QCD Corrections to $\bar{B} \to X_s l^+ l^-$ in the Standard Model and Beyond

Christoph Bobeth

September 2003

Physik Department T31
Prof. A. J. Buras

Physik–Department
Technische Universität München
Institut für Theoretische Physik
Lehrstuhl Univ.-Prof. Dr. Andrzej J. Buras

QCD Corrections to $\bar{B} \to X_s l^+ l^-$ in the Standard Model and Beyond

Christoph Bobeth

Vollständiger Abdruck der Fakultät für Physik der Technischen Universität München zur Erlangung des akademischen Grades eines

Doktors der Naturwissenschaften (Dr. rer. nat.)

genehmigten Dissertation.

Vorsitzender: Univ.-Prof. Dr. Stephan Paul

Prüfer der Dissertation:

1. Univ.-Prof. Dr. Andrzej J. Buras
2. Univ.-Prof. Dr. Manfred Lindner

Die Dissertation wurde am 28. August 2003 bei der Technischen Universität München eingereicht und durch die Fakultät für Physik am 11. September 2003 angenommen.

Abstract

The inclusive semileptonic B decay $\bar{B} \to X_s l^+ l^-$ will be discussed in this work. Here X_s denotes an arbitrary state of total strangeness -1 and the leptons are considered to be $l = e$ or μ. The theoretical predictions of inclusive quantities are preferable with respect to exclusive ones since non-perturbative effects are under control in the framework of heavy quark expansion (HQE). The non-perturbative corrections are small in certain regions of the dilepton invariant mass spectrum whereas the major contribution consists in the perturbatively calculable parton decay $b \to s l^+ l^-$.

We will extent the existing next-to leading order (NLO) QCD calculation of the parton result to the next-to-next-to leading order (NNLO) in QCD within the Standard Model (SM) of elementary particle physics. In particular, the NNLO matching contributions to the Wilson coefficients of the operators mediating $b \to s l^+ l^-$ will be calculated.

These results are used in the evaluation of the dilepton invariant mass distribution at the parton level taking into account the NNLO renormalization group evolution of the Wilson coefficients and the NNLO matrix element calculation of the corresponding operators. As a result we are able to reduce a large uncertainty of $\pm 16\%$ to $\pm 6\%$ of the dilepton invariant mass distribution which was mainly due to the renormalization scale of the top-quark mass.

Furthermore, we will include all known $\Lambda^2_{\rm QCD}/m_c^2$ and $\Lambda^3_{\rm QCD}/m_b^3$ non-perturbative corrections in the calculation of the dilepton invariant mass distribution at the hadronic level. The analysis will be restricted to low values of the dilepton invariant mass in the region $\hat{s} \in [0.05, 0.25]$ and to high values in the region $\hat{s} \in [0.64, 0.78]$. The HQE is not invalidated by intermediate hadron resonances in both regions and allows predictions without model-dependencies. The poorly known matrix elements of heavy quark effective theory (HQET) operators of the $\Lambda^3_{\rm QCD}/m_b^3$ corrections introduce further theoretical uncertainty.

The uncertainties of the branching ratio of the low- and high-$\hat{s}$ regions originating from the residual renormalization scale dependence and the poorly known parameters of HQET are analyzed. The residual renormalization scale dependencies are found to be of the order of $\pm 10\%$ and $\pm 16\%$ (compared to $\pm 20\%$ and $\pm 22\%$ at NLO order) in the low- and high-$\hat{s}$ region, respectively. Additionally, the HQET parameters of the order $\Lambda^3_{\rm QCD}/m_b^3$ induce an uncertainty of 5% in the low-$\hat{s}$ region and a large uncertainty of 15% in the high-$\hat{s}$ region.

Apart from the Standard Model we will consider also a special scenario of the Minimal Supersymmetric Standard Model (MSSM) with a heavy decoupled gluino and a minimal flavor violation inspired texture of soft supersymmetry breaking parameters. Analogously to the SM within this scenario the complete set of NNLO matching contributions to the Wilson coefficients of the operators mediating $b \to s l^+ l^-$ will be evaluated. Such corrections can become numerically important when approximate cancellations occur among the new physics contributions and/or the SM one. The impact of the NNLO corrections on the dilepton invariant mass distribution will be discussed in connection with the reduction of renormalization scale uncertainties.

Contents

1 Introduction

The current description of particle physics – the so called Standard Model (SM) – has been formed as a result of a combination of many theoretical concepts combined with experimental observations. As a quantum field theory being locally gauge invariant the ideas of quantum theory, relativistic field theory and group theory are needed. The SM successfully incorporates almost[1] all known properties of three out of the four known fundamental interactions – the strong, the weak and the electro-magnetic force – which is reflected by the invariance under local transformations of the non-abelian gauge symmetry $SU(3)_C \otimes SU(2)_W \otimes U(1)_Y$.

In principle local gauge invariance implies massless gauge bosons and consequently predicts long range forces. Therefore local gauge theories might not appear to be the proper description of the observed short range weak force mediated by massive gauge bosons. This apparent shortcoming can be solved with the help of spontaneous symmetry breaking achieved through the Higgs mechanism [1–4]. Furthermore, the proof of the renormalizability of local non-abelian (Yang-Mills) gauge theories [5] in the early 70ties was extended to spontaneously broken gauge theories [6]. Both, the Higgs mechanism and the proof of renormalizability were the foundations of the application of local gauge theories to describe short range weak interactions and the starting point of the formulation of the SM.

The spontaneous breaking of the gauge symmetry is necessary to properly model the short range interactions and requires the introduction of at least one scalar particle – the so called Higgs particle. Up to now the Higgs particle escaped the direct detection at high energy colliders being the last missing part for the experimental confirmation of the SM. The formally as massless introduced gauge and "matter" fields (leptons and quarks) acquire masses due to their couplings to the Higgs field. Thus the Higgs mechanism represents the mass generation mechanism of gauge and "matter" fields.

As a consequence of the spontaneous symmetry breaking the couplings of the W boson to quarks are given in terms of the elements of the Cabibbo-Kobayashi-Maskawa (CKM) matrix $(V_{\mathrm{CKM}})_{ij}$ [7,8] that arises from the diagonalization of the quark mass matrices. In the SM it is this very matrix that is responsible for *all* weak decays of hadrons as well as for CP non-conservation[2]. CP violation was first observed in 1964 in kaon decay [11] and recently for the first time in the B meson system in the decay $B \to J/\psi K_S^0$ [12]. The CKM matrix plays a fundamental role in the description of weak decays and the origin of CP violation requiring an exact knowledge and understanding of these parameters. Theoretical predictions of weak hadron decays suffer generally from uncertainties due to non-perturbative strong interaction effects preventing a straightforward determination of the CKM matrix elements. Their

[1] The experimental evidence for neutrino oscillations [9, 10] can be accommodated for example within the SM by adding right-handed neutrinos, however there exist also other theoretically more favorable and attractive alternatives.

[2] A different source of CP violation appears in QCD when including non-trivial topological effects due to the "Θ-term" known as the *strong CP problem*.

improved understanding is therefore desirable in order to test the SM and perhaps to find new physics effects.

The investigation of B meson decays promises to provide these kind of insights. Especially the high value of the b-quark mass in the range of $4-5$ GeV leads to a special role of B mesons for flavor physics studies. The theory of *inclusive* and also *exclusive* B decays has been dramatically improved in the last decade. Especially the *heavy quark expansion* (HQE) approach combined with *heavy quark effective theory* (HQET) methods applied to inclusive semileptonic and radiative B decays offers a quite systematic treatment of non-perturbative effects in a model independent way. Remarkably the perturbatively calculable parton decay emerges as the leading contribution to physical observables whereas non-perturbative corrections are suppressed by $\Lambda^2_{\mathrm{QCD}}/m_Q^2$ with m_Q being the heavy quark mass. It should be emphasized that the validity of the HQE depends strongly on the kinematical configuration under consideration which can limit the reliability and applicability of this approach in practice.

The class of *flavor changing neutral current* (FCNC) B decays forms a special group among B processes from a theoretical point of view. Within the SM their decay rate is naturally suppressed as they proceed only at the loop level in perturbation theory. This mechanism seems to be confirmed by the present experimental data through the fact that the branching ratios of FCNC decays are tiny. So far the experimental results are in agreement with the expected range of magnitude predicted by the SM, however still some decay channels are unobserved. The "loop" suppression of FCNC processes leads to a strong dependence on virtually exchanged particles, such as the top quark or the electroweak gauge bosons in the SM. With respect to the consideration of physics beyond the SM the sensitivity of FCNC processes to the exchange of unknown particles makes them attractive because they provide tests of the SM and constrain parameter spaces of new physics models.

Among the rare FCNC processes the radiative and semileptonic channels mediated at the parton level by $b \to s\gamma$ and $b \to s l^+ l^-$, respectively, are experimentally observed. The experimental and theoretical situations of the inclusive decay $\bar{B} \to X_s\gamma$ have progressed to a very involved point. The present data from CLEO, BaBar, Belle and ALEPH give the current world average [13] for the branching ratio $\bar{B} \to X_s\gamma$

$$\mathcal{B}[\bar{B} \to X_s\gamma\ (E_\gamma > 1.6\ \mathrm{GeV})]_{\mathrm{exp}} = (3.28^{+0.41}_{-0.36}) \times 10^{-4} \tag{1.1}$$

with an error of around 12%. The measurement of $\bar{B} \to X_s\gamma$ requires the introduction of a lower cut on the photon energy in the B meson rest-frame being typically $E_\gamma > 2.0\,\mathrm{GeV}$ [14] to exclude the dominant charm background. The extrapolation of the branching ratio to lower energy ranges down to 1.6 GeV with the help of theoretical models introduces besides the statistical and systematical error also theoretical model dependencies. So far these model dependencies do not dominate the total error of the experimental result but this might easily happen in the near future. With the expected high luminosity of the B factories (BaBar and Belle), an experimental accuracy below 10% appears to be achievable.

In the meantime the theoretical prediction of $\bar{B} \to X_s\gamma$ has reached an advanced level including a huge variety of corrections. As mentioned before within the HQE the leading contribution is the perturbatively calculable parton decay $b \to s\gamma$ inclusive bremsstrahlung corrections. It is known up to next-to leading order in QCD (NLO) as well as all enhanced logarithmic and $1/\sin^2\theta_W$ electroweak corrections. Further the leading non-perturbative $\Lambda^2_{\mathrm{QCD}}/m_Q^2$ $\{Q = c, b\}$ corrections are calculated. A careful reconsideration of this process [15]

has shown that the numerical value of the theoretical result can vary between $(3.28 \pm 0.33) \times 10^{-4}$ and $(3.57 \pm 0.30) \times 10^{-4}$ depending on the choice of the renormalization scheme of the charm quark mass between the pole mass scheme and the modified minimal subtraction ($\overline{\rm MS}$) scheme, respectively. This strong scheme dependence stems from two-loop matrix elements of four-quark operators to $b \to s\gamma$, being the leading contribution because of the vanishing one-loop matrix elements. Although the choice of the $\overline{\rm MS}$ scheme is preferred this discrepancy due to higher order QCD corrections can only be resolved by their explicit calculation. Beside this perturbative uncertainty a further theoretical uncertainty arises due to the unknown non-perturbative corrections associated to the same diagrams [16].

The reliability of the theoretical predictions depends crucially on the kinematical configuration under consideration and often theoretically favored kinematical regions, where non-perturbative corrections are under control, are rather restricted. On the other side the experimental investigation requires theoretical input to extrapolate the results to kinematical regions that are not accessible due to large backgrounds or small experimental efficiencies. The ultimate solution of the inclusive decay $\bar{B} \to X_s\gamma$ towards establishing a physical observable by means of adequate cuts on kinematical variables such as the photon energy and a reduced dependence on the renormalization scheme of the charm quark mass due to the inclusion of higher order QCD corrections still deserves experimental and theoretical efforts. The present SM prediction of the branching ratio of $\bar{B} \to X_s\gamma$ coincides with the measurement within the uncertainties. Despite the current errors the agreement of the experimental result and the SM prediction is quite impressive and the decay $\bar{B} \to X_s\gamma$ is known to put non-trivial constraints on the parameter spaces of models beyond the SM.

While the measurement of the decay $\bar{B} \to X_s\gamma$ is being consolidated, the Belle Collaboration succeeded about one year ago for the first time to measure the branching ratio of the inclusive decay $\bar{B} \to X_s l^+ l^-$ with $(l = e, \mu)$ [17]

$$\mathcal{B}[\bar{B} \to X_s l^+ l^-]_{\rm exp} = \left(6.1 \pm 1.4^{+1.4}_{-1.1}\right) \times 10^{-6} \tag{1.2}$$

for dilepton masses larger than 0.2 GeV. The statistical significance of this result amounts to $5.4\,\sigma$. Very recently also the BaBar Collaboration announced a similar preliminary value obtained with a statistical significance of $4.6\,\sigma$ [18]

$$\mathcal{B}[\bar{B} \to X_s l^+ l^-]_{\rm exp} = \left(6.3 \pm 1.6^{+1.8}_{-1.5}\right) \times 10^{-6}. \tag{1.3}$$

The large background due to the decays $B \to X_s J/\psi \to X_s l^+ l^-$ and $B \to X_s \psi' \to X_s l^+ l^-$ which interfere with the decay $\bar{B} \to X_s l^+ l^-$ is vetoed explicitely by cuts on the dilepton invariant mass distribution. The theoretical uncertainties which would be induced by the inclusion of such intermediate $c\bar{c}$ states are by far the most dominant. Because of the non-perturbative nature of these states, the dilepton invariant mass distribution can be only roughly estimated when the invariant mass of the lepton pair is not significantly below the J/ψ resonance. It remains questionable whether integrating the dilepton invariant mass distribution over this domain can reduce the theoretical uncertainty below $\pm 20\%$ [19].

On the contrary, for small dilepton invariant masses (accessible to $l = e$ or μ), a relative precise determination of the decay distribution is possible using perturbative methods and non-perturbative corrections within the framework of HQE. The dominant non-perturbative $\Lambda^2_{\rm QCD}/m^2_Q$ $(Q = c, b)$ corrections were found to be small, of the order of a few percent, for

dilepton invariant masses in the range $0.05 < \hat{s} \equiv (p_{l^-} + p_{l^+})^2/m_{b,pole}^2 < 0.25$. Thus, the $\bar{B} \to X_s l^+ l^-$ decay distribution integrated over this region of the dilepton invariant mass should be perturbatively predictable as the $\bar{B} \to X_s \gamma$ decay rate, i.e. up to about 10% uncertainty.

Unfortunately, the theoretical prediction of the perturbatively calculable part in the SM, even though performed up to next-to leading (NLO) order in QCD [20–24], has not reached this precision. The formally leading order term is (quite accidentally) suppressed, which makes it as small as some of the NLO contributions. The theoretical uncertainties due to renormalization scale dependencies of the NLO result are of the order of 20%. Consequently, some of the formally next-to-next-to leading (NNLO) terms can have an effect larger than 10% on the dilepton invariant mass distribution. This can be easily verified by varying the renormalization scale at which the top quark mass is renormalized in the formulae of Refs. [23, 24].

In view of the small non-perturbative corrections and the large uncertainties in the NLO calculation we will extend the analysis of the decay $\bar{B} \to X_s l^+ l^-$ up to the NNLO level within the SM and a minimal flavor violation inspired scenario of the Minimal Supersymmetric Standard Model (MSSM) with decoupled heavy gluino. For these purposes Chapter 2 provides a short introduction to the SM to remind the reader of the origin of several ideas, terms and definitions as well as to set up our notation.

Chapter 3 covers the subject of effective theories being a necessary tool for the evaluation of B decays. The theoretical framework of weak B processes is based on the different mass scales involved in the decay allowing for a systematic factorization of high and low energy scale effects with the help of an *operator product expansion* (OPE). This results in an effective theory Lagrangian which describes the interactions of the light degrees of freedom (leptons and light quarks) in terms of effective interaction vertices – the so called *operators*. The effect of the decoupled heavy degrees of freedom is absorbed into the effective coupling constants – *Wilson coefficients* – which can be calculated reliably in perturbation theory. With the help of the renormalization group equation (RGE) the framework of effective theories allows further the resummation of large logarithmic terms due to radiative corrections to all orders in perturbation theory.

The sensitivity of FCNC B decays to physics beyond the SM provides the possibility to find constraints on parameter spaces of new physics models. Chapter 4 is devoted to the description of the particle spectrum of the Minimal Supersymmetric Standard Model (MSSM) and the relevant parts of the interaction Lagrangian for B decays. Furthermore a minimal flavor violation inspired scenario with heavy decoupled gluinos will be described. The initial matching conditions for the operators mediating $\bar{B} \to X_s l^+ l^-$ will be evaluated later within this new physics scenario up to NNLO.

The results of the NNLO analysis of the decay $\bar{B} \to X_s l^+ l^-$ will be presented in Chapter 5. This includes a summary of the matching conditions of the SM and the here considered supersymmetric scenario at the matching scale. In a second step the renormalization group running will be given up to next-to-next-to leading logarithmic (NNLL) approximation, resulting in the effective Lagrangian at the low energy scale. Collecting the known formulae of the perturbative calculation of the matrix elements $b \to s l^+ l^-$ the remaining scale dependencies of the dilepton invariant mass spectrum and the branching ratio obtained by integration over the dilepton invariant mass below the J/ψ resonance will be discussed. In order to pass from the perturbatively calculated parton level to the final hadronic B meson observables the non-perturbative corrections will be included and the final uncertainties investigated.

Finally, we conclude in Chapter 6 and give a short outlook. Technical details and the analytic formulae for the Wilson coefficients are presented in the appendices. Appendix A summarizes the relevant parts of the MSSM interaction Lagrangian to setup the notation. Appendix B contains a list of unphysical operators needed for the complete off-shell calculation of two-loop contributions to the Wilson coefficients. Appendix C contains the analytic results of the matching contributions to the Wilson coefficients in the SM and the considered MSSM scenario. Appendix D lists further auxiliary functions that enter the results of Appendix C.

2 The Standard Model

This chapter provides a short introduction to the notions and notations of the Standard Model (SM) of electroweak and strong interactions of elementary particle physics.

The Principle of Local Gauge Invariance

Elementary particle physics is described by relativistic quantum field theories. Thereby the fundamental interactions of spin 1/2 fermion fields are derived from the *principle of local gauge invariance* (Weyl 1932, Yang-Mills 1954) with a certain gauge group $G_{\rm loc}$. Observations have taught us that matter is composed out of spin 1/2 fermion fields establishing them as the suitable description of elementary particle physics. Once these *matter fields* and their transformation laws under $G_{\rm loc}$ are specified the theory is essentially determined. The matter fields of the real world are spin 1/2 particles, *leptons and colored quarks*. The electroweak interactions of the leptons and quarks exhibit a symmetry under the group $SU(2)_W \otimes U(1)_Y$ and the strong interactions of the quarks under the group $SU(3)_C$, C denoting the *color charge*. Thus the electroweak and strong interactions are derived from the gauge group [25–27]

$$G_{\rm loc} = SU(3)_C \otimes SU(2)_W \otimes U(1)_Y. \tag{2.1}$$

Discarding mass terms of spin 1/2 particles they are described by the relativistic massless Dirac field ψ which decomposes into two independent fields (Weyl fields), a left-handed and a right-handed

$$\psi_L = \frac{1-\gamma_5}{2}\psi \equiv P_L\psi, \qquad \psi_R = \frac{1+\gamma_5}{2}\psi \equiv P_R\psi, \tag{2.2}$$

yielding the free matter Lagrangian for N left-handed and N right-handed distinct massless spin 1/2 particles

Group	Gauge fields	Coupling	Generators	
$U(1)_Y$	B_μ	g_1	Y	hyper charge
$SU(2)_W$	W^a_μ	g_2	$\tau^a = \sigma^a/2,\ a = 1,2,3$	σ^a Pauli matrices
$SU(3)_C$	G^a_μ (gluons)	g_s	$\mathbf{T}^a = \lambda^a/2,\ a = 1,\ldots,8$	λ^a Gell-Mann matrices

Table 2.1: Notation of the gauge fields, the coupling constants and the generators of the group factors of $G_{\rm loc}$

$$\mathcal{L}_{\text{Fermion}} = \sum_{a=1}^{N} \left\{ \bar{\psi}_{La}\, i\partial\!\!\!/\, \psi_{La} + \bar{\psi}_{Ra}\, i\partial\!\!\!/\, \psi_{Ra} \right\}. \tag{2.3}$$

The principle of local gauge invariance requires $\mathcal{L}_{\text{Fermion}}$ to be locally invariant under transformations of G_{loc} such as

$$\psi_L \to U_L(x)\psi_L, \quad \psi_R \to U_R(x)\psi_R, \qquad U_L(x), U_R(x) \in G_{\text{loc}}. \tag{2.4}$$

The local gauge invariance can only be achieved by introducing a set of spin 1 gauge fields $V_{n,\mu}$ that couple minimally to the spin 1/2 fields by the introduction of the covariant derivative

$$\partial_\mu \to D_\mu = \partial_\mu + i \sum_n g_n \sum_{a=1}^{N_n} T_n^a V_{n,\mu}^a. \tag{2.5}$$

Since G_{loc} is a direct product of the simple group factors $SU(3)_C$, $SU(2)_W$ and $U(1)_Y$ the generators belonging to two different group factors will commute. As a consequence the gauge potential of G_{loc} can be written as a sum of products where the single addends correspond to the group factors. Each product consists out of a coupling constants g_n and a gauge potential $V_{n,\mu}$ with n denoting the gauge group factor and μ being the Lorentz indices of the gauge fields. The components of the gauge fields $V_{n,\mu}^a$ must transform according to the adjoint representation of the corresponding group. Furthermore, by T_n^a we denote the generators of the group and N_n gives the number of generators of each group factor. Table 2.1 shows the relevant parts to G_{loc}.

Matter – Gauge Interactions

The matter field content of the SM consists of three generations whereas each generation is composed of a neutrino ν_i, a charged lepton l_i, and the up- and down-type quarks u_i and d_i. The transformation laws of the chiral components of these fields under the $SU(3)_C$, $SU(2)_W$ and $U(1)_Y$ are summarized in Table 2.2. Only the fundamental (nontrivial representation of lowest dimension) and the trivial (singlet) representations show up.

Using the definitions and transformation properties listed in Table 2.2 $\mathcal{L}_{\text{Fermion}}$ contains the gauge interaction of the spin 1/2 fermion fields and the spin 1 gauge boson fields

$$\mathcal{L}_{\text{Fermion}} = \sum_{k=1}^{3} \left\{ \bar{L}_L^k\, iD\!\!\!/\, L_L^k + \bar{E}_R^k\, iD\!\!\!/\, E_R^k + \bar{Q}_L^k\, iD\!\!\!/\, Q_L^k + \bar{U}_R^k\, iD\!\!\!/\, U_R^k + \bar{D}_R^k\, iD\!\!\!/\, D_R^k \right\} \tag{2.6}$$

with k numbering the generations. When the covariant derivative

$$D_\mu = \partial_\mu + ig_1 B_\mu Y + ig_2 W_\mu^a \tau^a + ig_s G_\mu^a \mathbf{T}^a \tag{2.7}$$

acts on a fermion field, Y, τ^a and $\mathbf{T}^a$ are given in the same representation to which the fermion belongs. For example all leptons are put into the trivial representation of $SU(3)_C$ with

Group	Multiplet	Representation
$SU(3)_C$	leptons	1 color singlets
	quarks	3 color triplets
	antiquarks	3^* anticolor triplets
$SU(2)_W$	$L_L^1 \equiv \begin{pmatrix} \nu_e \\ e \end{pmatrix}_L,\ Q_L^1 \equiv \begin{pmatrix} u \\ d' \end{pmatrix}_L$	
	$L_L^2 \equiv \begin{pmatrix} \nu_\mu \\ \mu \end{pmatrix}_L,\ Q_L^2 \equiv \begin{pmatrix} c \\ s' \end{pmatrix}_L$	$2 = 2^*$
	$L_L^3 \equiv \begin{pmatrix} \nu_\tau \\ \tau \end{pmatrix}_L,\ Q_L^3 \equiv \begin{pmatrix} t \\ b' \end{pmatrix}_L$	
	$E_R^1 \equiv e_R,\ \ U_R^1 \equiv u_R,\ \ D_R^1 \equiv d'_R$ $E_R^2 \equiv \mu_R,\ \ U_R^2 \equiv c_R,\ \ D_R^2 \equiv s'_R$ $E_R^3 \equiv \tau_R,\ \ U_R^3 \equiv t_R,\ \ D_R^3 \equiv b'_R$	1
$U(1)_Y$	$Y = Q - T_3$	phase transformation

Table 2.2: The transformation laws of the matter fields under the particular group factors of the SM local gauge group G_{loc}. Note that the left-handed and right-handed fields transform different under the group $SU(2)_W$. Further the down quarks represent the gauge eigenstates of electro-weak interactions denoted by primes.

$\mathbf{T}^a = 0$ and consequently the covariant derivative becomes simplified to $D_\mu = \partial_\mu + ig_1 B_\mu Y + ig_2 W_\mu^a \tau^a$. Further simplification takes place for right-handed leptons as they in addition also transform according to the trivial representation of $SU(2)_W$ resulting in $D_\mu = \partial_\mu + ig_1 B_\mu Y$.

Free Gauge Field Sector

By adding the locally gauge invariant kinetic term

$$\mathcal{L}_{\text{Gauge}} = -\frac{1}{4} B_{\mu\nu} B^{\mu\nu} - \frac{1}{4} W^a_{\mu\nu} W^{a,\mu\nu} - \frac{1}{4} G^a_{\mu\nu} G^{a,\mu\nu} \tag{2.8}$$

the gauge fields describe physical degrees of freedom i.e. they become dynamical variables. The antisymmetric abelian and non-abelian field strength tensors are

$$\begin{aligned} B_{\mu\nu} &= \partial_\mu B_\nu - \partial_\nu B_\mu, \\ W^a_{\mu\nu} &= \partial_\mu W^a_\nu - \partial_\nu W^a_\mu - g_2 \epsilon^{abc} W^b_\mu W^c_\nu, \\ G^a_{\mu\nu} &= \partial_\mu G^a_\nu - \partial_\nu G^a_\mu - g_s f^{abc} G^b_\mu G^c_\nu, \end{aligned} \tag{2.9}$$

where ϵ^{abc} and f^{abc} denote the $SU(2)$ and $SU(3)$ structure constants, respectively.

Higgs – Gauge Interaction

The local gauge invariance enforces the existence of spin 1 gauge bosons transforming in the adjoint representation. However, local gauge invariance requires them to be massless. Further the different transformation properties of the left-handed and right-handed fermion fields under the $SU(2)_W$ symmetry also forbids mass terms of fermions, since they have the non-invariant form $\bar{\psi}\psi = \bar{\psi}_L \psi_R + \bar{\psi}_R \psi_L$.

The only known possibility to maintain the local gauge invariance[1] of the theory and to introduce masses for gauge and fermion fields is the mechanism of spontaneous symmetry breaking, the so called *Higgs mechanism* (Higgs 1964 [1–4], Weinberg 1967 [25–27]). The Higgs mechanism necessitates the introduction of a spin 0 $SU(2)_W$ doublet of two complex scalar fields (Higgs field) with the hypercharge $Y_\Phi = +1/2$

$$\Phi = \begin{pmatrix} \phi^+ \\ \phi^{0\prime} \end{pmatrix} \tag{2.10}$$

including a potential $V(\Phi^\dagger \Phi)$ which respects renormalizability

$$\mathcal{L}_{\text{Higgs}} = (D_\mu \Phi)^\dagger (D^\mu \Phi) - V(\Phi^\dagger \Phi) = (D_\mu \Phi)^\dagger (D^\mu \Phi) + \mu^2 \Phi^\dagger \Phi - \lambda (\Phi^\dagger \Phi)^2. \tag{2.11}$$

In the Higgs potential $V(\Phi^\dagger \Phi)$ two new parameters μ and λ appear.

[1] The issue of local gauge invariance is crucial for the Slavnov-Taylor identities [28, 29] which are needed for the proof of renormalizability and unitarity [5, 6] of the S-Matrix.

Higgs – Matter Interaction

The interaction of the Higgs field and the spin 1/2 fields are $G_{\rm loc}$–invariant *Yukawa* type couplings

$$\mathcal{L}_{\rm Yukawa} = \sum_{k,k'=1}^{3} \left\{ \bar{Q}_L^k \, Y_{kk'}^U \, \tilde{\Phi} \, U_R^{k'} + \bar{Q}_L^k \, Y_{kk'}^D \, \Phi \, D_R^{k'} + \bar{L}_L^k \, Y_{kk'}^E \, \Phi \, E_R^{k'} \right\} + \text{h.c.} \; . \tag{2.12}$$

The matrices $Y^{U,D,E}$ (Yukawa couplings) are arbitrary complex 3×3 matrices acting in the generation-space and $\tilde{\Phi} \equiv i\sigma_2 \Phi^*$ is the charge conjugated Higgs field.

Summarizing, the SM Lagrangian on the classical level before spontaneous symmetry breaking is given by the sum

$$\mathcal{L}_{\rm SM} = \mathcal{L}_{\rm Fermion} + \mathcal{L}_{\rm Higgs} + \mathcal{L}_{\rm Gauge} + \mathcal{L}_{\rm Yukawa}, \tag{2.13}$$

thereby being locally invariant under $G_{\rm loc}$ transformations.

Throughout the introduction of the SM the right-handed neutrinos were omitted leading to the prediction of massless neutrinos. Obviously, the SM has to be extended bearing in mind the fact that neutrino oscillation experiments (see for example [9,10]) have shown that neutrinos do have a non-vanishing mass. The right-handed neutrinos transform as singlets under the gauge group $G_{\rm loc}$ and hence are neutral with respect to all gauge interactions. For this reason they do not interact with the remaining particles via gauge interactions. A Yukawa type coupling of the form $\bar{L}^k Y_{kk'}^N \tilde{\Phi} N_R^{k'}$ were N_R^k denotes the right-handed neutrinos and Y^N the Yukawa coupling can be considered once the Higgs sector is introduced to spontaneously break the electroweak symmetry. This term is not forbidden by the symmetry $G_{\rm loc}$ and allows for the possibility that the SM could also accommodate neutrino masses. Analogously to the quark mass generation by means of the Higgs mechanism such a Yukawa term would yield a flavor mixing matrix in the lepton sector and both, lepton and neutrino masses.

However, for example such a simple extension does not provide an explanation of the smallness of neutrino masses. Here models based on the seesaw mechanism [30–32] are more attractive since they offer the possibility to relate the neutrino masses to scales where new physics is expected to enter. Disregarding the fact of the existence of neutrino masses in the following right-handed neutrinos shall be omitted because neutrino mass effects are completely negligible for the purpose of rare B decays.

Spontaneous Symmetry Breaking

To generate the mass terms of the spin 1 gauge bosons of the electroweak interaction and spin 1/2 matter fields the $SU(2)_W \otimes U(1)_Y$ symmetry will be broken spontaneously by means of the Higgs mechanism to the remaining $U(1)_Q$ of the electromagnetic interaction, observed in the real world by the experiment (electric charge conservation).

A symmetry G is said to be spontaneously broken, if the system chooses one special ground state among a set of degenerated ground states which are connected by transformations under G. Such a situation arises in systems in which the lowest lying state that still respects the symmetry G does not coincides with the state of minimum energy (ground state).

	ν_L^e	e_L^-	e_R^-	u_L	u_R	d_L	d_R
Q	0	-1	-1	2/3	2/3	-1/3	-1/3
T_3	1/2	-1/2	0	1/2	0	-1/2	0
Y	-1/2	-1/2	-1	1/6	2/3	1/6	-1/3

Table 2.3: The electric charge Q, the third component of the weak isospin T_3 and the hypercharge Y assignments of the matter fields in the SM.

Concerning the Higgs potential $V(\Phi^\dagger\Phi)$, the classical Higgs field configuration with minimum energy in the case of $\mu^2 < 0$ is a uniform field Φ_0 with the value zero. In the quantized theory the corresponding quantity is the vacuum expectation value (VEV) $\langle\Phi_0^\dagger\Phi_0\rangle = 0$.

For the choice of $\mu^2 > 0$ the norm of the constant field configuration which minimizes the potential becomes nonzero

$$\langle\Phi_0^\dagger\Phi_0\rangle = \frac{2\mu^2}{\lambda} \equiv \frac{v^2}{2}. \tag{2.14}$$

All these vectors Φ_0 are connected by a transformation under $SU(2)_W \otimes U(1)_Y$ and fixing Φ_0 to one special direction will break the symmetry spontaneously. Since in the real world the symmetry under electromagnetic gauge transformations $U(1)_Q$ is unbroken, Φ_0 has to be fixed in such a way to yield $U(1)_Q$ as the remaining unbroken symmetry, resulting (up to a phase convention) into the unique solution

$$\Phi_0 = \frac{1}{\sqrt{2}}\begin{pmatrix}0\\ v\end{pmatrix}. \tag{2.15}$$

The conserved electric charge Q is then given by the Gell-Mann–Nishijima relation

$$Q = Y + T_3. \tag{2.16}$$

Since the charges Q of leptons and quarks are known, the hypercharges Y are fixed by the above relation, as summarized in Table 2.3.

In order to extract the physical content of the Lagrangian in the presence of the classical background of the Higgs field it is convenient to introduce new Higgs fields with subtracted background by the replacement

$$\Phi = \begin{pmatrix}\phi^+\\ \frac{1}{\sqrt{2}}(v + H + i\phi^0)\end{pmatrix}. \tag{2.17}$$

As a result of the Higgs mechanism the Lagrangian contains the unphysical *would-be Goldstone fields* $\phi^\pm, \phi^0$ and the physical massive spin 0 Higgs boson H. Further the terms proportional to v in $\mathcal{L}_{\text{Higgs}}$ and $\mathcal{L}_{\text{Yukawa}}$ can be interpreted as mass terms of the spin 1 gauge boson fields and spin 1/2 fermion fields, respectively. The diagonalization of these terms by

means of unitary redefinitions of the gauge and fermion fields yields the Lagrangian in the mass eigenstate basis.

Physical Particle Spectrum

The mass eigenstate of the Higgs particle is H with the corresponding tree-level mass relation $M_H = \sqrt{2}\mu$.

The mass eigenstates of the gauge bosons are

$$W_\mu^\pm = \frac{1}{\sqrt{2}}\left(W_\mu^1 \mp iW_\mu^2\right), \qquad \begin{pmatrix} A_\mu \\ Z_\mu \end{pmatrix} = \begin{pmatrix} c_W & s_W \\ -s_W & c_W \end{pmatrix} \begin{pmatrix} B_\mu \\ W_\mu^3 \end{pmatrix}, \tag{2.18}$$

the two charged W bosons, the neutral Z boson and the neutral and massless photon A. Here the weak mixing angle (also Weinberg angle) θ_W appears in the transformation of the neutral gauge bosons

$$s_W \equiv \sin\theta_W = \frac{g_1}{\sqrt{g_1^2+g_2^2}}, \qquad c_W \equiv \cos\theta_W = \frac{g_2}{\sqrt{g_1^2+g_2^2}} = \frac{M_W}{M_Z}. \tag{2.19}$$

The covariant derivative takes the form (with $\tau^\pm \equiv \tau^1 \pm i\tau^2$)

$$D_\mu = \partial_\mu + i\frac{g_2}{\sqrt{2}}(W_\mu^+\tau^+ + W_\mu^-\tau^-) + i\frac{g_2}{c_W}(\tau_3 - s_W^2 Q)Z_\mu + ieQA_\mu. \tag{2.20}$$

To acquire the usual photon–fermion coupling of quantum electrodynamics (QED) the equality

$$e = s_W g_2 = c_W g_1 = \frac{g_1 g_2}{\sqrt{g_1^2+g_2^2}} = \sqrt{4\pi\alpha} \tag{2.21}$$

must hold, where $\alpha \approx 1/137$ denotes the fine structure constant. The tree-level mass relations are

$$M_W \equiv M_{W^-} = M_{W^+} = \frac{v}{2}g_2, \qquad M_Z = \frac{v}{2}\sqrt{g_1^2+g_2^2}, \qquad M_A = 0. \tag{2.22}$$

In order to obtain $M_A = 0$ when carrying out the Higgs mechanism it is necessary to fix the hypercharge of the Higgs doublet to the unique value $Y_\Phi = +1/2$.

Mass terms of the leptons and quarks arise from the diagonalization of terms proportional to v in $\mathcal{L}_{\text{Yukawa}}$-terms by unitary field redefinitions of the form

$$\begin{aligned} &L_L \to V_L^E L_L, && U_L \to V_L^U U_L, && D_L \to V_L^D D_L, \\ &E_R \to V_R^E E_R, && U_R \to V_R^U U_R, && D_R \to V_R^D D_R. \end{aligned} \tag{2.23}$$

Note that contrary to the lepton sector the two components of Q_L denoted by U_L and D_L have to be diagonalized by two different unitary matrices in order to diagonalize the Y^U and Y^D terms of $\mathcal{L}_{\text{Yukawa}}$ simultaneously. As a consequence the charged current coupling of quarks and W bosons becomes non-diagonal

$$\begin{aligned}\mathcal{L}_{udW} &\sim \frac{g_2}{\sqrt{2}}(\bar{u},\bar{c},\bar{t})\,\gamma^\mu P_L (V_L^U)^\dagger\, V_L^D \begin{pmatrix} d \\ s \\ b \end{pmatrix} W_\mu^+ + \text{h.c.}, \\ &\equiv \frac{g_2}{\sqrt{2}}\; J^{\dagger\,\mu} W_\mu^+ + \text{h.c.}. \end{aligned} \tag{2.24}$$

and the mass-eigenstates of the down quarks (denoted by omitting the primes, see Table 2.2) are not the gauge eigenstates of electroweak interactions. The coupling strengths of the flavor off diagonal quark transitions are given by the elements of the unitary matrix $V_{\text{CKM}} \equiv (V_L^U)^\dagger\, V_L^D$, the so called Cabibbo-Kobayashi-Maskawa (CKM) matrix. Finally the fermion masses can be obtained by diagonalizing $Y^{U,D,E}$ with the help of the biunitary transformations

$$M_U = \frac{v}{\sqrt{2}}(V_L^U)^\dagger Y^U V_R^U, \qquad M_D = \frac{v}{\sqrt{2}}(V_L^D)^\dagger Y^D V_R^D, \qquad M_E = \frac{v}{\sqrt{2}}(V_L^L)^\dagger Y^E V_R^L. \tag{2.25}$$

where the left-handed neutrinos remain massless.

3 Effective Theories

The observed physical particle spectrum in experiments consists to a large extent of hadrons that are mesons or baryons. These particles are described by quark bound states in the SM which arise due to the strong interaction (QCD) given by the $SU(3)_C$ non-abelian group factor of the SM gauge group G_{loc} (2.1). The investigation of B meson decays requires therefore the consideration of bound states of quarks. The arising problem is already indicated by the fact that the observed degrees of freedom (hadrons) are not the degrees of freedom of the SM Lagrangian (quarks). It is a general property of non-abelian gauge field theories that the coupling constant (in the case of QCD $\alpha_s \equiv g_s^2/(4\pi)$) becomes large at small momenta. As a consequence the quarks are strongly bound due to their interaction with gluon fields inside the hadrons, they are "glued together" and are not recognizable as quarks anymore which is called *confinement*. The large coupling constant prevents the application of perturbation theory to calculate observables. The typical scale at which the strong coupling α_s becomes non-perturbative is of the order of $\Lambda_{\text{QCD}} \approx 300\text{MeV}$.

Fortunately non-abelian gauge field theories also possess the property of a decreasing coupling constant at high momenta referred to as *asymptotic freedom* [33–35] where a perturbative calculation is possible. In this sense observables depending on QCD corrections only at high virtual momenta offer the possibility to gain insights into QCD with the help of perturbation theory, for example QCD corrections to the Z-boson physics.

The FCNC B decays are caused by the electroweak interactions of the quarks inside the meson. They are characterized by the fact, that scales of the external momenta and masses ($\sim 5\,\text{GeV}$) are small in comparison to scales of the masses of virtually exchanged particles responsible for the quark decays, i.e. in the SM the electroweak gauge bosons ($\sim 80\,\text{GeV}$) and the heavy top quark ($\sim 175\,\text{GeV}$). Beyond the SM usually additional heavy particles can contribute to FCNC decays. Although the confinement in general cannot be solved the full SM can be replaced by an effective theory. Thereby degrees of freedom involving scales at which QCD can be treated perturbatively and which are usually responsible for the FCNC B decays have been factorized (decoupled) into effective coupling constants since they are too short ranged to contribute to bound state effects. The effective theory then describes only the QCD interactions of the light quarks including there bound states, requiring the application of non-perturbative methods to evaluate the matrix elements.

In the following the ideas for the derivation of such an effective low energy theory will be presented. Since the perturbative methods in quantum field theories lead to infinities the concept of *renormalization* has to be applied and a short introduction will be given. As a consequence of the renormalization procedure in intermediate steps the use of a *renormalization scale* becomes necessary. However, physical observables and "bare" parameters have to be renormalization scale independent which implies the existence of so called *renormalization group equations* (RGE). This leads to the concept of *running* coupling constants and masses. Furthermore large logarithms induced by radiative corrections can be resummed to

all orders in the coupling constant with the help of RGE's within the effective theory often referred to as *RGE improved perturbation theory*.

3.1 Effective Theory

In quantum field theory the Lagrangian in terms of fields and parameters plays a central role. It enters the generating functional of the Green functions describing the quantum field theory. Further the Lehmann-Symanzik-Zimmermann reduction formula yields the S-Matrix elements within an scattering picture of asymptotic free particles (leptons or hadrons) derived from the Green functions. The S-Matrix elements themselves represent transition probabilities providing the link to the experiment to determine the parameters of the Lagrangian. However, fields and parameters do not have the status of physical observables.

Intuitively, an effective theory reproduces S-Matrix elements of a given theory (*full theory*) within the range of validity of a certain applied approximation. The effective theory Lagrangian $\mathcal{L}_{\text{eff}} = \mathcal{L}_{\text{eff}}(\{\Phi_i^{\text{eff}}\}, \{\alpha_j^{\text{eff}}\})$ is given in terms of a set of fields $\{\Phi_i^{\text{eff}}\}$ and parameters $\{\alpha_j^{\text{eff}}\}$. A priori there exists no relation of these fields and parameters to their counterparts $\{\Phi_I\}$ and $\{\alpha_J\}$ of the full theory. Only a derivation of $\mathcal{L}_{\text{eff}}$ from $\mathcal{L}_{\text{full}}$ would yield such relations

$$\{\Phi_i^{\text{eff}}\} = \{\Phi_i^{\text{eff}}\}\Big(\{\Phi_I\}, \{\alpha_J\}\Big), \qquad \{\alpha_j^{\text{eff}}\} = \{\alpha_j^{\text{eff}}\}\Big(\{\Phi_I\}, \{\alpha_J\}\Big). \tag{3.1}$$

For the derivation of the effective theory it is sufficient to consider Green functions since the S-Matrix elements are fully determined by them. The Green functions relevant for weak decays of hadrons within the SM are characterized by

- light external particles such as light quarks, leptons and gauge bosons (photon or gluon),
- the weak quark and lepton currents are nonlocal and the non-locality is determined by the momentum transfer and the masses of the electroweak gauge boson and the top-quark propagators,
- the details of the electroweak interaction describing the real production of heavy particles are irrelevant for processes with small external momenta $\sqrt{s} \ll M_W$.

To sketch the derivation of the relations (3.1) we introduce the n-point Green function as the vacuum expectation value of the time-ordered product of n Heisenberg fields $\Phi_{\alpha_i}(x_i)$

$$G_{\alpha_1,\ldots,\alpha_n}(x_1,\ldots,x_n) = \langle 0|\mathbf{T}\Phi_{\alpha_1}(x_1)\ldots\Phi_{\alpha_n}(x_n)|0\rangle. \tag{3.2}$$

The transformation of the Heisenberg fields to the corresponding fields $\Phi^I_{\alpha_i}(x_i)$ of the interaction picture then yields

$$G_{\alpha_1,\ldots,\alpha_n}(x_1,\ldots,x_n) = \frac{\left\langle 0\left|\mathbf{T}\Phi^I_{\alpha_1}(x_1)\ldots\Phi^I_{\alpha_n}(x_n)\exp\left[i\int d^4x\ \mathcal{L}_{\text{int}}[\Phi^I_{\alpha_i}(x)]\right]\right|0\right\rangle}{\left\langle 0\left|\mathbf{T}\exp\left[i\int d^4x\ \mathcal{L}_{\text{int}}[\Phi^I_{\alpha_i}(x)]\right]\right|0\right\rangle} \tag{3.3}$$

as can be found for example in [36]. Thereby $\mathcal{L}_{\rm int}[\Phi^I_{\alpha_i}(x)]$ denotes the interaction part of the Lagrangian, the time-ordered product $\mathbf{T}$ extends over the entire expression and further the denominator cancels vacuum-vacuum sub-diagrams which are not connected to external points appearing in the numerator. The Green functions can be expressed in terms of the "connected" Green functions which will be denoted in the following by

$$G^c_{\alpha_1,\ldots,\alpha_n}(x_1,\ldots,x_n) = \Big\langle 0\Big|\mathbf{T}\Phi^I_{\alpha_1}(x_1)\ldots\Phi^I_{\alpha_n}(x_n)\exp\Big[i\int d^4x\ \mathcal{L}_{\rm int}[\Phi^I_{\alpha_i}(x)]\Big]\Big|0\Big\rangle_c. \tag{3.4}$$

As two representative parts of the SM interaction Lagrangian involved in B decays the QCD and electroweak interactions of the up- and down-quarks and the respective gauge bosons, G^a_μ and $W^\pm_\mu$ will be considered

$$\mathcal{L}_{\rm int} = \mathcal{L}_{\rm QCD} + \mathcal{L}_{udW} \tag{3.5}$$

with $\mathcal{L}_{udW}$ given in (2.24). The insertion of the SM interaction Lagrangian into (3.4) and the properties of the $\mathbf{T}$-product yield then

$$\begin{aligned} G^c_{\alpha_1,\ldots,\alpha_n}(x_1,\ldots,x_n) = \Big\langle 0\Big|&\mathbf{T}\Phi^I_{\alpha_1}(x_1)\ldots\Phi^I_{\alpha_n}(x_n)\\ &\times\exp\Big[i\int d^4x\ \mathcal{L}_{\rm QCD}(x)\Big]\ \exp\Big[i\int d^4x\ \mathcal{L}_{udW}(x)\Big]\Big|0\Big\rangle_c. \end{aligned} \tag{3.6}$$

The perturbative expansion with respect to electroweak interactions can be obtained expanding the exponential function containing the electroweak part of the interaction – $\mathcal{L}_{udW}$

$$\begin{aligned} G^c_{\alpha_1,\ldots,\alpha_n}(x_1,\ldots,x_n) = \sum_{n=0}^{\infty}\frac{i^n}{n!}\int\left(\prod_{m=1}^{n}d^4y_m\right)\Big\langle 0\Big|&\mathbf{T}\Phi^I_{\alpha_1}(x_1)\ldots\Phi^I_{\alpha_n}(x_n)\\ &\times\exp\Big[i\int d^4x\ \mathcal{L}_{\rm QCD}(x)\Big]\ \left(\prod_{m=1}^{n}d^4y_m\ \mathcal{L}_{udW}(y_m)\right]\Big)\Big|0\Big\rangle_c. \end{aligned} \tag{3.7}$$

This result still contains all orders in the strong coupling constant and the exponential function containing $\mathcal{L}_{\rm QCD}$ will not be expanded whereas the electroweak interactions will be treated in perturbation theory. For example a $\Delta B = \pm 1$ process of four external quarks is represented by the term $n = 2$ of (3.7) in lowest order of perturbation theory in the electroweak coupling

$$\begin{aligned} G^c_{\alpha_1,\ldots,\alpha_4}(x_1,\ldots,x_4) &= -\frac{1}{2}\int d^4y_1d^4y_2\Big\langle 0\Big|\mathbf{T}\Phi^I_{\alpha_1}(x_1)\ldots\Phi^I_{\alpha_n}(x_4)\\ &\quad\times\exp\Big[i\int d^4x\ \mathcal{L}_{\rm QCD}(x)\Big]\ \Big(\mathcal{L}_{udW}(y_1)\ \mathcal{L}_{udW}(y_2)\Big)\Big|0\Big\rangle_c\\ &= -\frac{g_2^2}{4}\int d^4y_1d^4y_2\Big\langle 0\Big|\mathbf{T}\Phi^I_{\alpha_1}(x_1)\ldots\Phi^I_{\alpha_n}(x_4)\ \exp\Big[i\int d^4x\ \mathcal{L}_{\rm QCD}(x)\Big]\\ &\quad\times\Big(J^{\dagger\,\mu}(y_1)W^+_\mu(y_1)J^{\dagger\,\nu}(y_2)W^-_\nu(y_2)+\text{h.c.}\Big)\Big|0\Big\rangle_c. \end{aligned} \tag{3.8}$$

The application of the Wick-theorem and the subsequent contraction of the W-boson fields gives the W-boson propagator $i\,\Delta^W_{\mu\nu}(y_1 - y_2,\, M_W)$ being a complex function and thus the last line in (3.8) becomes

$$G^c_{\alpha_1,\ldots,\alpha_4}(x_1,\ldots,x_4) = -i\frac{g_2^2}{4}\int d^4y_1 d^4y_2\ \Delta^W_{\mu\nu}(y_1-y_2,\,M_W)\Big\langle 0\Big|\mathbf{T}\Phi^I_{\alpha_1}(x_1)\ldots\Phi^I_{\alpha_n}(x_4) \times \exp\Big[i\int d^4x\ \mathcal{L}_{\mathrm{QCD}}(x)\Big]\Big(J^{\dagger\,\mu}(y_1)J^{\dagger\,\nu}(y_2)+\mathrm{h.c.}\Big)\Big|0\Big\rangle_c . \tag{3.9}$$

At this point the product of the non-local quark currents can be replaced by an operator product expansion (OPE) [37] resulting in a series of local interactions $\mathcal{O}_i\left(\frac{y_1+y_2}{2}\right)$ (*Operators*) and according complex coefficient functions $C_i^{\mu\nu}(y_1-y_2)$ (*Wilson coefficients*)

$$\mathbf{T}J^{\dagger\,\mu}(y_1)J^{\dagger\,\nu}(y_2) = \sum_i C_i^{\mu\nu}(y_1-y_2)\mathcal{O}_i\left(\frac{y_1+y_2}{2}\right). \tag{3.10}$$

Strictly speaking the above equation represents an operator identity. The local operators have quantum numbers of a $\Delta B = \pm 1$ transition and are sorted by rising dimension. In general they are built out of quark fields and the gluon and photon field strength tensors. Further also "equation of motion (EOM) vanishing" [see Appendix B] and other non-physical operators appear in the complete set of the operators. The complex Wilson coefficients $C_i^{\mu\nu}(x)$ are divergent functions in the limit $x \to 1$ whereby the degree of divergence reduces with the increasing dimension of the corresponding operator. The insertion of (3.10) into (3.9) and a subsequent variable transformation yields

$$G^c_{\alpha_1,\ldots,\alpha_4}(x_1,\ldots,x_4) = -i\frac{g_2^2}{4}\sum_i\int d^4\tilde{y}_1\Big[\int d^4\tilde{y}_2\ \Delta^W_{\mu\nu}(\tilde{y}_2,\,M_W)C_i^{\mu\nu}(\tilde{y}_2)\Big] \times\Big\langle 0\Big|\mathbf{T}\Phi^I_{\alpha_1}(x_1)\ldots\Phi^I_{\alpha_n}(x_4)\exp\Big[i\int d^4x\ \mathcal{L}_{\mathrm{QCD}}(x)\Big]\mathcal{O}_i(\tilde{y}_1)\Big|0\Big\rangle_c ,$$

$$G^c_{\alpha_1,\ldots,\alpha_4}(x_1,\ldots,x_4) = -i\frac{g_2^2}{4}\sum_i\int d^4\tilde{y}_1\ \tilde{C}_i \times\Big\langle 0\Big|\mathbf{T}\Phi^I_{\alpha_1}(x_1)\ldots\Phi^I_{\alpha_n}(x_4)\exp\Big[i\int d^4x\ \mathcal{L}_{\mathrm{QCD}}(x)\Big]\mathcal{O}_i(\tilde{y}_1)\Big|0\Big\rangle_c . \tag{3.11}$$

Here the W-boson is "integrated out" when performing the $\tilde{y}_2$-integration and the result is denoted by $\tilde{C}_i$. The Wilson coefficients $\tilde{C}_i$ turn out to be independent of the structure of the external states. In practice it is sufficient to use the approximation of massless quarks simplifying the calculations. The factorization achieved by the OPE corresponds to a factorization of short-distance physics represented by the Wilson coefficients and long-distance physics parameterized by the matrix elements of the operators.

The details of the electroweak interaction as for example real W-boson production or the real production of other heavy particles are not relevant concerning low energy processes with

a typical momentum transfer of $\sqrt{s} \ll M_W$. The same result (3.11) can be also obtained from an effective theory Lagrangian of the form

$$\mathcal{L}_{\rm int} = \mathcal{L}_{\rm QCD} - \frac{2G_F}{\sqrt{2}} \sum_i c_i \mathcal{O}_i. \tag{3.12}$$

Here $G_F \equiv \sqrt{2} g_2^2/(8M_W^2)$ is the Fermi constant, c_i are the effective coupling constants corresponding to the set of effective parameters $\{\alpha_j^{\rm eff}\}$ of (3.1) and $\mathcal{O}_i$ are effective interaction vertices of the same form as in the OPE but expressed in terms of effective fields $\{\Phi_i^{\rm eff}\}$. The result obtained using the effective Lagrangian and expanding up to the first order in G_F ($n = 1$) following the above derivation yields

$$G^c_{\alpha_1,\ldots,\alpha_4}(x_1,\ldots,x_4) = -i\frac{2G_F}{\sqrt{2}} \sum_i \int d^4\tilde{y}_1 \; c_i \\ \times \Big\langle 0 \Big| \mathbf{T} \Phi^I_{\alpha_1}(x_1) \ldots \Phi^I_{\alpha_n}(x_4) \exp\Big[i \int d^4x \; \mathcal{L}_{\rm QCD}(x) \Big] \mathcal{O}_i(\tilde{y}_1) \Big| 0 \Big\rangle_c . \tag{3.13}$$

At this point the effective coupling constants can be fixed by the requirement of the equality of the full theory (3.11) and the effective theory result (3.13). The determination of c_i from the full theory is called *matching* and the considered example yields the relation

$$c_i = M_W^2 \tilde{C}_i. \tag{3.14}$$

Here the fields are the same that appear in the full and effective theory Lagrangian. However, in practical calculations also the expansion in the strong coupling constant becomes necessary and in the course of the explicite evaluation of Green functions a renormalization of fields and parameters has to be performed. This renormalization corresponds to a redefinition of the fields and parameters which can be chosen differently for the full and effective theory Green functions. In general one starts the matching with n-point Green functions of smallest n and proceeds with the calculation of higher n-point Green function until all fields and parameters of the effective theory are fully determined.

3.2 Renormalization

The perturbative expansion of Green functions in coupling constants is a well defined procedure which can be illustrated by Feynman graphs and the corresponding analytic expressions can be easily found by the application of the Feynman rules. When going beyond the tree-level approximation the analytic expressions of the Green functions contain integrations over virtual momenta which turn out to be infinite. To allow for a proper treatment of the divergencies, a *regularization* procedure is needed. This amounts to a modification of the theory so that the possibly divergent expressions become well defined and that in a suitable limit the original (divergent) theory is recovered. For gauge theories it is convenient to use the method of *dimensional regularization* [38–42] which guarantees gauge invariance of the regularized

theory. Further, with regard to the application of the RGE the *mass-independent* renormalization scheme of *minimal subtraction* (MS) [43] and the *modified minimal subtraction* ($\overline{\text{MS}}$) [44] are most adequate.

Dimensional Regularization

The method of dimensional regularization consists in the analytical continuation of the $D = 4$ dimensional space-time to $D = 4 - 2\epsilon$. This requires the generalization of the Dirac algebra to $D \neq 4$ dimensions. Thereby a problem concerning the correct definition of the Dirac matrix γ_5 occurs. Assuming the anitcommutativity of γ_5 with the D dimensional Dirac matrices γ_μ, i.e. the naive dimensional regularization (NDR), will lead to inconsistencies in the evaluation of closed Fermi lines. For example calculations adopting the NDR scheme are not able to reproduce chiral anomalies correctly. Several schemes which consistently define the Dirac algebra have been proposed having in common complicated and tedious algebraic manipulations. For example in the 't Hooft-Veltman (HV) [38, 45, 46] scheme γ_5 anti-commutes with the 4-dimensional parts of the Dirac matrices γ_μ and commutes with the elements of the $(D-4)$ dimensional subspace of the Dirac matrices.

However, in many practical calculations the appearance of Dirac traces containing γ_5 can be avoided. In the special case of $\Delta F = 1$ nonleptonic effective Lagrangian this was shown in [47]. The considerations given there also apply to rare B decays such as $\bar{B} \to X_s\gamma$ and $\bar{B} \to X_s l^+ l^-$ and the NDR scheme will be used.

Renormalization

The procedure of renormalization is based on the idea that the fields and parameters of the Lagrangian are so called *bare* parameters, in the following indicated by the index "B". After having modified the theory with the help of regularization (here dimensional regularization) the bare Green functions expressed in bare fields and parameters are finite, however in the limit of $D \to 4$ or equivalently $\epsilon \to 0$ the original divergent expression will be recovered. In particular, using dimensional regularization it depends on an arbitrary scale parameter μ. This scale parameter has to be introduced by the requirement of a dimensionless coupling and is called *renormalization scale*. The multiplicative renormalization introduces the renormalized fields and parameters and their respective renormalization constants as follows

$$\begin{aligned} g^{\text{B}} &= Z_g g \mu^\epsilon, & m^{\text{B}} &= Z_m m, & \xi^{\text{B}} &= Z_3 \xi, \\ \Psi^{\text{B}} &= \sqrt{Z_2}\Psi, & A_\mu^{a,\text{B}} &= \sqrt{Z_3} A_\mu^a. \end{aligned} \tag{3.15}$$

Here g represents the coupling constants, m masses, ξ gauge parameters, Ψ spin 1/2 fields and A_μ^a gauge fields. The renormalization constants Z_i are free available additional parameters and it is helpful to transform them into *counterterms*

$$\begin{aligned} \mathcal{L}_{\bar{\Psi}\Psi A} &\sim g^{\text{B}} \, [\bar{\Psi}^{\text{B}} \gamma^\mu \mathbf{T}^a \Psi^{\text{B}}] A_\mu^{a,\text{B}} = Z_g Z_2 \sqrt{Z_3} \, \mu^\epsilon g \, [\bar{\Psi}\gamma^\mu \mathbf{T}^a \Psi] A_\mu^a \\ &= \mu^\epsilon g \, [\bar{\Psi}\gamma^\mu \mathbf{T}^a \Psi] A_\mu^a + (Z_g Z_2 \sqrt{Z_3} - 1) \mu^\epsilon g \, [\bar{\Psi}\gamma^\mu \mathbf{T}^a \Psi] A_\mu^a \end{aligned} \tag{3.16}$$

as shown for the $\bar{\Psi}\Psi A_\mu$-coupling above. The first term has the same form as the Lagrangian expressed in bare fields and parameters and reproduces therefore the same result for the regularized Green functions inclusive the divergencies in the limit $\epsilon \to 0$. The same applies to the second term, called "counterterm". However, the renormalization constants Z_i are still arbitrary. Especially they can be chosen in a way that the parts diverging in the limit $\epsilon \to 0$ cancel between the first- and the counterterm. As a result the Green functions become finite depending on the renormalized parameters and the renormalization scale μ. It is essential that all potentially divergent parts cancel since only then the regularization can be removed by the limit $\epsilon \to 0$. Furthermore the renormalization constants Z_i diverge in the limit $\epsilon \to 0$ and depend in general on the renormalized parameters and the renormalization scale μ.

The ambiguity of the renormalization procedure consists in the possibility to change the renormalization constants by arbitrary finite terms. Such terms do not affect the existence of the limit $\epsilon \to 0$ and result in different renormalized fields and parameters. A special choice of the finite terms of the renormalization constants is called *renormalization scheme* implying that renormalized parameters are renormalization-scheme-dependent. In particular physical observables can be calculated in different renormalization schemes and the corresponding renormalized parameters obtained from experiments will be different. The method of renormalization is meaningful for theories which lead to renormalization-scheme-independent relations between physical observables although the parameters of the theory are renormalization-scheme-dependent.

The renormalization procedure yields finite Green functions due to the special choice of the renormalization constants Z_i. In the following the coupling renormalization constant Z_g will be discussed. In practice the application of dimensional regularization and perturbation theory leads to a typical expansion of the renormalization constant of the form

$$Z_g = 1 + g\frac{1}{\epsilon}a_{11} + g^2\Big[\frac{1}{\epsilon}a_{12} + \frac{1}{\epsilon^2}a_{22}\Big] + \ldots\ . = 1 + \sum_{n=1}^{\infty}\frac{a_n(g)}{\epsilon^n} \tag{3.17}$$

The Laurent series in the regulator ϵ clearly shows the divergencies in the limit $\epsilon \to 0$. Of course a redefinition of the renormalized parameters

$$g = g' + b_1(m')\epsilon + b_2(m')\epsilon^2 + \ldots, \tag{3.18}$$

where the coefficients even could depend on additional parameters, indicated by m', would yield the modification

$$Z_{g'} = \sum_{n=1}^{\infty} c'_n(g', m')\epsilon^n + c'_0(g', m') + \sum_{n=1}^{\infty}\frac{a'_n(g', m')}{\epsilon^n} \tag{3.19}$$

and correspond to a change of the renormalization scheme. The special choice of the renormalization constant in (3.17) is called *minimal subtraction* (MS) scheme because here just the divergent parts become subtracted. The coefficients $a_n = a_n(g)$ depend only on the renormalized coupling and implicitly on the renormalization scale μ, but not on mass parameters, referred to as a mass-independent renormalization scheme. The relation between coupling constants in two different schemes can be established with the help of the relation

$$g^{\mathrm{B}} = Z_g g\mu^\epsilon = Z_{g'}g'\mu^\epsilon. \tag{3.20}$$

3.3 The Renormalization Group Equation

The expansion of the bare coupling constant is similar to the expansion of the renormalization constant Z_g. Its concrete form can be obtained from the insertion of (3.17) into (3.15). Therefore it also diverges in the limit $\epsilon \to 0$. However, the bare renormalization constant must not depend on the renormalization scale μ because the μ dependence is introduced when renormalizing g^{B} multiplicatively. The μ independence of g^{B} implies that the μ dependence of the renormalized coupling g and its renormalization constant Z_g must cancel

$$0 = \mu \frac{d}{d\mu} g^{\mathrm{B}} = \mu \frac{d}{d\mu} \Big[\mu^{\epsilon} g(\mu) Z_g(\mu) \Big]. \tag{3.21}$$

Assuming a mass-independent renormalization scheme this leads to the renormalization group equation (RGE) of the renormalized coupling of the following form

$$\mu \frac{d}{d\mu} g = -\epsilon g - g Z_g^{-1} \mu \frac{d}{d\mu} Z_g \equiv -\epsilon g + \beta(g) \equiv \beta(\epsilon, g). \tag{3.22}$$

The function $\beta(g)$ is the *renormalization group function* of the coupling constant. In the MS scheme it takes a very simple form and is given as

$$\beta(g) = g^2 \frac{d\ a_1(g)}{dg} \tag{3.23}$$

using the expansion (3.17). Remarkably only the coefficients of the $1/\epsilon$ poles enter the β-function whereas the coefficient of higher poles in $1/\epsilon$ are determined recursively by the relation

$$g^2 \frac{d\ a_{n+1}}{dg} = \beta(g) \frac{d}{dg} \Big[g\ a_n(g) \Big]. \tag{3.24}$$

The explicite g-dependence of the coefficients a_n can be calculated in perturbation theory.

The RGE establishes a relation between the renormalization scale in the MS scheme when changing the scale μ. This relation is a consequence of the uniqueness of the bare coupling constant as already mentioned above. In other words this implies that a change of the scale μ requires a change of the renormalized coupling in order not to change the renormalization constant Z_g because a change of Z_g would correspond to a change of the renormalization scheme.

For example the β function of the strong coupling constant has the perturbative expansion

$$\beta(g_s) = -g_s^3 \beta_0 - g_s^5 \beta_1 - g_s^7 \beta_2 - \ldots \qquad \beta_0 = 11 - \frac{2}{3} n_f. \tag{3.25}$$

Restricting to the lowest order in perturbation theory only the coefficient β_0 is needed which is given for the MS scheme. Here n_f denotes the number of active quark flavors. The solution of (3.22) in terms of $\alpha_s = g_s^2/4\pi$ relates the strong coupling α_s renormalized in the MS scheme at the scale μ to a different scale μ_0

$$\alpha_s(\mu) = \frac{\alpha_s(\mu_0)}{1 + \frac{\alpha_s(\mu_0)}{4\pi}\beta_0 \ln\frac{\mu^2}{\mu_0^2}}. \tag{3.26}$$

This result explains the increasing of the coupling constant when going to smaller scales leading to the non-perturbative behavior of QCD. For $\mu < \mu_0$ the logarithm has a negative sign whereas the coefficient β_0 is positive for $n_f < 17$. Further the coupling constant decreases in the case $\mu > \mu_0$ resulting in weakly interacting quarks at very high scales. In contrast the leading coefficient β_0^{QED} of the electric coupling constant e is negative justifying the application of perturbation theory also at low energy scales.

To reveal a very important property of RGEs making them attractive for applications, the solution (3.26) will be reexpanded in $\alpha_s(\mu_0)$. Such an reexpansion yields

$$\begin{aligned}\alpha_s(\mu) &= \alpha_s(\mu_0)\Big[1 - \alpha_s(\mu_0)\beta_0 \ln\frac{\mu^2}{\mu_0^2} + \alpha_s(\mu_0)^2\beta_0^2 \ln^2\frac{\mu^2}{\mu_0^2} - \alpha_s(\mu_0)^3\beta_0^3 \ln^3\frac{\mu^2}{\mu_0^2} + \dots\Big] \\ &= \alpha_s(\mu_0)\sum_{n=0}^{\infty}(-1)^n\Big[\alpha_s(\mu_0)\beta_0 \ln\frac{\mu^2}{\mu_0^2}\Big]^n. \end{aligned} \tag{3.27}$$

Apparently, for small changes of the scale $\mu \sim \mu_0$ the logarithm $\ln \mu^2/\mu_0^2$ multiplying $\alpha_s(\mu_0)$ in every term of the expansion with the same power in n is approximately ~ 1 and a truncation of the series will reproduce the exact result of (3.26). However, for very different scales $\mu \ll \mu_0$ or $\mu \gg \mu_0$ the higher order terms in n become more and more relevant. These higher order terms in the coupling constant are included in the exact solution (3.26) of the RGE which can be therefore interpreted as a resummation of large logarithmic terms to all orders in perturbation theory.

The MS scheme yields particularly simple RGE. A very important application is the use of the RGE in effective theories where analogous equations can be derived for the effective couplings considered in (3.14). The perturbative solution of these coupled differential equations can be found in section 5.2.

4 The Minimal Supersymmetric Standard Model

The minimal supersymmetric extension of the SM is called the Minimal Supersymmetric Standard Model (MSSM). In this section the physical particle content and the relevant mass matrices in terms of the fundamental parameters of the MSSM will be introduced. Further details of the MSSM interaction Lagrangian relevant to FCNC B decays as used for the calculation of matching conditions to the initial Wilson coefficients of $\bar{B} \to X_s l^+ l^-$ can be found in Appendix A.

The complexity of the generic MSSM tends to tedious and extensive calculations to obtain general results of higher order corrections. Thus assuming the gluino to be heavy and by further assumptions about the soft supersymmetry breaking parameters, we will restrict to a scenario inspired by minimal flavor violation (MFV). Within this scenario only charged and neutral Higgs particles, charginos and up squarks will contribute to FCNC B decays. Furthermore the effects of the decoupled gluino on the remaining MSSM particle interactions within this scenario will be explained.

4.1 The MSSM Lagrangian

The Minimal Supersymmetric Standard Model (MSSM) is the supersymmetric extension of the SM with minimal particle content and R-parity conservation. The Lagrangian of the MSSM is locally invariant under the SM gauge group (2.1) and further under a global $N = 1$ supersymmetric transformation which requires the existence of one superpartner particle to every SM degree of freedom differing by spin 1/2. Further it is essential to introduce two Higgs doublets with opposite hypercharge $Y = \pm 1$ to obtain an under $N = 1$ supersymmetric transformations invariant and an anomaly free extension of the SM. The electroweak symmetry $SU(2)_W \otimes U(1)_Y$ will be broken analogously to the SM to the $U(1)_{\text{em}}$ with the help of the Higgs mechanism.

The SM particles and their superpartners are organized in supermultiplets having identical quantum numbers and differing by spin 1/2. Since the quantum numbers fix the gauge interactions within exact supersymmetry no new parameters will be introduced except for the Higgs sector being extended compared to the SM. However, here the supersymmetry restricts the form of the Higgs potential to just one parameter μ appearing as the Higgs coupling in the superpotential. Therefore exact supersymmetry reduces the number of parameters by one compared to the SM.

The invariance under the supersymmetric transformation implies that SM particles and their corresponding superpartners will have the same mass. However, so far no experimental evidence of these superpartners has been found, which strongly indicates that supersymmetry

must be broken if realized in nature at energy scales currently accessible to particle physics experiments. To be viable *soft supersymmetry breaking* terms have to be added to the MSSM Lagrangian. These terms introduce about 100 additional parameters. The characteristic mass scale M_{soft} of these parameters determines the mass splitting between the known SM particles and their superpartners and should not be much larger than $10^3\,\text{GeV}$. Otherwise, the successful solution to the hierarchy problem becomes lost since the M^2_{soft} corrections to the Higgs (mass)^2 would be unnaturally large compared to the electroweak breaking scale of 174 GeV.

The superpotential of the MSSM is chosen to respect conservation laws such as baryon and lepton number conservation as in the SM. This is achieved by the postulation of the existence of a multiplicative quantum number P_R called R-parity. The corresponding symmetry is a discrete Z_2 symmetry. R-parity is given in terms of the baryon number B, the lepton number L and the spin s

$$P_R = (-1)^{3(B-L)+2s}. \tag{4.1}$$

SM particles and the Higgs bosons have even R-parity ($P_R = +1$), while all of their superpartners differing by spin 1/2 have odd R-parity ($P_R = -1$). The interactions of the MSSM conserve R-parity yielding +1. As a consequence the superpartners of the SM particles can only be produced in pairs and the lightest supersymmetric particle (LSP) is stable. The existence of the LSP in the MSSM provides for example a good candidate for the cold dark matter of the universe.

The construction of the supersymmetric Lagrangian, the form of the soft supersymmetry breaking terms, the electroweak symmetry breaking, the gauge fixing and the resulting physical spectrum of mass eigenstates inclusive the Feynman rules describing their interaction can be found in [48–51].

In the following we will present the physical particle spectrum of the MSSM, but will follow a slightly modified notation than the one given in [48–51].

The Higgs Sector

Contrary to the SM in the MSSM it is essential to introduce two Higgs supermultiplets to give all fermions masses when breaking spontaneously the electroweak symmetry. As a consequence the physical Higgs spectrum of the MSSM is enlarged. It consists of the CP-even Higgs fields h^0 and H^0, one CP-odd Higgs field A^0 and two charged Higgs fields $H^\pm$. The masses and mixing angles of the Higgs sector obey the following tree–level relations

$$M^2_{A^0} = M^2_H - M^2_W, \tag{4.2a}$$

$$M^2_{h^0,H^0} = \frac{1}{2}\left\{ M^2_{A^0} + M^2_Z \mp \sqrt{(M^2_{A^0} + M^2_Z)^2 - 4M^2_Z M^2_{A^0} \cos^2 2\beta} \right\}, \tag{4.2b}$$

$$\sin 2\alpha = -\sin 2\beta \left(\frac{M^2_{H^0} + M^2_{h^0}}{M^2_{H^0} - M^2_{h^0}} \right), \tag{4.2c}$$

where M_H and M_{A^0} are the masses of the charged and CP-odd Higgs boson, respectively, and M_{h^0,H^0} and α are the masses and mixing angle in the CP-even Higgs sector. At tree–level

the Higgs sector of the MSSM is described by the two free parameters chosen to be $\tan\beta$ and M_H. The parameter $\tan\beta$ is given by the ratio v_2/v_1 of the VEV's of the two scalar Higgs doublets that they acquire to break the electroweak symmetry spontaneously. The use of tree–level relations is quite adequate when considering B decays at leading order in electroweak couplings and evaluating only strong corrections to these processes.

The Chargino Sector

The charginos are the mass eigenstates resulting from the mixing of the charged higgsinos (the superpartners of the charged scalar Higgs fields) and the charged winos (superpartners of the $SU(2)_W$ gauge bosons – the "gauginos"). The chargino mass matrix is given by

$$M_{\tilde{\chi}} = \begin{pmatrix} M_2 & \sqrt{2}M_W \sin\beta \\ \sqrt{2}M_W \cos\beta & \mu \end{pmatrix}. \tag{4.3}$$

Here μ is the parameter of the Higgs coupling in the superpotential and M_2 the Wino soft supersymmetry breaking mass parameter. This matrix can be cast in diagonal form by means of a biunitary transformation

$$U^* M_{\tilde{\chi}} V^\dagger = \mathrm{diag}(M_{\tilde{\chi}_1}, M_{\tilde{\chi}_2}), \tag{4.4}$$

$M_{\tilde{\chi}_{1,2}}$ being the chargino masses with $M_{\tilde{\chi}_1} < M_{\tilde{\chi}_2}$.

The Neutralino Sector

The mass eigenstates originating from the mixing of the neutral higgsinos (the superpartners of the neutral scalar Higgs fields) and the neutral wino and bino (superpartners of the neutral $SU(2)_W$ and $U(1)_Y$ gauge boson, respectively) are called neutralinos. The neutralino mass matrix

$$M_{\tilde{\chi}^0} = \begin{pmatrix} M_1 & 0 & -M_Z s_W \cos\beta & M_Z s_W \sin\beta \\ 0 & M_2 & M_Z c_W \cos\beta & -M_Z c_W \sin\beta \\ -M_Z s_W \cos\beta & M_Z c_W \cos\beta & 0 & -\mu \\ M_Z s_W \sin\beta & -M_Z c_W \sin\beta & -\mu & 0 \end{pmatrix}, \tag{4.5}$$

is symmetric and can be diagonalized by the orthogonal matrix N

$$N^* M_{\tilde{\chi}^0} N^\dagger = \mathrm{diag}(M_{\tilde{\chi}^0_1}, M_{\tilde{\chi}^0_2}, M_{\tilde{\chi}^0_3}, M_{\tilde{\chi}^0_4}) \tag{4.6}$$

with $M_{\tilde{\chi}^0_1} < M_{\tilde{\chi}^0_2} < M_{\tilde{\chi}^0_3} < M_{\tilde{\chi}^0_4}$. Here M_1 is the bino soft supersymmetry breaking mass parameter and s_W and c_W are the sine and cosine of the Weinberg angle, respectively.

The Gluino Sector

The superpartners of the $SU(3)_C$ gauge bosons are called gluinos, which do not mix. They are the only color octet fermions in the MSSM and form eight Majorana spinors in the

four component notation. Their common mass $|M_3|$ originates from the soft supersymmetry breaking part of the MSSM Lagrangian.

The Squark Sector

The squarks (scalar quarks) are the scalar partners of the quarks in the chiral supermultiplets. Their 6×6 mass-squared matrix will be given in the super-CKM basis [51], in which the quark mass matrices are diagonal and both quarks and squarks are rotated simultaneously. For the up-squarks $(\tilde{u}_L, \tilde{c}_L, \tilde{t}_L, \tilde{u}_R, \tilde{c}_R, \tilde{t}_R)$ and down-squarks $(\tilde{d}_L, \tilde{s}_L, \tilde{b}_L, \tilde{d}_R, \tilde{s}_R, \tilde{b}_R)$ this yields

$$M^2_{\tilde{u}} = \begin{pmatrix} M^2_{U_{LL}} & M^2_{U_{LR}} \\ M^{2\dagger}_{U_{LR}} & M^2_{U_{RR}} \end{pmatrix}, \qquad M^2_{\tilde{d}} = \begin{pmatrix} M^2_{D_{LL}} & M^2_{D_{LR}} \\ M^{2\dagger}_{D_{LR}} & M^2_{D_{RR}} \end{pmatrix}, \tag{4.7}$$

where the 3×3 submatrices are given by

$$M^2_{U_{LL}} = M^2_{\tilde{U}_L} + M^2_U + \frac{1}{6} M^2_Z \cos 2\beta (3 - 4s^2_W)\mathbf{1}, \tag{4.8a}$$

$$M^2_{U_{LR}} = M_U (A^*_U - \mu \cot \beta \mathbf{1}), \tag{4.8b}$$

$$M^2_{U_{RR}} = M^2_{\tilde{U}_R} + M^2_U + \frac{2}{3} M^2_Z \cos 2\beta s^2_W \mathbf{1}, \tag{4.8c}$$

$$M^2_{D_{LL}} = M^2_{\tilde{D}_L} + M^2_D - \frac{1}{6} M^2_Z \cos 2\beta (3 - 2s^2_W)\mathbf{1}, \tag{4.9a}$$

$$M^2_{D_{LR}} = M_D (A^*_D - \mu \tan \beta \mathbf{1}), \tag{4.9b}$$

$$M^2_{D_{RR}} = M^2_{\tilde{D}_R} + M^2_D - \frac{1}{3} M^2_Z \cos 2\beta s^2_W \mathbf{1}. \tag{4.9c}$$

$\mathbf{1}$ denotes the 3×3 unit matrix. A_U and A_D are the soft supersymmetry breaking trilinear couplings of the squark and Higgs fields which can be arbitrary complex. $M^2_{\tilde{U}_{L,R}}$ and $M^2_{\tilde{D}_{L,R}}$ are the soft supersymmetry breaking squark mass-squared matrices which have to be hermitian so that the Lagrangian is real. Due to the $SU(2)_W$ gauge invariance of the soft supersymmetry breaking part of the MSSM Lagrangian these matrices are connected by the CKM matrix

$$M^2_{\tilde{D}_L} = V^\dagger_{\mathrm{CKM}} M^2_{\tilde{U}_L} V_{\mathrm{CKM}}. \tag{4.10}$$

The matrices $M^2_{\tilde{u}}$ and $M^2_{\tilde{d}}$ are diagonalized by unitary squark field redefinitions (the squark mixing matrices Γ^U and Γ^D) yielding the mass eigenstate basis of the squarks

$$\Gamma^U M^2_{\tilde{u}} \Gamma^{U\dagger} = \mathrm{diag}(m^2_{\tilde{u}_1}, \ldots, m^2_{\tilde{u}_6}), \qquad \Gamma^D M^2_{\tilde{d}} \Gamma^{D\dagger} = \mathrm{diag}(m^2_{\tilde{d}_1}, \ldots, m^2_{\tilde{d}_6}). \tag{4.11}$$

For later use it is convenient to define the 6×3 submatrices

$$(\Gamma^{U_L})_{ai} = (\Gamma^U)_{ai}, \qquad (\Gamma^{U_R})_{ai} = (\Gamma^U)_{a,i+3}, \tag{4.12a}$$

$$(\Gamma^{D_L})_{ai} = (\Gamma^D)_{ai}, \qquad (\Gamma^{D_R})_{ai} = (\Gamma^D)_{a,i+3}, \tag{4.12b}$$

where i runs over 1, 2, 3.

The Slepton Sector

The sleptons (scalar leptons) are the superpartners of the leptons in the chiral supermultiplet whereas the scalar superpartners of the neutrinos are called sneutrinos (scalar neutrinos). The 6×6 and the 3×3 mass-squared matrices of the sleptons and the sneutrinos in the super-CKM basis are

$$M_{\tilde{l}}^2 = \begin{pmatrix} M_{E_{LL}}^2 & M_{E_{LR}}^2 \\ M_{E_{LR}}^{2\dagger} & M_{E_{RR}}^2 \end{pmatrix}, \qquad M_{\tilde{\nu}}^2 = \left(M_{\tilde{L}_L}^2 + \frac{1}{2} M_Z^2 \cos 2\beta \mathbf{1} \right), \tag{4.13}$$

where the 3×3 submatrices are given by

$$M_{E_{LL}}^2 = M_{\tilde{L}_L}^2 + M_E^2 - \frac{1}{2} M_Z^2 \cos 2\beta (1 - 2s_W^2)\mathbf{1}, \tag{4.14a}$$

$$M_{E_{LR}}^2 = M_E (A_E^* - \mu \tan\beta \mathbf{1}), \tag{4.14b}$$

$$M_{E_{RR}}^2 = M_{\tilde{L}_R}^2 + M_E^2 - M_Z^2 \cos 2\beta s_W^2 \mathbf{1}. \tag{4.14c}$$

Again $\mathbf{1}$ denotes the 3×3 unit matrix. A_E is the soft supersymmetry breaking trilinear coupling of the slepton and Higgs fields and $M_{\tilde{L}_{L,R}}^2$ are the soft supersymmetry breaking squark mass-squared matrices. Similarly to the squark mixing matrices we define the slepton and sneutrino mixing matrices

$$\Gamma^E M_{\tilde{l}}^2 \Gamma^{E\dagger} = \mathrm{diag}(m_{\tilde{l}_1}^2, \ldots, m_{\tilde{l}_6}^2), \qquad \Gamma^N M_{\tilde{\nu}}^2 \Gamma^{N\dagger} = \mathrm{diag}(m_{\tilde{\nu}_1}^2, m_{\tilde{\nu}_2}^2, m_{\tilde{\nu}_3}^2), \tag{4.15}$$

which yield the mass eigenstates of sleptons and sneutrinos. As before we introduce the 6×3 submatrices for the sleptons, Γ^E and Γ^N

$$(\Gamma^{E_L})_{ai} = (\Gamma^E)_{ai}, \qquad (\Gamma^{E_R})_{ai} = (\Gamma^E)_{a,i+3}. \tag{4.16}$$

Flavor-changing Interactions

The parts of the MSSM interactions relevant to FCNC B decays are

- $u - d - H^{\pm}$: up-quark – down-quark – charged Higgs,

- $\tilde{u} - d - \tilde{\chi}^{\pm}$: up-squark – down-quark – chargino,
- $\tilde{d} - d - \tilde{\chi}^{0}$: down-squark – down-quark – neutralino,
- $\tilde{d} - d - \tilde{g}$: down-squark – down-quark – gluino,

and their explicit form can be found in Appendix A. In the following the impact of the four listed flavor-changing interactions are discussed.

The discussion will be restricted to $\Delta B = 1$ FCNC decays such as for example $\bar{B} \to X_s\gamma$, $\bar{B} \to X_s l^+ l^-$ or $\bar{B} \to X_s \nu\bar{\nu}$, however similar results can be obtained for $\Delta B = 2$ decays. $\Delta B = 1$ FCNC processes are characterized by the quark level transitions $b \to q$ with $q = \{d, s\}$. In the SM they are mediated at leading order in electroweak interactions via virtual "up-quark – W boson" states. Due to the dependence of the $u - d - W$ vertex on the CKM matrix elements, the amplitude of such a process has the generic form

$$\mathcal{A}(b \to q) = V_{uq}^* V_{ub}\, \mathcal{A}_u^W + V_{cq}^* V_{cb}\, \mathcal{A}_c^W + V_{tq}^* V_{tb}\, \mathcal{A}_t^W = \sum_{i=\{u,c,t\}} V_{iq}^* V_{ib}\, \mathcal{A}_i^W \tag{4.17}$$

with $\mathcal{A}_i^W = \mathcal{A}_i^W(M_W, m_i)$ being a function of the up-quark and the W boson masses[1]. The contribution due to the $u - d - H^{\pm}$ vertex is similar to the SM $u - d - W$ vertex, as can be seen from the explicit form given in Appendix A. The above equation extends to

$$\mathcal{A}(b \to q) = \sum_{i=\{u,c,t\}} V_{iq}^* V_{ib}\, \left(\mathcal{A}_i^W + \mathcal{A}_i^H\right), \tag{4.18}$$

where $\mathcal{A}_i^H = \mathcal{A}_i^H(M_W, m_i, M_H, \tan\beta)$ depends additionally on the charged Higgs mass and the parameter $\tan\beta$. In the SM and the charged Higgs sector of the MSSM the sum over the virtual states has to be performed over the three up-quarks u, c and t, whereas the "mixing angles" are represented by the CKM matrix elements. In the limit of equal quark masses $m_u = m_c = m_t \equiv m$ the unitarity of the CKM matrix[2] would imply

$$\mathcal{A}(b \to q) = \left(\mathcal{A}^W + \mathcal{A}^H\right) \sum_{i=\{u,c,t\}} V_{iq}^* V_{ib} \to 0 \tag{4.19}$$

vanishing FCNC amplitudes.

The situation becomes more complex when the supersymmetric partners are considered, contributing via virtual "gaugino/higgsino – squark"[3] states. In contrast to the SM and the charged Higgs contributions now the sum over the virtual states has to be performed over a large number of particles. The "mixing angles", namely the matrices U, V of the chargino sector, N of the neutralino sector, Γ^U, Γ^D of the squark sector and Γ^E, Γ^N of the slepton sector, take a complicated functional dependence on the fundamental parameters

[1] These functions can also depend on the lepton masses for example in the process $\bar{B} \to X_s\nu\bar{\nu}$ appearing in box-diagrams, however in practical calculations terms proportional to lepton masses are negligible. The discussion could be extended by applying the same arguments to these terms as well.

[2] Apart of the unitarity of V_{CKM} further $V_{\mathrm{CKM}} \to 1$ in the limit of degenerated quark masses.

[3] As already noticed before also virtual lepton states can contribute to B decays implying that their supersymmetric partners, the sleptons, contribute as well.

of the MSSM, especially the soft supersymmetry breaking parameters. In particular these parameters can play a special role for FCNC decays. For example in [52,53] it was shown that in the absence of soft supersymmetry breaking terms, in other words when supersymmetry becomes restored at high energies, the FCNC process $\bar{B} \to X_s\gamma$ vanishes. This implies, if supersymmetry is realized in nature then the observed branching ratio of $\bar{B} \to X_s\gamma$ is sensitive to the soft supersymmetry breaking parameters. In general the amplitudes of FCNC processes take a complicated form, not allowing for a simple discussion as in the SM or charged Higgs case. The explicit one loop results relevant to the B decays can be found for example in [54, 55].

In the next section we will present a minimal flavor violation inspired scenario. There the mixing matrices of down-squarks will be chosen not in the general form of the MSSM but flavor diagonal causing a vanishing contribution due to neutralinos and gluinos to FCNC B decays at leading order in electroweak coupling constants.

4.2 MSSM with MFV and Gluino Decoupling

In this section we describe the main assumptions leading to the considered supersymmetric scenario underlying the calculations, a scenario inspired by *minimal flavor violation* (MFV) and the heavy gluino effective theory describing the MSSM degrees of freedom with decoupled gluino.

Minimal Flavor Violation

The scenario of minimal flavor violation was inspired by model independent investigations of FCNC B decays [59–64] in the framework of effective theories. Here *model independent* is understood independently of a particular specified full theory that generates the effective Lagrangian describing B decays. A general model independent analysis should include all possible operators into the effective theory Lagrangian allowed by symmetries. However, this usually leads to a loss of predictive power and therefore as a starting point such analysis usually employ the SM effective Lagrangian. A necessary precondition of such investigations is that the not specified extensions of the SM, would generate the same effective Lagrangian. More concrete this means that the relevant operators are the same as in the SM implying that Wilson coefficients of additional operators are zero or at least strongly suppressed compared to the SM Wilson coefficients and hence negligible. In such a case the impact of new physics (NP) to the theoretical expressions of physical observables in addition to the SM can be added by the simple reparametrization of the Wilson coefficients of the SM $C^{\rm SM} \to C^{\rm SM} + C^{\rm NP}$. The model independent analysis of physical observables with experimental data in the absence of new operators becomes considerably simpler and provides bounds on the magnitude of $C^{\rm NP}$ and in turn on the parameter spaces of the NP models.

Model-independent analysis of the CKM matrix with the help of the unitarity triangle also depend strongly on new flavor violating interactions when considering extensions of the SM. Assuming that no additional flavor violating couplings occur in the considered new physics scenarios and that FCNC processes are entirely governed by the CKM matrix allow the application of the SM unitarity triangle analysis. This further assumption guarantees the same CKM-dependence of $C^{\rm NP}$ as in the SM and is called minimal flavor violation. Under such conditions for example the construction of a universal unitarity triangle [65] is possible.

The general MSSM does not fulfill either assumptions. Integrating out the heavy particles i.e. the heavy gauge bosons, Higgs particles and supersymmetric partners will yield additional operators in the effective Lagrangian. Furthermore the soft supersymmetry breaking terms contain additional sources of flavor violating interactions contributing also to FCNC B decays. This raises the question how the structure of the MSSM parameters – especially the soft supersymmetry breaking terms – should be constrained to fall under the class of one or both of the introduced assumptions. The restriction of the general form of the MSSM parameters in order to fulfill certain assumptions will be referred to as a *scenario in the context of the MSSM*. No conclusive answer can be given to these questions.

To prevent the generation of new operators contributing to FCNC B decays due to Higgs mediation the value of $\tan\beta$ should be small [66–72]. Apart from the generation of new operators high values of $\tan\beta$ also induce large radiative corrections at higher orders which should be included besides the here considered QCD corrections. It has been shown that these corrections can be substantial once taken into account in the framework of effective theories [68, 69, 71–74]. Thereby a mass hierarchy of the MSSM was assumed in which all supersymmetric partners are much heavier than the Higgs bosons and the SM particles. In a first step the superpartners were integrated out yielding the SM with an extended Higgs sector as an effective theory containing the effects of higher order corrections due to $\tan\beta$ in effective couplings. In a second step the remaining heavy SM and Higgs particles were integrated out leaving as dynamical degrees of freedom the light quarks, the leptons and their QCD×QED interactions. In view of these complications throughout small values of $\tan\beta$ in the range

$$2 \lesssim \tan\beta \lesssim 5 \tag{4.20}$$

will be used.

The scenario of minimal flavor violation underlies the wish that FCNC B decays, but also all other flavor-changing decays, are exclusively governed by the CKM matrix. Concerning the neutralino and gluino interactions contributing to FCNC B decays [see (A.3)] it should be noted, that they are completely governed by soft supersymmetry breaking parameters. For example the coupling of left-handed down-quarks to down-squarks and gluinos is

$$\sim \overline{\tilde{g}_a}\, \tilde{d}_i^{\dagger}\, [\Gamma^{D_L}]_{ij} \mathbf{T}^a\, d_L^j \tag{4.21}$$

with $i = 1, \ldots, 6$ and $j = 1, 2, 3$, mixing the flavors of quarks and squarks arbitrarily. The matrix Γ^{D_L} is determined diagonalizing the 6×6 mass-squared matrix of the down-squarks $M_{\tilde{d}}^2$ in (4.7). However, no flavor mixing occurs in the special case of a flavor diagonal mixing matrix Γ^D. In turn for example the transition $(b \to \tilde{g}_a \tilde{b}_1)$ is nonzero whereas the transition $(\tilde{g}_a \tilde{b}_1 \to s)$ becomes zero and hence no contribution to FCNC down-quark transitions such as $(b \to s)$ can arise. The same applies to the couplings of right-handed down-quarks to down-squarks and gluinos and furthermore to the "down-quark – down-squark – neutralino" couplings.

The mixing matrix Γ^D will be flavor diagonal if $M_{\tilde{d}}^2$ itself possesses a block diagonal structure with respect to the four 3×3 submatrices shown in (4.7). Only if this requirement is fulfilled the neutralino and gluino interactions will match into the MFV assumption. The block diagonal structure of $M_{\tilde{d}}^2$ implies that

$$A_D \equiv \mathrm{diag}(A_d,\, A_s,\, A_b), \tag{4.22}$$

$$M^2_{\tilde{D}_L} \equiv \mathrm{diag}(m^2_{\tilde{d}_L},\, m^2_{\tilde{s}_L},\, m^2_{\tilde{b}_L}) \qquad M^2_{\tilde{D}_R} \equiv \mathrm{diag}(m^2_{\tilde{d}_R},\, m^2_{\tilde{s}_R},\, m^2_{\tilde{b}_R})$$

are diagonal matrices.

To avoid flavor violation beyond the CKM matrix in FCNC up-quark transitions as for example $(t \to c)$ due to neutralino and gluino interactions the above extends to the up-squark sector where the following matrices

$$A_U \equiv \mathrm{diag}(A_u,\, A_c,\, A_t), \tag{4.23}$$

$$M^2_{\tilde{U}_L} \equiv \mathrm{diag}(m^2_{\tilde{u}_L},\, m^2_{\tilde{c}_L},\, m^2_{\tilde{t}_L R}) \qquad M^2_{\tilde{U}_R} \equiv \mathrm{diag}(m^2_{\tilde{u}_R},\, m^2_{\tilde{c}_R},\, m^2_{\tilde{t}_R})$$

have to be diagonal.

Finally the $SU(2)_W$ gauge invariance requires relation (4.10) to hold which restricts the matrices $M^2_{\tilde{U}_L}$ and $M^2_{\tilde{D}_L}$ to be equal and proportional to the 3×3 unit matrix

$$M^2_{\tilde{U}_L} = M^2_{\tilde{D}_L} \equiv m^2_{\tilde{q}_L} \mathbf{1}. \tag{4.24}$$

The above considerations restrict the general form of the soft supersymmetry breaking parameters severely. There are no contributions to flavor-changing quark transitions from neutralino and gluino interactions. The same does not apply to chargino interactions as can be seen from (A.3) and (A.4). For example the coupling of right-handed down-quarks to up-squarks and charginos has the form

$$\sim \frac{g_2}{\sqrt{2} M_W \cos\beta}\, \overline{\tilde{\chi}^-_i}\, \tilde{u}^\dagger_a \, \left(U_{i2} [\Gamma^{U_L}]_{ab} [V_{\mathrm{CKM}}]_{bc} [M_D]_{cc} \right) d^c_L \tag{4.25}$$

with $a = 1, \ldots, 6$ and $b, c = 1, 2, 3$. Here the off-diagonal entries of the CKM matrix allow for flavor-changing transitions such as $(b \to \tilde{u}_1 \tilde{\chi}^-)$ followed by $(\tilde{u}_1 \tilde{\chi}^- \to s)$ and hence for example FCNC transitions such as $(b \to s)$ are mediated by virtual "up-squark – chargino" states. The flavor-changing interaction is governed by the CKM matrix coinciding with the idea of minimal flavor violation.

Gluino Decoupling

The consideration of QCD corrections to B decays in the MSSM includes gluon and gluino corrections. Within perturbation theory the evaluation of two loop diagrams containing gluinos as QCD corrections will tend to rather lengthy results. Further it would require the consideration of additional four-quark operators[4] generated by gluino exchange which mix under the renormalization group evolution into the operators already present in the SM operator basis. To avoid the necessity to take into account two loop diagrams containing

[4] A leading order analysis of the decay $\bar{B} \to X_s \gamma$ was performed in [56] including gluino induced four-quark operators.

gluinos and to consider a larger operator basis it is useful to assume in a first step the gluino to be heavier than all the other particles i.e. assuming the mass hierarchy

$$\mu_{\tilde{g}} \sim \mathcal{O}(M_{\tilde{g}}) \quad \gg \quad \mu_W \sim \mathcal{O}(M_W, m_t, M_H, M_{\tilde{\chi}^\pm}, m_{\tilde{u}}) \quad \gg \quad m_b \quad \gg \quad \Lambda_{\rm QCD}. \tag{4.26}$$

Due to this mass hierarchy a successive construction of effective field theories is possible. In the first step the gluino will be integrated out resulting in an effective theory of the remaining supersymmetric particles – the "effective MSSM". Thereby neglecting all the $1/M_{\tilde{g}}$ effects the "down-quark – up-squark – chargino" couplings $X^{U_{L,R}}$ [see (A.3) and (A.4)] become changed. The result within the "effective MSSM" renormalized in the $\overline{\rm MS}$ scheme using NDR is given as follows

$$X_i^{U_L} = -g_2 \left[a_g V_{i1}^* \Gamma^{U_L} - a_Y V_{i2}^* \Gamma^{U_R} \frac{M_U}{\sqrt{2} M_W \sin\beta} \right] V_{\rm CKM}, \tag{4.27}$$

$$X_i^{U_R} = g_2 \, a_Y \, U_{i2} \Gamma^{U_L} V_{\rm CKM} \frac{M_D}{\sqrt{2} M_W \cos\beta}. \tag{4.28}$$

The effect of the decoupled gluino, with mass $M_{\tilde{g}}$, is contained in the functions a_g and a_Y [57], which are given by

$$a_g = 1 - \frac{\alpha_s(\mu)}{4\pi} \left[\frac{7}{3} + 2 \ln \left(\frac{\mu^2}{M_{\tilde{g}}^2} \right) \right], \qquad a_Y = 1 + \frac{\alpha_s(\mu)}{4\pi} \left[1 + 2 \ln \left(\frac{\mu^2}{M_{\tilde{g}}^2} \right) \right], \tag{4.29}$$

and μ being the matching scale.

This approach limits the validity of the results with respect to the parameter space of the general MSSM, nevertheless it is interesting to compute the QCD corrections to $\bar{B} \to X_s l^+ l^-$ within this restricted setup and to investigate their size. Indeed similar analysis of the inclusive decay $\bar{B} \to X_s \gamma$ [57, 58] have shown that QCD corrections can be of the magnitude of the current experimental uncertainty. Once the experimental situation improves the inclusion of these corrections will be essential also in $\bar{B} \to X_s l^+ l^-$ when performing scans over the MSSM parameter space. The reliability of constraints derived from such scans depends crucially on theoretical uncertainties due to higher order corrections. The numerical analysis will demonstrate the improvement of theoretical predictions within the SM and the considered MSSM scenario.

5 $\bar{B} \to X_s l^+ l^-$

The rare B decays mediated at the parton level by the transition $b \to s l^+ l^-$ $(l = \mu, e)$ provide a sensitive probe of flavor dynamics, the least tested sector of the SM. As loop induced flavor-changing neutral current (FCNC) processes they are also sensitive to possible effects of new physics at the electroweak scale. The experimental situation of these rare B decay modes seems promising as they are in the reach of the present B physics experiments BELLE [75] at KEK and BaBar [76] at SLAC. Both succeeded recently to observe for the first time some *exclusive* channels. A complete list of the status of the individual exclusive channels can be found in Table 5.1.

About one year ago the BELLE Collaboration has also reported the first measurement of the branching fraction of the *inclusive* decay mode $\bar{B} \to X_s l^+ l^-$ combined from the two channels $\bar{B} \to X_s e^+ e^-$ and $\bar{B} \to X_s \mu^+ \mu^-$ [17]

$$\begin{aligned}
\mathcal{B}[\bar{B} \to X_s e^+ e^-] &= \left(5.0 \pm 2.3^{+1.3}_{-1.1}\right) \times 10^{-6}, \qquad (3.4\sigma) \\
\mathcal{B}[\bar{B} \to X_s \mu^+ \mu^-] &= \left(7.9 \pm 2.1^{+2.1}_{-1.5}\right) \times 10^{-6}, \qquad (4.7\sigma) \\
\mathcal{B}[\bar{B} \to X_s l^+ l^-] &= \left(6.1 \pm 1.4^{+1.4}_{-1.1}\right) \times 10^{-6}, \qquad (5.4\sigma)
\end{aligned} \tag{5.1}$$

for dilepton masses bigger than 0.2 GeV/c^2. Very recently similar preliminary results were reported also by the Babar Collaboration [18]

$$\begin{aligned}
\mathcal{B}[\bar{B} \to X_s e^+ e^-] &= \left(6.6 \pm 1.9^{+1.9}_{-1.6}\right) \times 10^{-6}, \qquad (4.0\sigma) \\
\mathcal{B}[\bar{B} \to X_s \mu^+ \mu^-] &= \left(5.7 \pm 2.8^{+1.7}_{-1.4}\right) \times 10^{-6}, \qquad (2.2\sigma) \\
\mathcal{B}[\bar{B} \to X_s l^+ l^-] &= \left(6.3 \pm 1.6^{+1.8}_{-1.5}\right) \times 10^{-6}. \qquad (4.6\sigma)
\end{aligned} \tag{5.2}$$

The numbers in brackets in (5.1) and (5.2) are the statistical significance of the respective decay channel whereas the quoted errors of these results are the statistical and systematical, respectively. The systematic error also includes uncertainties from modeling signal decays with the help of theoretical models.

The experimental results of the decays $\bar{B} \to X_s l^+ l^-$ promise to yield much needed information complementary to that from other sources such as $\bar{B} \to X_s \gamma$, $\bar{B} \to X_s \nu \bar{\nu}$, $B\bar{B}$ – mixing, CP violation and rare K decays. A substantial further improvement of the accuracy of the results from BELLE and BaBar is expected in the forthcoming future.

The special interest in *inclusive* rare decays such as $\bar{B} \to X_s \gamma$, $\bar{B} \to X_s l^+ l^-$ and $\bar{B} \to X_s \nu \bar{\nu}$ is governed by the fact that their theoretical treatment is fairly well under control. In particular the rate for $\bar{B} \to X_s l^+ l^-$ is dominated, in the region of the dilepton

Decay mode	Belle Collaboration $\mathcal{B} \times 10^6$	St.Sig.	BaBar Collaboration $\mathcal{B} \times 10^6$	St.Sig.
$\bar{B}^0 \to K^0 e^+ e^-$	< 0.5	90%C.L.	$-0.21^{+0.23}_{-0.16} \pm 0.08$	$< 3\sigma$
$\bar{B}^+ \to K^+ e^+ e^-$	$0.63^{+0.19}_{-0.17} \pm 0.03 \pm 0.03$	5.1σ	$1.05^{+0.25}_{-0.22} \pm 0.07$	8.4σ
$\bar{B} \to K e^+ e^-$	$0.48^{+0.15}_{-0.13} \pm 0.03 \pm 0.01$	4.6σ	$0.74^{+0.18}_{-0.16} \pm 0.05$	7.8σ
$\bar{B}^0 \to K^{*0} e^+ e^-$	$1.29^{+0.57+0.12}_{-0.49-0.09} \pm 0.04$	$< 3\sigma$	$1.11^{+0.56}_{-0.47} \pm 0.11$	$< 3\sigma$
$\bar{B}^+ \to K^{*+} e^+ e^-$	$2.02^{+1.27+0.22}_{-1.01-0.23} \pm 0.07$	$< 3\sigma$	$0.20^{+1.34}_{-0.87} \pm 0.28$	$< 3\sigma$
$\bar{B} \to K^* e^+ e^-$	$1.49^{+0.52+0.11}_{-0.46-0.13} \pm 0.03$	3.6σ	$0.98^{+0.50}_{-0.42} \pm 0.11$	$< 3\sigma$
$\bar{B}^0 \to K^0 \mu^+ \mu^-$	$0.56^{+0.29}_{-0.23} \pm 0.04 \pm 0.03$	3.1σ	$1.63^{+0.82}_{-0.63} \pm 0.14$	4.1σ
$\bar{B}^+ \to K^+ \mu^+ \mu^-$	$0.45^{+0.14}_{-0.12} \pm 0.03 \pm 0.01$	4.6σ	$0.07^{+0.19}_{-0.11} \pm 0.02$	$< 3\sigma$
$\bar{B} \to K \mu^+ \mu^-$	$0.48^{+0.12}_{-0.11} \pm 0.03 \pm 0.02$	5.6σ	$0.45^{+0.23}_{-0.19} \pm 0.04$	$< 3\sigma$
$\bar{B}^0 \to K^{*0} \mu^+ \mu^-$	$1.33^{+0.42}_{-0.37} \pm 0.09 \pm 0.06$	4.4σ	$0.86^{+0.79}_{-0.58} \pm 0.11$	$< 3\sigma$
$\bar{B}^+ \to K^{*+} \mu^+ \mu^-$	< 1.8	90%C.L.	$3.07^{+2.58}_{-1.78} \pm 0.42$	$< 3\sigma$
$\bar{B} \to K^* \mu^+ \mu^-$	$1.17^{+0.36}_{-0.31} \pm 0.08 \pm 0.06$	4.4σ	$1.27^{+0.76}_{-0.61} \pm 0.16$	$< 3\sigma$
$\bar{B} \to K l^+ l^-$	$0.48^{+0.10}_{-0.09} \pm 0.03 \pm 0.01$	7.4σ	$0.65^{+0.14}_{-0.13} \pm 0.04$	8.4σ
$\bar{B} \to K^* l^+ l^-$	$1.15^{+0.26}_{-0.24} \pm 0.07 \pm 0.04$	5.9σ	$0.88^{+0.33}_{-0.29} \pm 0.10$	3.3σ

Table 5.1: Results of the measurement of branching ratios and the corresponding statistical significance of the exclusive channels by the BELLE [77] and BaBar [78] experiment. The first and the second error are the statistical and systematic error, respectively. The third error corresponds to the model dependence.

invariant mass $s \equiv q^2 = (p_{l^-} + p_{l^+})^2$ away from resonance backgrounds, by perturbatively calculable contributions. Within the heavy quark expansion (HQE) formalism it can be formally justified that the free b quark decay emerges as the leading contribution to $\bar{B} \to X_s l^+ l^-$ and furthermore power corrections of the form $(\Lambda_{\rm QCD}/m_b)^n$ and $(\Lambda_{\rm QCD}/m_c)^n$ can be systematically treated within the HQE framework.

This chapter is devoted to the presentation of the current status of the perturbatively calculable contributions within the SM and the scenario of the MSSM as outlined in section 4.2. So far this program was performed up to the NLL level [23,24] in the SM completely. As the results of this calculation still suffer from large renormalization scale uncertainties of the order of $\sim 20\%$ in the near past a great deal of effort was spent to reduce them. Nowadays the most important parts of the NNLL contributions relevant for the SM were completed providing an improved prediction of $\bar{B} \to X_s l^+ l^-$.

The formalism of effective theories, which is conventionally used in the analysis of weak B decays, allows to separate the calculation into three distinct steps.

1. The matching of the full theory and the effective theory amplitudes to determine the Wilson coefficients at the electroweak scale $\mu_0 \sim M_W$ – which can be regarded as *integrating out heavy degrees of freedom.*

2. The renormalization group evolution of the Wilson coefficients down to the relevant low energy scale $\mu \sim m_b$ – thereby resumming large logarithms to all orders in the strong coupling constant α_s – *renormalization group improved perturbation theory.*

3. The calculation of physical observables such as branching ratios or various asymmetries. This step requires the evaluation of matrix elements of the effective theory operators between the physical states of interest and the inclusion of the corresponding bremsstrahlung corrections. The leading contribution is the perturbatively calculable decay at the parton level, formally justified by HQE.

Subsequently the dependence of the results on the matching scale μ_0 and the low energy scale $\mu \sim m_b$ as the main theoretical uncertainty in the perturbative calculable contributions will be discussed. The inclusion of non-perturbative corrections allows finally the prediction of the hadronic branching ratio integrated in a restricted domain of $\hat{s}$ where the theoretical uncertainties are well under control.

5.1 Matching Results

The framework of effective theories applied to electroweak decays are a convenient tool to resum QCD corrections to all orders with the help of renormalization group methods. As a first step the mass hierarchy of the SM and many of its extensions allows for integrating out systematically heavy degrees of freedom of masses $M_{\text{heavy}} \geq M_W$. The effect of the decoupled degrees of freedom will be contained in the effective theory coupling constants, the so-called Wilson coefficients.

The effective theory Lagrangian relevant to the inclusive decay $\bar{B} \to X_s l^+ l^-$ resulting from the SM and the considered scenario of the MSSM has the following form

$$\begin{aligned}\mathcal{L}_{\text{eff}} &= \mathcal{L}_{\text{QCD}\times\text{QED}}(u,d,s,c,b,e,\mu,\tau) \\ &+ \frac{4G_{\text{F}}}{\sqrt{2}}\left[V_{us}^* V_{ub}\left(C_1^c \mathcal{O}_1^u + C_2^c \mathcal{O}_2^u + C_{11}^c \mathcal{O}_{11}^u\right) + V_{cs}^* V_{cb}\left(C_1^c \mathcal{O}_1^c + C_2^c \mathcal{O}_2^c + C_{11}^c \mathcal{O}_{11}^c\right)\right] \\ &+ \frac{4G_{\text{F}}}{\sqrt{2}} \sum_{i\in A}\left[\left(V_{us}^* V_{ub} + V_{cs}^* V_{cb}\right) C_i^c + V_{ts}^* V_{tb}\, C_i^t\right] \mathcal{O}_i, \end{aligned} \tag{5.3}$$

with $A = \{3\ldots10,\ 31\ldots36,\ \textit{evanescent}\}$ numbering the relevant operators $\mathcal{O}_i^Q$ and the corresponding Wilson coefficients C_i^Q. Here G_F is the Fermi constant and furthermore we refrain from using unitarity of the CKM matrix V_{CKM}

$$V_{us}^* V_{ub} + V_{cs}^* V_{cb} + V_{ts}^* V_{tb} = 0. \tag{5.4}$$

The first term in eq. (5.3) consists of kinetic terms of the light particles – the leptons and the five light quark flavors – as well as their QCD and QED interactions while the remaining terms consist of $\Delta B = -\Delta S = 1$ gauge-invariant local operators[1] up to dimension 6 built out of those light fields[2]. The operators $\mathcal{O}_i^Q$ entering the effective Lagrangian can be divided into three classes. The *physical* operators

[1] The operators conserve flavors other than B and S.

[2] The s-quark mass is neglected here, i.e. it is assumed to be negligibly small when compared to m_b. No such assumption is made concerning m_c or m_τ.

$$\mathcal{O}_1^Q = (\bar{s}\,\gamma_\mu P_L \mathbf{T}^a\, Q)(\bar{Q}\,\gamma^\mu P_L \mathbf{T}^a\, b), \quad \mathcal{O}_2^Q = (\bar{s}\,\gamma_\mu P_L\, Q)(\bar{Q}\,\gamma^\mu P_L\, b),$$

$$\mathcal{O}_3 = (\bar{s}\,\gamma_\mu P_L\, b)\sum_q (\bar{q}\,\gamma^\mu\, q), \qquad \mathcal{O}_5 = (\bar{s}\,\gamma_{\mu_1}\gamma_{\mu_2}\gamma_{\mu_3} P_L\, b)\sum_q (\bar{q}\,\gamma^{\mu_1}\gamma^{\mu_2}\gamma^{\mu_3}\, q),$$

$$\mathcal{O}_4 = (\bar{s}\,\gamma_\mu P_L \mathbf{T}^a\, b)\sum_q (\bar{q}\,\gamma^\mu \mathbf{T}^a\, q), \quad \mathcal{O}_6 = (\bar{s}\,\gamma_{\mu_1}\gamma_{\mu_2}\gamma_{\mu_3} P_L \mathbf{T}^a\, b)\sum_q (\bar{q}\,\gamma^{\mu_1}\gamma^{\mu_2}\gamma^{\mu_3} \mathbf{T}^a\, q),$$

$$\mathcal{O}_7 = \frac{e}{g^2} m_b\, (\bar{s}\,\sigma^{\mu\nu} P_R\, b)\, F_{\mu\nu}, \qquad \mathcal{O}_8 = \frac{1}{g} m_b\, (\bar{s}\,\sigma^{\mu\nu} P_R \mathbf{T}^a\, b)\, G^a_{\mu\nu},$$

$$\mathcal{O}_9 = \frac{e^2}{g^2}(\bar{s}\,\gamma_\mu P_L\, b)(\bar{l}\,\gamma^\mu\, l), \qquad \mathcal{O}_{10} = \frac{e^2}{g^2}(\bar{s}\,\gamma_\mu P_L\, b)(\bar{l}\,\gamma^\mu\gamma_5\, l), \tag{5.5}$$

consist of the current-current operators $\mathcal{O}^Q_{1,2}$ ($Q = \{u, c\}$), the QCD penguin operators $\mathcal{O}_{3,\ldots,6}$ ($q = \{u, d, s, c, b\}$), the electro-magnetic moment type operator $\mathcal{O}_7$, the chromo-magnetic moment type operator $\mathcal{O}_8$ and finally the semileptonic operators $\mathcal{O}_{9,10}$.

In addition to the physical operators several non-physical operators have to be included in the matching procedure of the full and effective theories. One group consists of the so-called *EOM-vanishing* operators $\mathcal{O}_{31,\ldots,36}$ listed in Appendix B. These operators vanish by the QCD×QED equation of motion (EOM) of the effective theory up to a total derivative. They appear in intermediate steps of the off-shell calculation of the processes $b \to s\gamma$ and $b \to sg$ and contribute to the final results of Wilson coefficients of physical operators when going beyond the leading order matching.

The second group of non-physical operators which have to be considered in the matching procedure consists of *evanescent* operators [see Appendix C]. Evanescent operators vanish algebraically in four dimensions [79–81], however in $D \neq 4$ dimensions they are indispensable because without considering them the physical and EOM-vanishing operators would not form a closed set under QCD renormalization[3]. Their choice defines the "MS" scheme applied for the renormalization of the effective theory. In general the usage of different schemes results in different expressions of Wilson coefficients, anomalous dimensions and matrix elements of the effective theory as these quantities do not correspond to physical observables. In the evaluation of amplitudes the scheme dependencies will cancel up to the considered order in perturbation theory. Here we choose the evanescent operators [see Appendix B] as used in the calculation of the anomalous dimensions relevant to $b \to s\gamma$, $b \to sg$ and $b \to sl^+l^-$ of references [82] and [83].

The specific structure of the operators $\mathcal{O}_i^Q$ yields $\Delta B = -\Delta S = 1$ off-shell $b \to s$+(light particles) amplitudes of the effective theory which reproduce the analog amplitudes of the SM and its extensions. The off-shell amplitudes of the effective and full theory are equal at the leading order in electroweak gauge couplings and up to $\mathcal{O}$[(external momenta and light masses)$^2/M^2_{\text{heavy}}$], but to all orders in strong interactions. Thus $\mathcal{L}_{\text{eff}}$ reproduces the SM amplitudes, both partonic and hadronic ones [84].

For a detailed description of the two-loop matching of photonic $\Delta B = 1$ penguins ($b \to s\gamma$) in the SM the interested reader is referred to section 5 of Ref. [85]. The matching calculation of the supersymmetric contributions proceeds analogously. Additional helpful details of the matching calculation of the MSSM contributions can be found also in section 4 of Ref. [86].

[3]This extends also to the renormalization of QED corrections which are not considered here.

As a result of the matching calculation the Wilson coefficients can be perturbatively expanded as follows

$$C_i^Q = C_i^{Q(0)} + \frac{\alpha_s}{4\pi} C_i^{Q(1)} + \frac{\alpha_s^2}{(4\pi)^2} C_i^{Q(2)} + \dots \,, \qquad Q = \{c, t\}. \tag{5.6}$$

Contributions to order α_s^n to each Wilson coefficient originate from n-loop diagrams which follows from the particular convention of powers of gauge couplings in the normalization of the operators $\mathcal{O}_{7,\dots,10}$ and $\mathcal{O}_{31,\dots,36}$.

The results of the matching computation of the Wilson coefficients of the physical operators $\mathcal{O}^Q_{1,\dots,10}$ can be summarized as follows. At the tree level only

$$C_2^{c(0)} = -1, \tag{5.7}$$

is non-zero. The one-loop and two-loop matching conditions are

$$\begin{aligned}
C_1^{c(1)} &= -15 - 6L, \\
C_2^{c(1)} &= 0, \\
C_3^{c(1)} &= 0, & C_3^{t(1)} &= 0, \\
C_4^{c(1)} &= \frac{7}{9} - \frac{2}{3}L, & C_4^{t(1)} &= [E_4]^0, \\
C_5^{c(1)} &= 0, & C_5^{t(1)} &= 0, \\
C_6^{c(1)} &= 0, & C_6^{t(1)} &= 0, \\
C_7^{c(1)} &= \frac{23}{36}, & C_7^{t(1)} &= -\frac{1}{2}[A_7]^0, \\
C_8^{c(1)} &= \frac{1}{3}, & C_8^{t(1)} &= -\frac{1}{2}[F_8]^0, \\
C_9^{c(1)} &= -\frac{1}{4s_W^2} - \frac{38}{27} + \frac{4}{9}L, & C_9^{t(1)} &= \frac{1-4s_W^2}{s_W^2}[C_9^{l\bar{l}}]^0 - \frac{1}{s_W^2}[B_9^{l\bar{l}}]^0 - [D_9]^0, \\
C_{10}^{c(1)} &= \frac{1}{4s_W^2}, & C_{10}^{t(1)} &= \frac{1}{s_W^2}([B_{10}^{l\bar{l}}]^0 - [C_9^{l\bar{l}}]^0),
\end{aligned} \tag{5.8}$$

$$\begin{aligned}
C_1^{c(2)} &= [T_1]^1 - \frac{7987}{72} - \frac{17}{3}\pi^2 - \frac{475}{6}L - 17L^2, \\
C_2^{c(2)} &= -\frac{127}{18} - \frac{4}{3}\pi^2 - \frac{46}{3}L - 4L^2, \\
C_3^{c(2)} &= \frac{680}{243} + \frac{20}{81}\pi^2 + \frac{68}{81}L + \frac{20}{27}L^2, & C_3^{t(2)} &= [G_3]^1, \\
C_4^{c(2)} &= -\frac{950}{243} - \frac{10}{81}\pi^2 - \frac{124}{27}L - \frac{10}{27}L^2, & C_4^{t(2)} &= [E_4]^1,
\end{aligned}$$

$$
\begin{aligned}
C_5^{c(2)} &= -\frac{68}{243} - \frac{2}{81}\pi^2 - \frac{14}{81}L - \frac{2}{27}L^2, & C_5^{t(2)} &= -\frac{1}{10}[G_3]^1 + \frac{2}{15}[E_4]^0,\\
C_6^{c(2)} &= -\frac{85}{162} - \frac{5}{108}\pi^2 - \frac{35}{108}L - \frac{5}{36}L^2, & C_6^{t(2)} &= -\frac{3}{16}[G_3]^1 + \frac{1}{4}[E_4]^0,\\
C_7^{c(2)} &= -\frac{713}{243} - \frac{4}{81}L, & C_7^{t(2)} &= -\frac{1}{2}[A_7]^1,\\
C_8^{c(2)} &= -\frac{91}{324} + \frac{4}{27}L, & C_8^{t(2)} &= -\frac{1}{2}[F_8]^1,\\
C_9^{c(2)} &= -\frac{1}{s_W^2} - \frac{524}{729} + \frac{128}{243}\pi^2 + \frac{16}{3}L + \frac{128}{81}L^2, & & \\
C_9^{t(2)} &= \frac{1-4s_W^2}{s_W^2}[C_9^{l\bar{l}}]^1 - \frac{1}{s_W^2}[B_9^{l\bar{l}}]^1 - [D_9]^1, & & \\
C_{10}^{c(2)} &= \frac{1}{s_W^2}, & C_{10}^{t(2)} &= \frac{1}{s_W^2}([B_{10}^{l\bar{l}}]^1 - [C_9^{l\bar{l}}]^1).
\end{aligned} \tag{5.9}
$$

In the above equations the abbreviation

$$L = \ln \frac{\mu_0^2}{M_W^2} \tag{5.10}$$

was used with μ_0 being the renormalization scale introduced by the renormalization of the Greens functions of the full and effective theory. As it is the very scale at which the heavy degrees of the full theory are integrated out and their effect is factorized from long distance interaction of the remaining light particles by matching the full and the effective theories it is also called the *matching scale*.

The various functions $[X]^n$ in eqs. (5.8) and (5.9) indicate their origin when matching the $b \to s$+(light particles) Greens functions of the full and effective theory

- $[A]$: on-shell part of 1PI $b \to s\gamma$,
- $[B^{l\bar{l}}]$: $b \to s l^+ l^-$ mediated by box-diagrams,
- $[C^{l\bar{l}}]$: $b \to s l^+ l^-$ mediated by Z-boson (Z-penguins),
- $[D]$: off-shell part of 1PI $b \to s\gamma$, contributing to $b \to s l^+ l^-$,
- $[E]$: off-shell part of 1PI $b \to sg$, contributing to $b \to sq\bar{q}$,
- $[F]$: on-shell part of 1PI $b \to sg$,
- $[G]$: 1PI two-loop diagrams $b \to sq\bar{q}$,
- $[T]$: two-loop diagrams $b \to sc\bar{c}$.

The index n corresponds to the number of loops of the diagrams which can be classified into $n = 0$ tree-level, $n = 1$ leading order (LO) and $n = 2$ next-to-leading order (NLO) contributions, see also the comment below eq. (5.6). Further each function $[X]^n$ receives contributions from different virtual particle exchange

$$[X]^n = \sum_{i=\{W,H,\tilde{\chi},4\}} [X]_i^n. \tag{5.11}$$

The "charm quark – W boson" contribution of the SM is explicitely given in the eqs. (5.7)-(5.9). For the "top quark – W boson" contribution of the SM and contributions due to MSSM particles we refer to the Appendix C. The index i corresponds to

- $i = W$: "top quark – W boson" loops (SM),
- $i = H$: "top quark – charged Higgs boson" loops,
- $i = \tilde{\chi}$: "chargino – up-squark" loops,
- $i = 4$: "chargino – up-squark" loops containing quartic squark vertex.

The SM result can be obtained by discarding the contributions $\{H, \tilde{\chi}, 4\}$ in the sum of eq. (5.11).

The results of the function $[X]^n$ listed in Appendix C are given in terms of the running $\overline{\rm MS}$ quark and squark masses $m_q \equiv m_q(\mu)$ and $m_{\tilde{q}} \equiv m_{\tilde{q}}(\mu)$, respectively. Alternatively, one can work with the pole masses, in which the following steps should be performed:

Step 1. Remove the contributions due to the quartic squark couplings denoted by $i = 4$ in (5.11).

Step 2. Use the shift from the $\overline{\rm MS}$ scheme to the corresponding pole masses[4]

$$m_t(\mu) = m_{t,pole}\left\{1 - \frac{\alpha_s(m_{t,pole})}{4\pi}\left[\frac{16}{3} - 4\ln\left(\frac{m_{t,pole}}{\mu}\right)^2\right]\right\}, \tag{5.12}$$

$$\begin{aligned} m_q(\mu) = m_{q,pole}&\left[1 - \frac{\alpha_s(m_{q,pole})}{4\pi}\frac{16}{3}\right]\left[\frac{\alpha_s(\mu)}{\alpha_s(m_{q,pole})}\right]^{\gamma_m^{(0)}/(2\beta_0)} \\ &\times\left\{1 + \left[\frac{\gamma_m^{(1)}}{2\beta_0} - \frac{\beta_1\gamma_m^{(0)}}{2\beta_0^2}\right]\frac{\alpha_s(\mu) - \alpha_s(m_{q,pole})}{4\pi}\right\} \quad (q = d, s, b), \end{aligned} \tag{5.13}$$

$$m_{\tilde{q}}(\mu) = m_{\tilde{q},pole}\left\{1 - \frac{\alpha_s(m_{\tilde{q},pole})}{4\pi}\left[\frac{14}{3} - 2\ln\left(\frac{m^{\tilde{q},pole}}{\mu}\right)^2\right]\right\}, \tag{5.14}$$

where

$$\beta_0 = 11 - \frac{2}{3}n_f, \qquad \beta_1 = 102 - \frac{38}{3}n_f, \qquad \gamma_m^{(0)} = 8, \qquad \gamma_m^{(1)} = \frac{404}{3} - \frac{40}{9}n_f, \tag{5.15}$$

[4]Note that only in the case of light quarks (d, s, b) it is necessary to resum the large logarithms.

and n_f is the number of active quark flavors. Observe that the shift in 5.14 involves only the gluonic corrections, since the contributions due to quartic squark couplings have already been considered in step 1. In this context, we would like to remark that the absence of the 'quartic' contributions in an on-shell scheme is related to the renormalization of the squark mass and mixing angle. For details, we refer the reader to [87].

5.2 Renormalization Group Evolution

In the previous section the Wilson coefficients resulting from the matching procedure within the context of the SM and a supersymmetric extension where presented. In these results products of the strong coupling and logarithms of the type $\alpha_s^n \ln^n(\mu_0^2/M_{\text{heavy}}^2)$ for $n = 1, 2$ appear. In principle the renormalization scale μ_0 is arbitrary and thus logarithms of this kind can lift the suppression by powers of α_s^n when going to higher order in perturbation theory invalidating the calculation. To control these logarithms one has to choose $\mu_0 \sim M_{\text{heavy}}$ which in turn fixes the Wilson coefficients to be determined from the full theory at this particular scale.

However, the renormalization group equations of the Wilson coefficients within the effective theory allow to scale them to the more appropriate scale for B decays of the order $\mu \sim m_b$ thereby resumming the displeasing large logarithms to all orders in the strong coupling α_s.

The renormalization group equation (RGE) of the Wilson coefficients[5] $\vec{C}$ is governed by the anomalous dimension matrix $\hat{\gamma}$

$$\mu \frac{d}{d\mu} \vec{C} = \hat{\gamma}^T \vec{C}. \tag{5.16}$$

It has the following general solution

$$\vec{C}(\mu) = \hat{U}(\mu, \mu_0)\, \vec{C}(\mu_0) \tag{5.17}$$

where

$$\begin{aligned} \hat{U}(\mu, \mu_0) &= T_g \exp \int_{g_s(\mu_0)}^{g_s(\mu)} dg_s' \frac{\hat{\gamma}^T(g_s')}{\beta(g_s')} \\ &= \hat{U}^{(0)}(\mu, \mu_0) + \frac{\alpha_s(\mu_0)}{4\pi} \hat{U}^{(1)}(\mu, \mu_0) + \frac{\alpha_s(\mu_0)^2}{(4\pi)^2} \hat{U}^{(2)}(\mu, \mu_0) + \dots \end{aligned} \tag{5.18}$$

is the evolution operator of the Wilson coefficients and β the renormalization group function of the strong coupling constant g_s. In the intermediate step of the above equation T_g denotes ordering of products of the anomalous dimension $\hat{\gamma}^T(g_s')$ such that their arguments g_s' increase from right to left. When using the perturbative results of the β- and $\hat{\gamma}$-functions

[5] Throughout this derivation we will suppress the index Q of the Wilson coefficients and the anomalous dimension matrices, labeling the CKM-sector of the effective theory they correspond to.

$$\beta(g_s) = -g_s\frac{\alpha_s}{4\pi}\beta_0 - g_s\frac{\alpha_s^2}{(4\pi)^2}\beta_1 - g_s\frac{\alpha_s^3}{(4\pi)^3}\beta_2 + \dots\ ,$$

$$\hat{\gamma}(g_s) = \frac{\alpha_s}{4\pi}\hat{\gamma}^{(0)} + \frac{\alpha_s^2}{(4\pi)^2}\hat{\gamma}^{(1)} + \frac{\alpha_s^3}{(4\pi)^3}\hat{\gamma}^{(2)} + \dots\ , \tag{5.19}$$

the result of the form given in the second line of eq. (5.18) can be obtained. Together with the perturbative expansion of the initial Wilson coefficients $\vec{C}(\mu_0)$ as shown in eq. (5.6) also the down-scaled Wilson coefficients $\vec{C}(\mu)$ can **a)** be organized in a systematic expansion in $\alpha_s(\mu_0)$ (or equivalently in $\alpha_s(\mu)$) and **b)** will contain also the resummed large logarithms to all orders in α_s.

The individual terms $\hat{U}^{(i)}(\mu,\mu_0)$ with $i = 0, 1, 2$ can be determined following Ref. [88, 89] with the help of the ansatz

$$\hat{U}(\mu,\mu_0) = \hat{K}[g_s(\mu)]\ \hat{U}^{(0)}(\mu,\mu_0)\ \hat{K}^{-1}[g_s(\mu_0)]. \tag{5.20}$$

Here $\hat{U}^{(0)}(\mu,\mu_0)$ represents the solution of (5.18) when restricting to the lowest order expansion of $\beta(g_s)$ and $\hat{\gamma}(g_s)$

$$\hat{U}^{(0)}(\mu,\mu_0) = \hat{V}\left[\frac{\alpha_s(\mu_0)}{\alpha_s(\mu)}\right]^{\frac{\hat{\gamma}_D^{(0)}}{2\beta_0}}\hat{V}^{-1} \tag{5.21}$$

with the diagonal matrix $\hat{\gamma}_D^{(0)} = \hat{V}^{-1}\hat{\gamma}^{(0)^T}\hat{V}$. The matrix $\hat{K}$ obeys then the differential equation

$$\left[\partial_{g_s}\hat{K}(g_s) - \frac{1}{g_s\beta_0}\hat{K}(g_s)\hat{\gamma}^{(0)^T}\right]\beta(g_s) = \hat{\gamma}^T(g_s)\hat{K}(g_s). \tag{5.22}$$

Inserting the perturbative expansion of $\hat{K}$ up to second order

$$\hat{K}(g_s) = \mathbf{1} + \frac{\alpha_s}{4\pi}\hat{J}_1 + \frac{\alpha_s^2}{(4\pi)^2}\hat{J}_2 + \dots\ , \tag{5.23}$$

$$\hat{K}^{-1}(g_s) = \mathbf{1} - \frac{\alpha_s}{4\pi}\hat{J}_1 - \frac{\alpha_s^2}{(4\pi)^2}(\hat{J}_2 - \hat{J}_1^2) + \dots\ , \tag{5.24}$$

determines the matrices $\hat{J}_1$ and $\hat{J}_2$

$$\hat{J}_1 = \hat{V}\hat{S}_1\hat{V}^{-1}, \qquad \hat{J}_2 = \hat{V}\hat{S}_2\hat{V}^{-1} \tag{5.25}$$

with

$$[\hat{S}_1]_{ij} = \frac{\beta_1}{2\beta_0^2}[\hat{\gamma}_D^{(0)}]_{ii}\delta_{ij} - \frac{[\hat{V}^{-1}\hat{\gamma}^{(1)^T}\hat{V}]_{ij}}{2\beta_0 + [\hat{\gamma}_D^{(0)}]_{ii} - [\hat{\gamma}_D^{(0)}]_{jj}}, \tag{5.26}$$

$$\begin{aligned}[\hat{S}_2]_{ij} = {} & \frac{\beta_2}{4\beta_0^2}[\hat{\gamma}_D^{(0)}]_{ii}\delta_{ij} - \frac{[\hat{V}^{-1}\hat{\gamma}^{(2)^T}\hat{V}]_{ij}}{4\beta_0 + [\hat{\gamma}_D^{(0)}]_{ii} - [\hat{\gamma}_D^{(0)}]_{jj}} \\ & + \sum_k \frac{2\beta_0 + [\hat{\gamma}_D^{(0)}]_{ii} - [\hat{\gamma}_D^{(0)}]_{kk}}{4\beta_0 + [\hat{\gamma}_D^{(0)}]_{ii} - [\hat{\gamma}_D^{(0)}]_{jj}} \left([\hat{S}_1]_{ik}[\hat{S}_1]_{kj} - \frac{\beta_1}{\beta_0}[\hat{S}_1]_{ij}\delta_{jk} \right).\end{aligned} \tag{5.27}$$

Then, using the expansion of the initial Wilson coefficients as given in (5.6), $\eta \equiv \alpha_s(\mu_0)/\alpha_s(\mu)$ and abbreviating $\hat{U}^{(0)} \equiv \hat{U}^{(0)}(\mu, \mu_0)$ the perturbative solution of (5.17) becomes

$$\begin{aligned}\vec{C}(\mu) = {} & \hat{U}^{(0)}\vec{C}^{(0)} \\ & + \frac{\alpha_s(\mu_0)}{4\pi}\left\{ \left[\frac{\hat{J}_1\hat{U}^{(0)}}{\eta} - \hat{U}^{(0)}\hat{J}_1 \right]\vec{C}^{(0)} + \hat{U}^{(0)}\vec{C}^{(1)} \right\} \\ & + \frac{\alpha_s(\mu_0)^2}{(4\pi)^2}\left\{ \left[\frac{\hat{J}_2\hat{U}^{(0)}}{\eta^2} - \frac{\hat{J}_1\hat{U}^{(0)}\hat{J}_1}{\eta} - \hat{U}^{(0)}(\hat{J}_2 - \hat{J}_1^2) \right]\vec{C}^{(0)} \right. \\ & \qquad \left. + \left[\frac{\hat{J}_1\hat{U}^{(0)}}{\eta} - \hat{U}^{(0)}\hat{J}_1 \right]\vec{C}^{(1)} + \hat{U}^{(0)}\vec{C}^{(2)} \right\}.\end{aligned} \tag{5.28}$$

In the above result the first term represents the leading logarithmic (LL) approximation of the scaled Wilson coefficients, the second term proportional to α_s the next-to leading logarithmic (NLL) contribution and the third term proportional to α_s^2 the next-to-next-to leading logarithmic (NNLL) contribution. The explicit results of the contributions of the initial Wilson coefficients $C_i^{Q(0)}$, $C_i^{Q(1)}$ and $C_i^{Q(2)}$ were presented in the preceding section in eqs. (5.7)–(5.9).

Concerning the expansion coefficients of the anomalous dimension of the physical operators $\mathcal{O}^Q_{1,\ldots,10}$ relevant to $b \to s l^+ l^-$ the first two terms $\hat{\gamma}^{(0)}$ and $\hat{\gamma}^{(1)}$ were known when the first partial NNLL calculation [85] was performed. In general the quantity $\hat{\gamma}^{(2)}$ affects the parts proportional to $\vec{C}^{(0)}$ of the α_s^2 contribution as can be seen in eq. (5.28). The only nonzero Wilson coefficient is $C_2^{c(0)}$ giving thus rise to contributions to $C_{7,8,9}^{c(2)}$. From the analysis of the decay $\bar{B} \to X_s\gamma$ [82] the entries of $\hat{\gamma}^{(2)}$ describing the mixing of the four-quark operators $\mathcal{O}^Q_{1,\ldots,6}$ into the magnetic operators $\mathcal{O}_{7,8}$ are known and $C_{7,8}^{c(2)}$ are determined completely leaving just the part of $C_9^{c(2)}$ proportional to $C_2^{c(0)}$ undetermined. This unknown quantity was abbreviated in [85] by $U_{92}^{c(2)}$ and the variation in the range of $U_{92}^{c(2)} \in [-10, 10]$ leads to a change of $\sim 2\%$ of the results.

Very recently the authors of Ref. [83] have checked the mixing of $\mathcal{O}^Q_{1,\ldots,6} \to \mathcal{O}_{7,8}$ and presented also the three-loop mixing of the four-quark operators $\mathcal{O}^Q_{1,\ldots,6}$ into the operator $\mathcal{O}_9$. In the same work the authors announced to present the results of the three-loop self-mixing of the four-quark operators $\mathcal{O}^Q_{1,\ldots,6}$ in a separate publication [90]. $U_{92}^{c(2)}$ depends also on these entries of $\hat{\gamma}^{(2)}$ and calculating them will complete the NNLL evolution of the Wilson coefficients $C_{1,\ldots,10}$.

5.3 Matrix Elements

The evolution of the initial Wilson coefficients from the matching scale μ_0 to the low energy scale $\mu \sim m_b$ with the RGE presented in the preceding section resums large logarithms of QCD corrections to all orders in the strong coupling constant α_s yielding as a final result the effective theory Lagrangian $\mathcal{L}_{\text{eff}}$ at the scale $\mu \sim m_b$. The effective Lagrangian describes light leptons and quarks and their QED×QCD interactions whereas the effects of short distance physics (electroweak interactions to first order and strong interactions to all orders in NNLL approximation) is integrated out being contained in the effective couplings - the Wilson coefficients. Once the missing entries of the anomalous dimension matrix $\hat{\gamma}^{(2)}$ are calculated the effective Lagrangian $\mathcal{L}_{\text{eff}}$ is known up to NNLL precision, the effects of the unknown entries were estimated to be at the order of the percent level [85].

Heavy Quark Expansion – Inclusive Decays

At this point it becomes unavoidable when calculating observables to connect the effective Lagrangian given in terms of quark and gluon degrees of freedom to hadronic transitions which are actually observed. This involves the consideration of hadronic matrix elements of quark-level operators which typically are incalculable due to the non-perturbative character of the bound state dynamics in the initial state and hadronization in the final state. Namely for $\bar{B} \to X_s l^+ l^-$

$$\langle l^+ l^- X_s | \mathcal{L}_{\text{eff}} | B \rangle \tag{5.29}$$

with B and X_s being the initial state and a hadronic final state with strangeness $S = -1$, respectively. The *inclusive* differential decay rate can be obtained by squaring the matrix elements and summing over the final states X_s yielding

$$d\Gamma = \frac{1}{2M_B} \sum_{X_s} d[PS](2\pi)^4 \delta^{(4)}(p_B - p_{X_s} - q) \langle B | i\mathcal{L}_{\text{eff}}^\dagger | X_s l^+ l^- \rangle \langle l^+ l^- X_s | i\mathcal{L}_{\text{eff}} | B \rangle. \tag{5.30}$$

Here M_B is the mass of the decaying B meson, $d[PS]$ the appropriate phase space differential, p_B and p_{X_s} are the momenta of the initial and final hadrons, respectively, and $\sqrt{q^2}$ is the invariant mass transfered to the lepton pair. In analogy to the optical theorem the squared matrix element can be replaced by the absorptive part of the forward scattering amplitude of the process $(B \to B)$ under the action of $\mathcal{L}_{\text{eff}}$

$$d\Gamma \sim \frac{1}{2M_B} \sum_{X_s} d[PS](2\pi)^4 \delta^{(4)}(p_B - p_{X_s} - q)\ \text{Im} \langle B | \hat{T}\{\mathcal{L}_{\text{eff}}^\dagger \mathcal{L}_{\text{eff}}\} | B \rangle. \tag{5.31}$$

The leptonic part of the non-local time-ordered product $\hat{T}\{\ldots\}$ can be treated perturbatively in α_{em}. The remaining hadronic part of the non-local time-ordered product $\hat{T}\{\ldots\}$ can be expanded into a series of local operators of increasing dimension using an operator product expansion (OPE) with coefficients that contain increasing powers of $1/m_b$. The general structure of the OPE

$$\hat{T}\{\mathcal{L}^\dagger_{\text{eff}}\mathcal{L}_{\text{eff}}\} \sim z_1(\bar{b}b) + \frac{z_2}{m_b^2}(\bar{b}g\sigma\cdot Gb) + \sum \frac{z_{qi}}{m_b^3}(\bar{b}\Gamma_i q)(\bar{q}\Gamma_i b) + \dots \tag{5.32}$$

again consists of Wilson coefficients z_i containing the short distance physics at scales of the order $\mu \sim m_b \gg \Lambda_{\text{QCD}}$ and operators whose matrix elements summarize the long distance physics of scales of the order $\mu \sim \Lambda_{\text{QCD}}$.

The matrix elements of these operators can be addressed systematically within the *heavy quark effective theory* (HQET) framework. As an example the matrix element of the leading dimension 3 operator $\bar{b}b$ within HQET can be expressed in terms of matrix elements of the heavy quark field h

$$\begin{aligned}\langle B|\bar{b}b|B\rangle &= 1 + \frac{1}{2m_b^2}\langle B|\bar{h}(iD)^2 h|B\rangle + \frac{1}{4m_b^2}\langle B|\bar{h}(g\sigma\cdot G)h|B\rangle + \dots \\ &= 2M_B\left[1 + \frac{1}{2m_b^2}(\lambda_1 + 3\lambda_2)\right] + \dots\ .\end{aligned} \tag{5.33}$$

The latter equation uses the HQET normalization of the states $\langle B|\bar{b}b|B\rangle = 2M_B$ and the parameterization of the matrix elements

$$\langle B|\bar{h}(iD)^2 h|B\rangle = 2M_B\lambda_1, \qquad \langle B|\bar{h}(g\sigma\cdot G)h|B\rangle = 12M_B\lambda_2. \tag{5.34}$$

Both parameters can be interpreted as the expectation value of the kinetic energy (λ_1) and the energy due to the chromo-magnetic moment (λ_2) of the heavy quark inside the heavy meson.

The discussion of limitations of eq. (5.33) when applied to $\bar{B} \to X_s l^+ l^-$ and the magnitude of non-perturbative effects to $\bar{B} \to X_s l^+ l^-$ is postponed. Finally we want to emphasize that the leading contribution within the HQE framework to the decay rate of inclusive decays is the free quark contribution described by z_1 whereas the first non-perturbative corrections are suppressed by $1/m_b^2$ [see eq. (5.32) and (5.33)].

Parton Decay

In the following we will summarize the calculation of the matrix elements at the parton level (free quark) $b \to s l^+ l^-$ within the effective theory. The calculation can be performed perturbatively in $\alpha_s(\mu)$ at the scale $\mu \sim m_b$.

Within the LL approximation the only operator mediating $b \to s l^+ l^-$ is $\mathcal{O}_9$ which receives a nonzero Wilson coefficient when solving the RGE due to the mixing of $\mathcal{O}_{1,\dots,6} \to \mathcal{O}_9$. It is a peculiarity of the $b \to s l^+ l^-$ decay that the magnitude of the NLL contribution is of the same size as the LL result and thus it is essential to include the NLL corrections to arrive at a reasonable estimate of physical observables.

The relevant matrix elements of the NLL analysis are the virtual gluon correction to the operator $\mathcal{O}_9$ and one-loop diagrams of the four-quark operators $\mathcal{O}^Q_{1,\dots,6}$ mediating $b \to s l^+ l^-$ [see Figure 5.1]. The calculation of the later shows that they are proportional to the tree-level matrix elements of the operators $\mathcal{O}_{7,9}$ and it has become customary to take them into account by introducing so called *effective Wilson coefficients* [see eq. (5.37)]. The result of

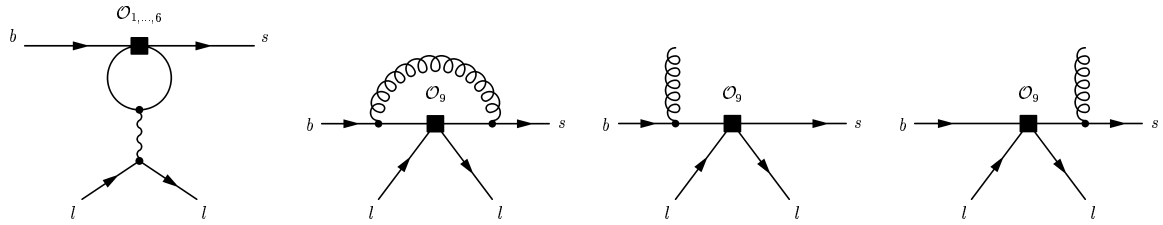

Figure 5.1: Matrix elements of the effective theory at NLL contributing to $b \to s l^+ l^-$. Diagram a) corresponds to the virtual corrections of the four-quark operators $\mathcal{O}^Q_{1,...,6}$ represented by $\mathcal{M}^{Q,\{3...6\}}_{7,1}$, $\mathcal{M}^{Q,\{1,2\}}_{9,1}$ and $\mathcal{M}^{Q,\{3...6\}}_{9,1}$ below. The diagram b) shows the gluon correction to the matrix element of $\mathcal{O}_9$ and diagrams c) and d) the corresponding bremsstrahlung corrections. The sum of the later three diagrams yields $\omega_{99}(\hat{s})$.

these one-loop matrix elements is given by the functions $h(0,\hat{s})$, $h(1,\hat{s})$ and $h(\hat{m}_c,\hat{s})$ which can be found in [23, 24]. Infrared singularities arising in the calculation of the one-gluon correction to the matrix element of the operator $\mathcal{O}_9$ cancel once the gluon bremsstrahlung corrections of the process $b \to s\, g\, l^+ l^-$ to this operator are taken into account, summarized below in the function $\omega_{99}(\hat{s})$.

In the partial NNLL analysis [85] consistently all NLO matching contributions to the initial Wilson coefficients in the SM were calculated [eq. (5.9)] and the evolution of the Wilson coefficients was partially performed to NNLL accuracy, parameterizing the remaining ignorance by $U^{c(2)}_{92}$. As a result the final μ_0 matching scale dependence of ($\pm 16\%$) of the NLL result becomes reduced to ($\pm 6\%$). However, as only the NLL matrix elements and bremsstrahlung corrections were included a μ low energy scale dependence of ($\pm 13\%$) remained. In a series of publications [91, 92] the most relevant parts of these virtual and bremsstrahlung corrections were calculated with the objective to further reduce the μ low energy scale dependence.

These NNLL corrections include **a)** the infrared finite virtual corrections to the matrix elements of the operators $\mathcal{O}_1$, $\mathcal{O}_2$ and $\mathcal{O}_8$. These corrections are proportional to the tree-level matrix elements of the operators $\mathcal{O}_7$ and $\mathcal{O}_9$ and are absorbed into the effective Wilson coefficients represented through the functions $F^{(j)}_i$ ($i = 1, 2, 8; j = 7, 9$) below. Further **b)** the virtual and the bremsstrahlung corrections to the matrix elements of $\mathcal{O}_7$, $\mathcal{O}_9$ and $\mathcal{O}_{10}$ were calculated. Both suffer from infrared- and collinear singularities which cancel when combined at the level of differential decay rates. The infrared finite sum of both yields the functions $\omega_{77}(\hat{s})$, $\omega_{79}(\hat{s})$ and $\omega_{99}(\hat{s})$ appearing in the dilepton invariant mass distribution[6]. Finally **c)** infrared finite bremsstrahlung corrections due to interferences between $\mathcal{O}_8$ and the operators $\mathcal{O}_{7,8,9,10}$ contained in $\frac{d\Gamma^{\rm Brems,A}}{d\hat{s}}$ and due to the interferences between $\mathcal{O}_{1,2}$ and $\mathcal{O}_{1,2,7,8,9,10}$ denoted by $\frac{d\Gamma^{\rm Brems,B}}{d\hat{s}}$ were considered in Ref. [92].

The final result of the dilepton invariant mass distribution is given in [94]

[6]The according results relevant to the double differential decay rate of the dilepton invariant mass and $\cos\theta$ are contained in analogous functions given in Ref. [94]. θ denotes the angle between the momenta of the positively charged lepton l^+ and the b-quark. The double-differential decay rate still contains the information about the angular distribution of the decay products that is important when considering forward-backward asymmetries. See also Ref. [93].

$$\frac{d\Gamma[b \to X_s l^+ l^-]}{d\hat{s}} = \left(\frac{\alpha_{\rm em}}{4\pi}\right)^2 \frac{G_F^2 m_{b,pole}^5 |V_{ts}^* V_{tb}|^2}{48\pi^3}(1-\hat{s})^2$$
$$\times \left\{(1+2\hat{s})\left(\left|\tilde{C}_9^{\rm eff}\right|^2 + \left|\tilde{C}_{10}^{\rm eff}\right|^2\right)[1+\frac{2\alpha_s}{\pi}\omega_{99}(\hat{s})] + 4\left(1+\frac{2}{\hat{s}}\right)\left|\tilde{C}_7^{\rm eff}\right|^2[1+\frac{2\alpha_s}{\pi}\omega_{77}(\hat{s})]\right.$$
$$\left. +12{\rm Re}\left(\tilde{C}_7^{\rm eff}\tilde{C}_9^{\rm eff*}\right)[1+\frac{2\alpha_s}{\pi}\omega_{79}(\hat{s})]\right\} + \frac{d\Gamma^{\rm Brems,A}}{d\hat{s}} + \frac{d\Gamma^{\rm Brems,B}}{d\hat{s}} \tag{5.35}$$

with $\alpha_s = \alpha_s(\mu)$ at the low energy scale. The effective Wilson coefficients can be split into top- and light-quark contributions

$$\tilde{C}_i^{\rm eff} = \tilde{C}_i^{t,{\rm eff}} + \frac{V_{cs}^* V_{cb}}{V_{ts}^* V_{tb}}\tilde{C}_i^{c,{\rm eff}} + \frac{V_{us}^* V_{ub}}{V_{ts}^* V_{tb}}\tilde{C}_i^{u,{\rm eff}}, \tag{5.36}$$

that are related to the evolved Wilson coefficients $C_i^Q(\mu)$ [see (5.28)] and virtual corrections to the matrix elements of the operators $\mathcal{O}_{1,\ldots,6}$ and $\mathcal{O}_8$. It is convenient to absorb these virtual corrections into the effective Wilson coefficients as follows

$$\begin{aligned}
\tilde{C}_7^{Q,{\rm eff}} &= \frac{4\pi}{\alpha_s(\mu)}C_7^Q(\mu) + \mathcal{M}_{7,1}^{Q,\{1,2\}} + \mathcal{M}_{7,1}^{Q,\{3\ldots6\}} + \mathcal{M}_{7,2}^{Q,\{1,2\}} + \mathcal{M}_{7,2}^{Q,\{3\ldots6\}} + \mathcal{M}_{7,2}^{Q,8},\\
\tilde{C}_9^{Q,{\rm eff}} &= \frac{4\pi}{\alpha_s(\mu)}C_9^Q(\mu) + \mathcal{M}_{9,1}^{Q,\{1,2\}} + \mathcal{M}_{9,1}^{Q,\{3\ldots6\}} + \mathcal{M}_{9,2}^{Q,\{1,2\}} + \mathcal{M}_{9,2}^{Q,\{3\ldots6\}} + \mathcal{M}_{9,2}^{Q,8},\\
\tilde{C}_{10}^{Q,{\rm eff}} &= \frac{4\pi}{\alpha_s(\mu)}C_{10}^Q(\mu), \qquad\qquad Q = \{u,c,t\}.
\end{aligned} \tag{5.37}$$

Here $\mathcal{M}_{\mathcal{O}_B,O}^{Q,\mathcal{O}_A}$ denotes the virtual corrections of matrix elements of the operators $\mathcal{O}_A$ which are proportional to the tree-level matrix element of the operator $\mathcal{O}_B$. The subindex O is 1 in the case of NLL corrections and 2 in the case of NNLL corrections. The following contributions are zero

$$\mathcal{M}_{7,1}^{Q,\{1,2\}} = \mathcal{M}_{7,2}^{t,\{1,2\}} = \mathcal{M}_{9,1}^{t,\{1,2\}} = \mathcal{M}_{9,2}^{t,\{1,2\}} = 0 \tag{5.38}$$

because the one-loop diagrams of $\mathcal{O}_{1,2}^Q$ insertions in diagram a) of Figure 5.1 are not proportional to the tree-level matrix element $\mathcal{O}_7$ and furthermore the Wilson coefficients of these operators in the top-sector are zero. The nonzero corrections are

$$
\begin{aligned}
\mathcal{M}_{7,1}^{Q,\{3\ldots6\}} &= -\frac{1}{3}\,C_3^Q(\mu) - \frac{4}{9}\,C_4^Q(\mu) - \frac{20}{3}\,C_5^Q(\mu) - \frac{80}{9}\,C_6^Q(\mu),\\
\mathcal{M}_{7,2}^{c,\{1,2\}} &= -\frac{\alpha_s(\mu)}{4\pi}\left(C_1^{c,(0)}F_1^{(7)}(\hat{s}) + C_2^{c,(0)}F_2^{(7)}(\hat{s})\right),\\
\mathcal{M}_{7,2}^{Q,8} &= -\frac{\alpha_s(\mu)}{4\pi}A_8^{Q,(0)}F_8^{(7)}(\hat{s}),\\
\mathcal{M}_{9,1}^{u,\{1,2\}} &= \sum_{i=1}^{2} C_i^Q(\mu)\gamma_{i9}^{Q(0)}\ln\frac{m_b}{\mu} + \left(\frac{4}{3}\,C_1^c(\mu) + C_2^c(\mu)\right)\,h(0,\hat{s}),\\
\mathcal{M}_{9,1}^{c,\{1,2\}} &= \sum_{i=1}^{2} C_i^Q(\mu)\gamma_{i9}^{Q(0)}\ln\frac{m_b}{\mu} + \left(\frac{4}{3}\,C_1^c(\mu) + C_2^c(\mu)\right)\,h(\hat{m}_c^2,\hat{s}),\\
\mathcal{M}_{9,1}^{Q,\{3\ldots6\}} &= \sum_{i=3}^{6} C_i^Q(\mu)\gamma_{i9}^{Q(0)}\ln\frac{m_b}{\mu} + \left(6\,C_3^Q(\mu) + 60C_5^Q(\mu)\right)h(\hat{m}_c^2,\hat{s})\\
&\quad + \left(-\frac{7}{2}\,C_3^Q(\mu) - \frac{2}{3}\,C_4^Q(\mu) - 38\,C_5^Q(\mu) - \frac{32}{3}\,C_6^Q(\mu)\right)\,h(1,\hat{s})\\
&\quad + \left(-\frac{1}{2}\,C_3^Q(\mu) - \frac{2}{3}\,C_4^Q(\mu) - 8\,C_5^Q(\mu) - \frac{32}{3}\,C_6^Q(\mu)\right)\,h(0,\hat{s})\\
&\quad + \frac{4}{3}\,C_3^Q(\mu) + \frac{64}{9}\,C_5^Q(\mu) + \frac{64}{27}\,C_6^Q(\mu),\\
\mathcal{M}_{9,2}^{c,\{1,2\}} &= -\frac{\alpha_s(\mu)}{4\pi}\left(C_1^{c,(0)}F_1^{(7)}(\hat{s}) + C_2^{c,(0)}F_2^{(7)}(\hat{s})\right),\\
\mathcal{M}_{9,2}^{Q,8} &= -\frac{\alpha_s(\mu)}{4\pi}A_8^{Q,(0)}F_8^{(9)}(\hat{s}).
\end{aligned}
\tag{5.39}
$$

The corrections $\mathcal{M}_{7,2}^{u,\{1,2\}}$, $\mathcal{M}_{9,2}^{u,\{1,2\}}$ relevant to the up-quark sector are not calculated yet. A discussion of these contributions within the context of the inclusive $\bar{B} \to X_d l^+ l^-$ decay can be found in [95]. We would like to note, that the effective Wilson coefficients of the up-quark sector are multiplied by $|(V_{us}^* V_{ub})/(V_{ts}^* V_{tb})| \sim 0.02$ and are suppressed. This suppression mechanism of the up-quark sector acts not in the inclusive $\bar{B} \to X_d l^+ l^-$ decay were $|(V_{ud}^* V_{ub})/(V_{td}^* V_{tb})| \sim 0.44$ is rather large. In the numerical analysis the known NLL matrix elements will be used. Further the numerical impact of the up-quark contribution on the dilepton invariant mass distribution will be investigated in the subsequent section. It turns out to be almost negligible for $\bar{B} \to X_s l^+ l^-$ of the order of 2% [see Figure 5.11].

The corrections $\mathcal{M}_{7,2}^{Q,\{3\ldots6\}}$ and $\mathcal{M}_{9,2}^{Q,\{3\ldots6\}}$ are proportional to the down-scaled Wilson coefficients $C_{3,\ldots,6}^{Q(0)}$ at the low energy scale μ. $C_{3,\ldots,6}^{Q(0)}$ are small in the SM compared to $C_{1,2}^{Q(0)}$ suggesting that the main corrections of the NNLL matrix elements are included within $\mathcal{M}_{7,2}^{Q,\{1,2\}}$ and $\mathcal{M}_{9,2}^{Q,\{1,2\}}$. A complete NNLL computation of $\bar{B} \to X_s l^+ l^-$ should include these corrections as well. In the case of $\bar{B} \to X_s \gamma$ the same diagrams with on-shell photons were calculated [96] effecting the branching ratio $\mathcal{B}[\bar{B} \to X_s \gamma]$ by a reduction of roughly 1%. It is important to note, that the calculation of the virtual corrections $\mathcal{M}_{7,2}^{Q,\{1,2\}}$ and $\mathcal{M}_{9,2}^{Q,\{1,2\}}$ [91]

containing the functions $F_i^{(j)}$ $(i = 1, 2, 8; j = 7, 9)$ involves an expansion in the ratios m_c/m_b, q/m_b and $q/2m_c$. This limits the range of validity to small values of the invariant mass of the dilepton system $q^2/m_{b,pole}^2 < 0.25$. In these functions the charm quark mass m_c is renormalized in the pole mass scheme.

Finally, to complete the NNLL prediction of $b \to s l^+ l^-$, apart from the missing two-loop virtual corrections to the matrix elements of the four-quark operators summarized above, also the two-loop virtual and bremsstrahlung corrections to the operator $\mathcal{O}_9$ deserve a calculation. Their consideration modify eq. (5.35) by the replacement

$$[1 + \frac{2\alpha_s}{\pi}\omega_{99}(\hat{s})] \quad \to \quad [1 + \frac{2\alpha_s}{\pi}\omega_{99}(\hat{s}) + \frac{2\alpha_s^2}{\pi^2}\omega_{99}^{(2)}(\hat{s})], \tag{5.40}$$

where $\omega_{99}^{(2)}(\hat{s})$ represents the infrared finite sum of the two-loop virtual and real corrections.

5.4 Numerical Results

The dilepton invariant mass distribution given in eq. (5.35) is the perturbatively calculated result appearing as the leading contribution in HQE. Due to renormalization it depends on two renormalization scales namely the matching scale μ_0 and the low energy scale μ. The matching scale has to be fixed in the matching procedure to values of the order of the heavy decoupled particles to avoid the appearance of large logarithms in the Wilson coefficients. Further, the low energy scale dependence enters due to the RGE running of the effective theory from the matching scale down to the more appropriate low energy scale and due to the renormalization of the matrix elements $b \to s l^+ l^-$ calculated within the effective theory [eq. (5.39)]. Since renormalization scales are introduced just as a regulator in the perturbative calculation, the scale dependence of physical observables should disappear after proper renormalization. However, as a consequence of restricting in practice the calculation to a finite order in perturbation theory a residual scale dependence of higher order remains. It is common to estimate theoretical uncertainties due to the unknown higher order corrections by the investigation of uncertainties arising due to the variation of the residual scale dependence.

Instead of the dilepton invariant mass distribution we will consider in this section the perturbative quantity $R_{\text{quark}}^{l^+l^-}(\hat{s})$, given below, to study the numerical importance of the NNLL corrections compared to the NLL predictions as well as the uncertainties due to yet unknown higher order contributions.

$$R_{\text{quark}}^{l^+l^-}(\hat{s}) = \frac{1}{\Gamma[b \to X_c e \bar{\nu}_e]} \frac{d}{d\hat{s}} \Gamma[b \to X_s l^+ l^-]. \tag{5.41}$$

The choice of normalizing the dilepton invariant mass distribution $d\Gamma[b \to X_s l^+ l^-]/d\hat{s}$ to the semileptonic decay rate

$$\Gamma[b \to X_c e \bar{\nu}_e] = \frac{G_F^2 m_{b,pole}^5}{192\pi^3} |V_{cb}|^2 \; f\left(\frac{m_{c,pole}^2}{m_{b,pole}^2}\right) \kappa\left(\frac{m_c^2}{m_b^2}\right) \tag{5.42}$$

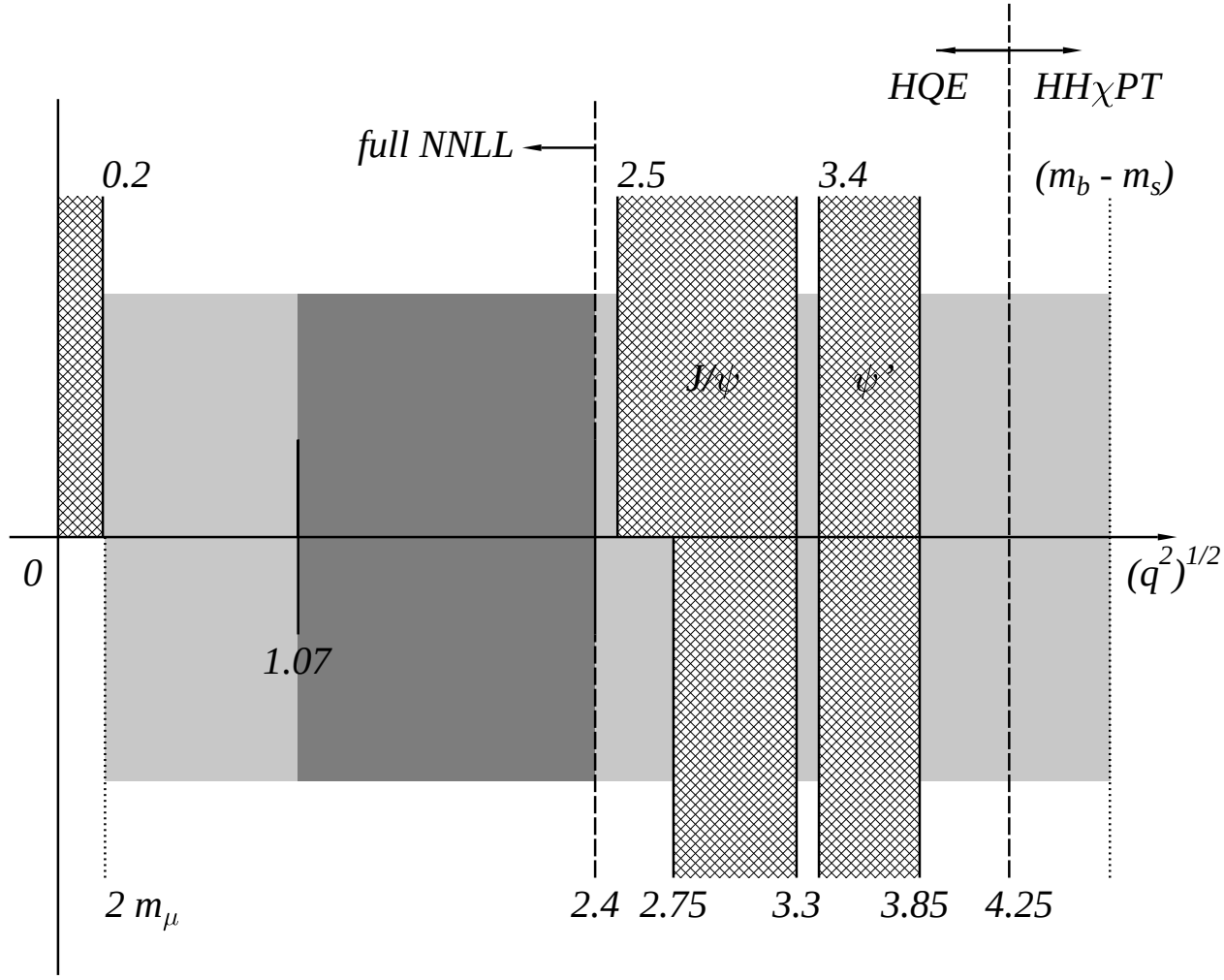

Figure 5.2: Cuts on the dilepton invariant mass $\sqrt{q^2}$ in units of GeV performed by the Belle Collaboration for the decay $\bar{B} \to X_s l^+ l^-$. The upper panel corresponds to the e^+e^- channel showing the lower cut of 0.2 GeV and the two cuts around the J/ψ and ψ' resonances as given in Table 5.5. The lower panel shows the according cuts of the $\mu^+\mu^-$ channel. The corresponding cuts applied by the BaBar Collaboration are much tighter [see Table 5.5] and are not displayed here. Further the low-$\hat{s}$ region according to $\hat{s} \in [0.05, 0.25]$ is indicated by the dark shaded area. The vertical dashed line at 2.4 GeV represents the upper boundary of the validity of the two-loop matrix element calculation restricting the full NNLL calculation to the area below. The vertical dashed line at 4.25 GeV corresponds to $s_m \approx 0.65$ up to which HQE can be trusted. As proposed in [124] for higher values of $\sqrt{q^2}$ other methods have to be used to estimate the dilepton invariant mass spectrum as for example HHχPT.

M_W	80.423 GeV	M_Z	91.187 GeV	$m_{t,pole}$	174.3 GeV
$m_{b,pole}$	4.8 GeV	$\alpha_s(M_Z)$	0.118	$\alpha_{\rm em}$	1/133
s_W^2	0.23124	G_F	$1.16639\,10^{-5}\,\text{GeV}^{-2}$	s_{12}	0.222
s_{13}	0.00349	s_{23}	0.041	$\delta_{\rm CKM}$	0.994838

Table 5.2: Input parameters used in the numerical analysis of the SM. For the CKM matrix the standard parameterization [99] with four independent parameters $s_{12},\ s_{13},\ s_{23}$ and $\delta_{\rm CKM}$ is used.

leads to a cancellation of the large uncertainties due to $m_{b,pole}^5$ and the CKM elements. The functions f and κ in (5.42) are the phase-space factor and the next-to-leading order QCD corrections to the semileptonic decay [97, 98], respectively.

The numerical analysis will be restricted in the following to a certain domain of $\hat{s}$. Figure 5.2 serves as an illustration of these regions in terms of the dilepton invariant mass $q^2 = \hat{s}\, m_{b,pole}^2$. The upper panel corresponds to dilepton final states $l^+l^- = e^+e^-$ and the lower panel to $\mu^+\mu^-$, respectively. Events with dilepton invariant masses smaller than $\sqrt{q^2} < 0.2\,\text{GeV}$ were rejected in both experimental analysis of the Belle and the Barbar Collaboration. This corresponds to the lower cut in the e^+e^- channel which coincides almost with the lower kinematical $\mu^+\mu^-$ production threshold. We will use throughout for both channels the common lower cut of $\sqrt{q^2} = 2m_\mu$ in the following. Further cuts were applied around the $c\bar{c}$ resonances J/ψ and ψ' given in Table 5.5 and the interested reader is referred to Section 5.5 for explanations. Apart from the experimental cuts the importance of the two vertical lines at $\sqrt{q^2} = 2.4\,\text{GeV}$ and $4.25\,\text{GeV}$ has to be emphazised.

The first vertical line at $\sqrt{q^2} = 2.4\,\text{GeV}$ corresponds to the upper boundary of the validity of the two-loop matrix element calculation performed in [91]. This implies that the full NNLL prediction of the dilepton invariant mass distribution is restricted to the domain $\hat{s} \in [4m_\mu^2/m_{b,pole}^2,\, 0.25]$. The second vertical line at $\sqrt{q^2} = 4.25\,\text{GeV}$ corresponds to the upper boundary up to which the HQE applied to $\bar{B} \to X_s l^+ l^-$ is expected to hold [124]. Again the reader is referred to Section 5.5 for more details. The use of the expression for the dilepton invariant mass spectrum derived within the formalism of HQE, especially the perturbatively calculated quantity $R_{\rm quark}^{l^+l^-}(\hat{s})$ in combination with the non-perturbative $(\Lambda_{\rm QCD}/m_Q)^n$ corrections given in Section 5.5, for values above $\sqrt{q^2} = 4.25\,\text{GeV}$ becomes meaningless.

Finally, the dark shaded area in the range $\sqrt{q^2} \in [1.07,\, 2.4]\,\text{GeV}$ and accordingly $\hat{s} \in [0.05,\ 0.25]$ is called the *low-$\hat{s}$ region*. Theoretically it is preferred since non-perturbative effects are under control as will be shown in Section 5.5.

To investigate the scale dependence of $R_{\rm quark}^{l^+l^-}(\hat{s})$ in the SM the numerical values of Table 5.2 are used.

5.4.1 The Standard Model

As a first analysis it is interesting to investigate the magnitude of the single terms contributing to the ratio $R_{\rm quark}^{l^+l^-}(\hat{s})$ within the SM. Five different contributions appear in (5.35) that are $|\tilde{C}_9^{\rm eff}|^2$, $|\tilde{C}_{10}^{\rm eff}|^2$, $|\tilde{C}_7^{\rm eff}|^2$, the interference term $\text{Re}(\tilde{C}_7^{\rm eff}\tilde{C}_9^{\rm eff*})$ and the bremsstrahlung

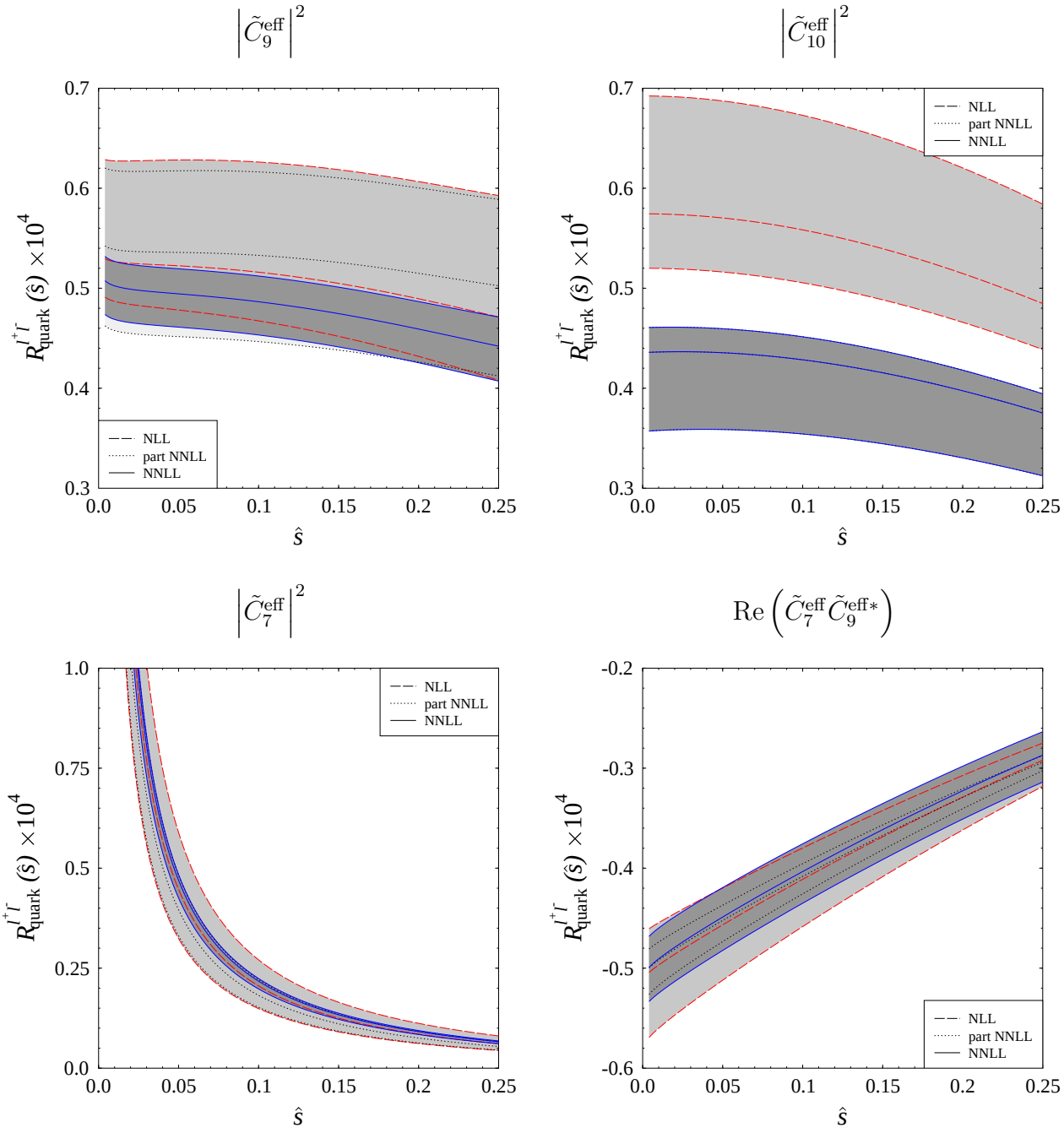

Figure 5.3: The scale dependencies at NLL, partial NNLL and NNLL order of the four parts $|\tilde{C}_9^{\text{eff}}|^2$, $|\tilde{C}_{10}^{\text{eff}}|^2$, $|\tilde{C}_7^{\text{eff}}|^2$ and $\text{Re}(\tilde{C}_7^{\text{eff}}\tilde{C}_9^{\text{eff}*})$ contributing to $R^{l^+l^-}_{\text{quark}}(\hat{s})$. In every plot all except one contribution are switched off in the calculation of $R^{l^+l^-}_{\text{quark}}(\hat{s})$ [see (5.41) and (5.35)]. The light-grey shaded regions correspond to the scale uncertainties of the NLL result and the dark-grey shaded to the scale uncertainties of the NNLL result, respectively.

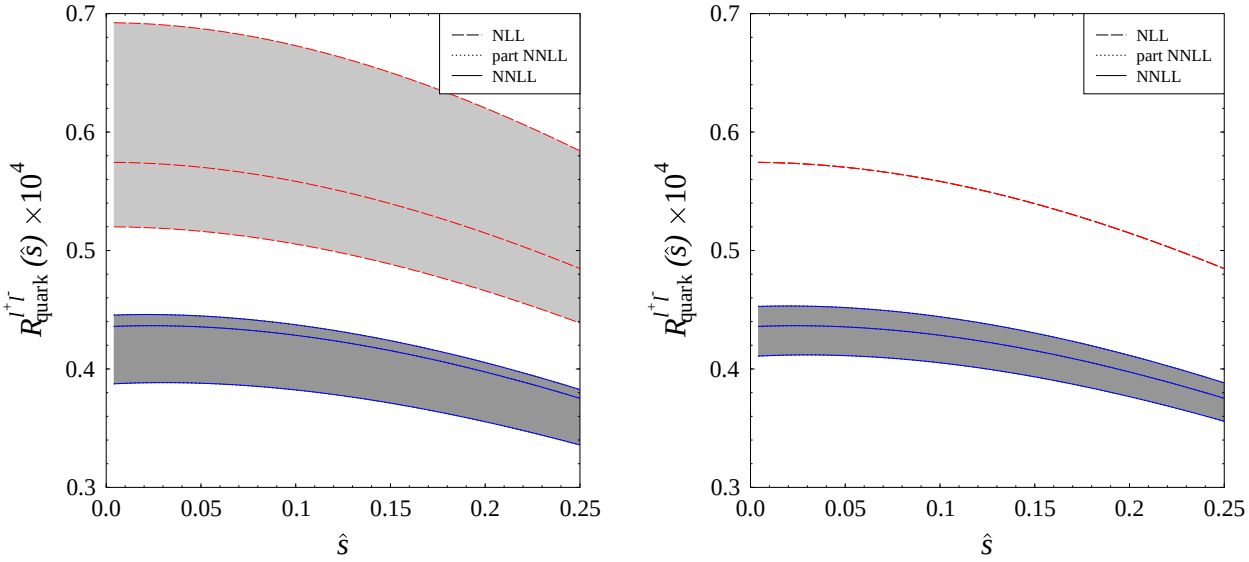

Figure 5.4: Renormalization scale dependence of the contribution $|\tilde{C}_{10}^{\text{eff}}|^2$ to $R^{l^+l^-}_{\text{quark}}(\hat{s})$. The left plot shows the matching scale μ_0 dependence while keeping the low energy scale $\mu = 5\,\text{GeV}$ fixed. The right plot shows the μ dependence while keeping $3/2\,\mu_0^c = \mu_0^t = 120\,\text{GeV}$ fixed.

corrections $\frac{d\Gamma^{\text{Brems,A}}}{d\hat{s}}$ and $\frac{d\Gamma^{\text{Brems,B}}}{d\hat{s}}$ of Ref. [92].

The result of $R^{l^+l^-}_{\text{quark}}(\hat{s})$ obtained by switching off all except one of these contributions is shown in Figure 5.3. Except for the tiny bremsstrahlung corrections being relevant only at the NNLL order the remaining four contributions are displayed at NLL, partial NNLL and NNLL order in the range $\hat{s} \in [4m_\mu^2/m_{b,pole}^2, 0.25]$. The dotted lines represent in all plots the partial NNLL result of Ref. [85] that can be obtained from eqs. (5.35) and (5.37) by setting all $\mathcal{M}_{\mathcal{O}_B,2}^{\mathcal{Q},\mathcal{O}_A}$, $\omega_{77}(\hat{s})$ and $\omega_{79}(\hat{s})$ to zero. The central curve of the NLL, partial NNLL and NNLL result corresponds to the following choice of renormalization scales: the low energy scale is set to the value $\mu = 5\,\text{GeV}$, the matching scale of the top sector to $\mu_0^t = 120\,\text{GeV}$ and the matching scale of the charm sector to $\mu_0^c = 80\,\text{GeV}$. The boundary curves of the accompanying grey shaded bands representing the renormalization scale uncertainties are obtained by varying the renormalization scales simultaneously in the ranges: $\mu \in [2.5,\, 10]\,\text{GeV}$ and $3/2\,\mu_0^c = \mu_0^t \in [60, 240]\,\text{GeV}$.

All four plots demonstrate the reduction of the renormalization scale dependence when going from NLL order to NNLL order. For example at the point $\hat{s} = 0.2$ the renormalization scale dependence of the contributions $|\tilde{C}_9^{\text{eff}}|^2$, $|\tilde{C}_{10}^{\text{eff}}|^2$, and $|\tilde{C}_7^{\text{eff}}|^2$ reduces from 16% $\to$ 7%, 14% $\to$ 12% and 30% $\to$ 6%, respectively. In the interference term $\text{Re}(\tilde{C}_7^{\text{eff}}\tilde{C}_9^{\text{eff}*})$ an accidental cancellation of the scale dependencies in the partial NNLL result occurs whereas the scale dependence of the NNLL result becomes only slightly reduced compared to the NLL, especially for larger values of $\hat{s}$. The by far largest scale uncertainty remains in the contribution $|\tilde{C}_{10}^{\text{eff}}|^2$. It should be noted that here the full NNLL result is already given by the partial NNLL result.

The contribution $|\tilde{C}_{10}^{\text{eff}}|^2$ to $R^{l^+l^-}_{\text{quark}}(\hat{s})$ is shown in Figure 5.4 once again this time varying the matching scale μ_0 (left plot) and the low energy scale μ (right plot) separately to shed

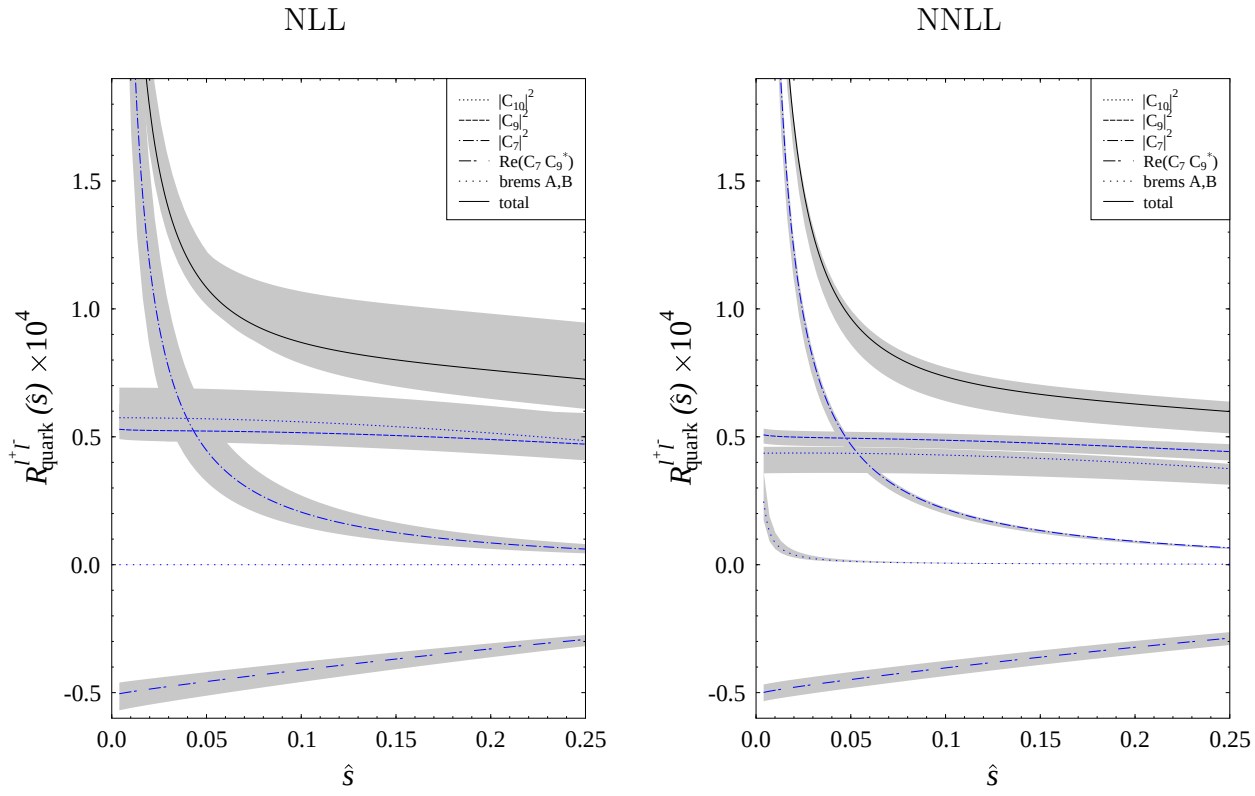

Figure 5.5: The final result of $R^{l^+l^-}_{\mathrm{quark}}(\hat{s})$ (solid line – "total") at NLL (left plot) and NNLL (right plot) order compared to the single contributions $|\tilde{C}_9^{\mathrm{eff}}|^2$, $|\tilde{C}_{10}^{\mathrm{eff}}|^2$, $|\tilde{C}_7^{\mathrm{eff}}|^2$ and $\mathrm{Re}(\tilde{C}_7^{\mathrm{eff}}\tilde{C}_9^{\mathrm{eff}*})$. In addition the NNLL order bremsstrahlung correction $\frac{d\Gamma^{\mathrm{Brems,A}}}{d\hat{s}}+\frac{d\Gamma^{\mathrm{Brems,B}}}{d\hat{s}}$ are shown, being almost negligible. The grey-shaded bands indicate the renormalization scale dependence obtained by varying μ_0 and μ as in Figure 5.3.

some light on the remaining scale dependency. At the NLL order the Wilson coefficient $\tilde{C}_{10}^{\mathrm{eff}}$ is independent of the low energy scale μ because of vanishing anomalous dimension. Therefore a variation of μ will not affect the NLL result as can be seen in the right plot. The matching scale μ_0 dependence of $\tilde{C}_{10}^{\mathrm{eff}}$ occurs implicitly due to its strong $\overline{\mathrm{MS}}$-top quark mass dependence. The variation of the μ_0 as in Figure 5.3 yields therefore the same result as shown there. At the NNLL order $\tilde{C}_{10}^{\mathrm{eff}}$ becomes μ dependent due to the inclusion of the one-loop matrix element of $\mathcal{O}_{10}$. The variation of the matching scale μ_0, while keeping $\mu = 5\,\mathrm{GeV}$ fixed, in the left plot exhibits a significant reduction of the μ_0 dependence due to the inclusion of the two-loop matching contributions to the Wilson coefficient. However, the remaining μ_0 dependence is as large as the μ dependence shown in the right plot when varying $\mu \in [2.5,\,10]\,\mathrm{GeV}$ while keeping $3/2\,\mu_0^c = \mu_0^t \in [60, 240]\,\mathrm{GeV}$ fixed. Both scale dependencies are equal in size and add up to the final result shown in Figure 5.3. A considerable improvement concerning the μ_0 and the μ dependence requires the calculation of higher order corrections.

The detailed discussion of the scale dependence of the particular contributions to $R^{l^+l^-}_{\mathrm{quark}}(\hat{s})$ has shown the importance of the inclusion of NNLL corrections. In the following the final scale dependence of $R^{l^+l^-}_{\mathrm{quark}}(\hat{s})$ resulting from the summation of all contributions will be

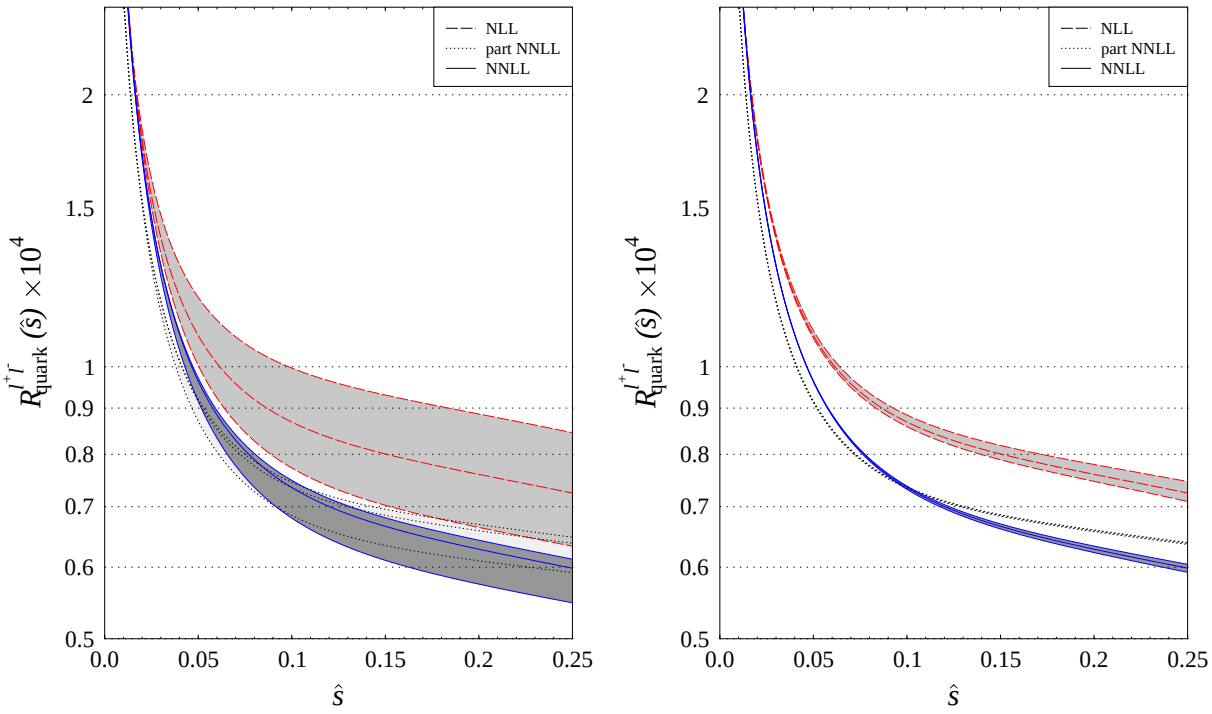

Figure 5.6: Reduction of the μ_0-matching scale dependence of $R^{l^+l^-}_{\text{quark}}(\hat{s})$. In the left plot the matching scale μ_0^t is varied while keeping the matching scale μ_0^c and the low energy scale μ fixed. In the right plot μ_0^c is varied while keeping μ_0^t and μ fixed. Note the logarithmic scale of the vertical axis.

considered. Figure 5.3 shows that the contributions due to $\tilde{C}_9^{\text{eff}}$ and $\tilde{C}_{10}^{\text{eff}}$ are similar in size varying only slightly over the examined range of $\hat{s}$. In general the magnitude of NNLL corrections tend to decrease somewhat the NLL result for $\tilde{C}_9^{\text{eff}}$ which has to be compared to a clear reduction of about 30% in the case of $\tilde{C}_{10}^{\text{eff}}$. The contribution of $\tilde{C}_7^{\text{eff}}$ changes strongly over the $\hat{s}$ region. It turns out to be small for values above $\hat{s} > 0.1$ whereas it dominates the other three contributions when approaching the lower boundary for $\hat{s}$. The size of the NNLL corrections is negligible although the scale dependencies become definitely smaller. Remarkably, the interference term $\text{Re}(\tilde{C}_7^{\text{eff}} \tilde{C}_9^{\text{eff}*})$ has opposite sign compared to the three contributions discussed before. It changes by about 30% in magnitude over the considered $\hat{s}$ range almost canceling for example the contribution of $\tilde{C}_9^{\text{eff}}$ for small values of $\hat{s}$. The NNLL corrections only mildly change the NLL result decreasing its absolute magnitude. In view of extensions of the SM it should be mentioned that the measured value of the branching ratio of $\bar{B} \to X_s \gamma$ provides a severe constraint of the absolute magnitude of $\tilde{C}_7^{\text{eff}}$, however not on its sign. New physics models that predict $\tilde{C}_7^{\text{eff}}$ with opposite sign compared to the SM could exhibit therefore an enhanced prediction of the channel $\bar{B} \to X_s l^+ l^-$ because then the sign of the interference term becomes reversed.

In Figure 5.5 the final result for $R^{l^+l^-}_{\text{quark}}(\hat{s})$ can be seen. The left plot shows the summed NLL result (solid line – "total") and also the single contributions to illustrate their magnitude. The shaded bands represent the scale dependencies arising from the variation of

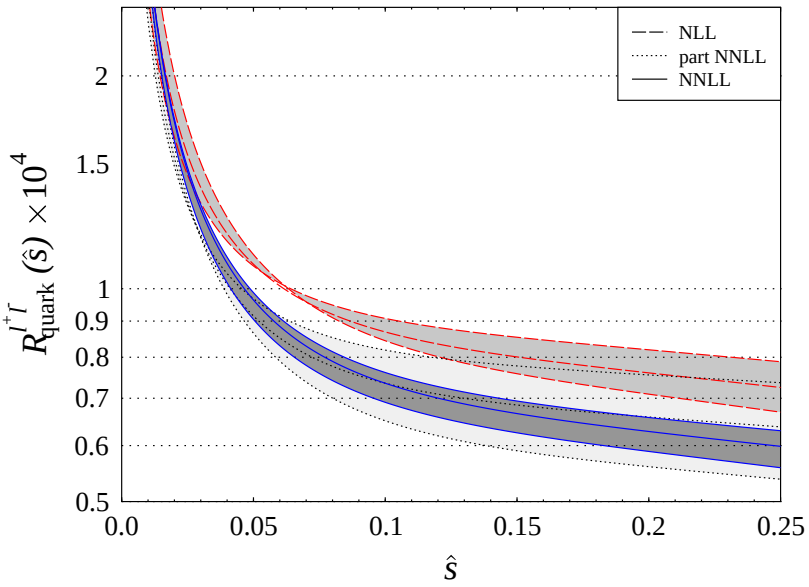

Figure 5.7: Reduction of the low energy scale μ dependence of $R^{l^+l^-}_{\rm quark}(\hat{s})$. Note the logarithmic scale of the vertical axis.

the renormalization scales μ and μ_0 as discussed in connection with Figure 5.3 above. Here again the central curves correspond to the choice of the scales $\mu = 5\,\text{GeV}$, $\mu_0^t = 120\,\text{GeV}$ and $\mu_0^c = 80\,\text{GeV}$. Moreover the contribution of the bremsstrahlung corrections $\frac{d\Gamma^{\text{Brems,A}}}{d\hat{s}}$ and $\frac{d\Gamma^{\text{Brems,B}}}{d\hat{s}}$ are shown being zero in the NLL case. These corrections to the NNLL result are very small [92] and can be seen in the right plot. Summarizing, in the SM the inclusion of the NNLL corrections to $R^{l^+l^-}_{\rm quark}(\hat{s})$ lead to a significant reduction of the renormalization scale and decrease the magnitude of the theoretical prediction as can be seen in the right plot.

To complete the discussion of the scale dependence of $R^{l^+l^-}_{\rm quark}(\hat{s})$ in the following the particular dependence on μ_0^t, μ_0^c and μ is discussed.

Figure 5.6 shows the dependence of $R^{l^+l^-}_{\rm quark}(\hat{s})$ on the matching scale μ_0 when using the NLL and the NNLL expression. In the left plot the matching scale μ_0^t of the top sector is varied by a factor of 2 around $\sqrt{M_W m_t}$ corresponding to $\mu_0^t = \{60,\ 120,\ 240\}\,\text{GeV}$ and the matching scale of the charm sector is fixed to the value $\mu_0^c = M_W \approx 80\,\text{GeV}$. Analogously the right plot corresponds to varying the matching scale μ_0^c of the charm sector by a factor of 2 around M_W according to the values $\mu_0^c = \{40,\ 80,\ 160\}\,\text{GeV}$ and keeping the matching scale of the top sector $\mu_0^t = \sqrt{M_W m_t} \approx 120\,\text{GeV}$ fixed. In both plots the low energy scale is set to $\mu = 5\,\text{GeV}$.

The importance of including the two-loop matching conditions in the top sector is clearly seen. For example at the point $\hat{s} = 0.2$ the dependence on μ_0 decreases from $\pm 16\%$ to around $\pm 6\%$. Actually in the top sector the NLL contribution is the leading one in comparison to the charm sector were the first nonzero contribution is the LL result. Most of the effect is due to the strong m_t-dependence of C_{10}^t and to the μ_0-dependence of the $\overline{\text{MS}}$ top quark mass as already discussed in connection with Figure 5.4.

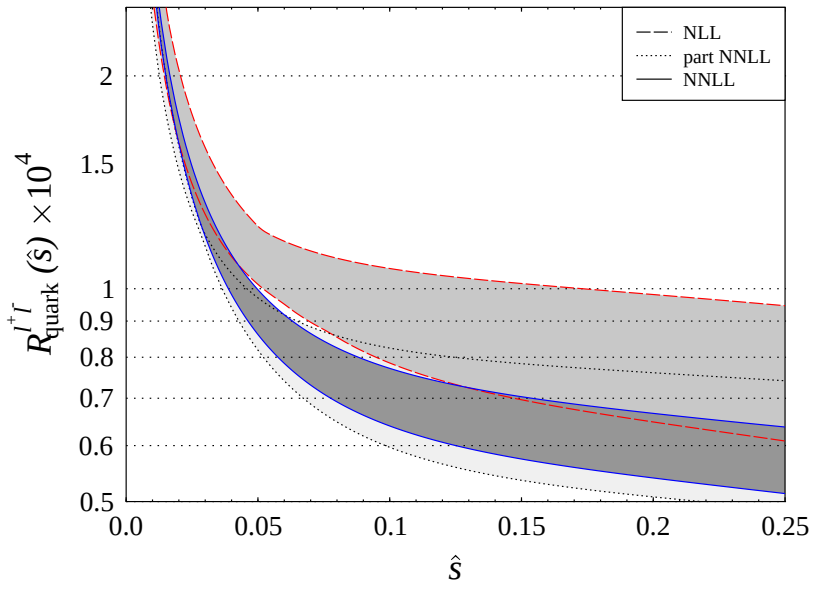

Figure 5.8: Reduction of the matching scale μ_0 and the low energy scale μ dependence of $R^{l^+l^-}_{\text{quark}}(\hat{s})$. Note the logarithmic scale of the vertical axis.

The inclusion of the two-loop matching conditions in the charm sector also reduces the matching scale dependence. However, in the combination of the LL and NLL results the matching scale dependence is already significantly smaller compared to the one of the NLL result of the top sector. The partial NNLL result exhibits a smaller μ_0 dependence [see right plot of Figure 5.6] compared to the full NNLL result because of the negligence of the terms $\mathcal{M}^{Q,\mathcal{O}_A}_{\mathcal{O}_B,2}$ which depend on $C_i^{c(1)}(\mu)$ and bear also a μ_0 dependence.

Apart from the reduction of the scale dependence the NNLL QCD corrections are in general quite sizeable decreasing the NLL result for example at the point $\hat{s} = 0.2$ by more than 20%.

The scale dependence of the NLL and the NNLL result of $R^{l^+l^-}_{\text{quark}}(\hat{s})$ on the low energy scale μ is shown in Figure 5.7. Again the partial NNLL result is portrayed by the dotted lines. The matching scale of the top sector and the charm sector are set to $\mu_0^t = \sqrt{M_W m_t} \approx 120\,\text{GeV}$ and $\mu_0^c = M_W \approx 80\,\text{GeV}$. The low energy scale μ is chosen to be $\mu = \{2.5,\ 5,\ 10\}\,\text{GeV}$.

Here the inclusion of all NNLL corrections to $R^{l^+l^-}_{\text{quark}}(\hat{s})$ does not decrease the μ-dependence of the NLL result significantly. In the NLL expression an accidental cancellation of the μ-dependence occurs among the different contributions to the differential decay rate in eq. (5.35). This cancellation becomes exact at $\hat{s} \approx 0.06$.

The analysis in Ref. [85] has shown that the strong μ-dependence of the partial NNLL result is mainly driven by the $\mathcal{O}(\alpha_s)$ term proportional to the product of $C^{c(1)}(\mu_0) = -15 - 6\ln(\mu_0^2/M_W^2)$ and the logarithm $\ln(m_b/\mu)$ of the one-loop matrix element of $\mathcal{O}_1^c$. The inclusion of the two-loop matrix element of the four-quark operators significantly reduces the μ-dependence.

Finally, the Figure 5.8 is obtained summarizing all the scale dependencies due to the

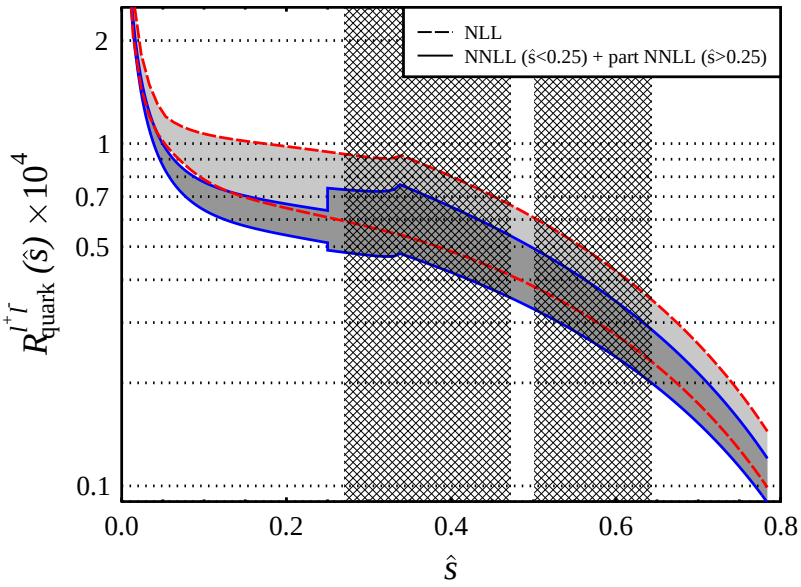

Figure 5.9: $R^{l^+l^-}_{\text{quark}}(\hat{s})$ calculated over the entire $\hat{s}$-range of validity of the HQE. The dashed lines show the NLL result and the uncertainties due to renormalization scale variation. The solid lines correspond to the full NNLL result up to $\hat{s} < 0.25$ and the partial NNLL result above $\hat{s} > 0.25$. The increased uncertainties of the partial NNLL prediction starting at the point $\hat{s} = 0.25$ can be clearly seen. Note the logarithmic scale of the vertical axis.

variation of the matching scales μ_0^t and μ_0^c about a factor of 2 around the values $\mu_0^t = \sqrt{M_W m_t}$ and $\mu_0^c = M_W$, respectively and the low energy scale between $\mu \in [2.5,\, 10]\,\text{GeV}$. As a survey this plot combines both plots of Figure 5.5.

Concluding within the SM the two-loop matching contributions calculated in (5.9) decrease the dilepton invariant decay distribution compared to the NLL calculation and reduce the theoretical uncertainty due to the matching scale μ_0 dependence. The inclusion of two-loop matrix elements and bremsstrahlung corrections improves the predictions due to a further reduction of the low energy scale μ dependence resulting in a almost complete NNLL prediction. As explained in the Section 5.3 the complete NNLL result still deserves the calculation of some two-loop matrix elements and more importantly the extension of the calculation to values of $\hat{s} > 0.25$. The authors of [93, 100, 101] report about a calculation of the two-loop matrix elements, valid in the entire range of $\hat{s}$, however the results are not yet publicly available. Therefore the perturbative quantity $R^{l^+l^-}_{\text{quark}}(\hat{s})$ can be calculated only at partial NNLL order for values above $\hat{s} > 0.25$.

Figure 5.9 summarizes the result of $R^{l^+l^-}_{\text{quark}}(\hat{s})$ within the SM over the entire $\hat{s}$-range of validity of the HQE. The full NNLL (solid lines) calculation can be used up to values of $\hat{s} < 0.25$ whereas for values above $\hat{s} > 0.25$ the partial NNLL order result is used. For comparison the dashed lines represent the NLL result. The bands correspond to the variation of renormalization scales as in Figure 5.8 rendering the perturbative uncertainties. The grided areas show the cuts applied by the Belle Collaboration around the J/ψ and ψ' resonances as

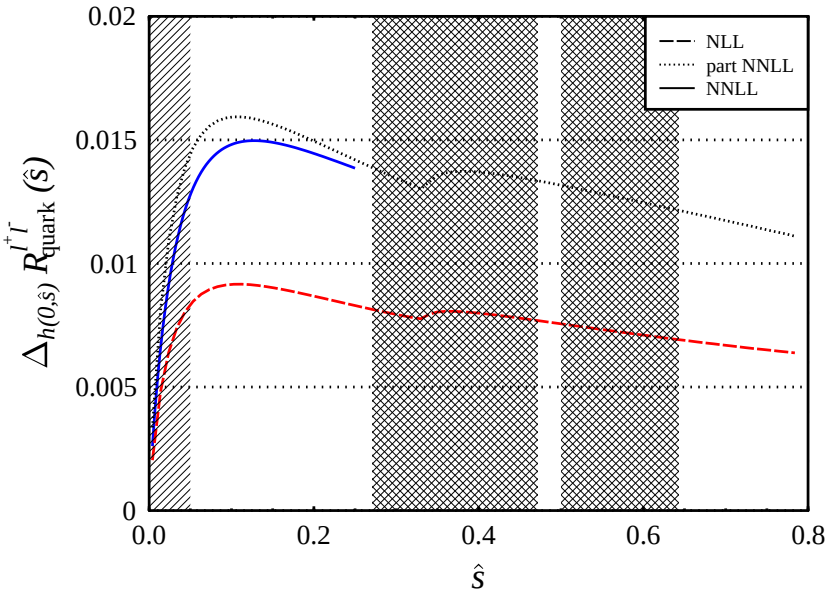

Figure 5.10: The relative contribution of the function $h(0,\hat{s})$ to $R^{l^+l^-}_{\text{quark}}(\hat{s})$ expressed through $\Delta_{h(0,\hat{s})} R^{l^+l^-}_{\text{quark}}(\hat{s})$.

given in Figure 5.2 and Table 5.5. In these regions the dilepton invariant mass distribution is also not accessible by the HQE due to intermediate $c\bar{c}$-resonances as will be explained in Section 5.5. For the time being it shall be just mentioned that the result of $R^{l^+l^-}_{\text{quark}}(\hat{s})$ is not valid in this two domains.

For later purposes the following two ratios are defined

$$\Delta_{h(0,\hat{s})} R^{l^+l^-}_{\text{quark}}(\hat{s}) \equiv \frac{R^{l^+l^-}_{\text{quark}}(\hat{s}) - R^{l^+l^-}_{\text{quark}}(\hat{s})\Big|_{h(0,\hat{s})=0}}{R^{l^+l^-}_{\text{quark}}(\hat{s})} \tag{5.43}$$

and

$$\Delta_{V^*_{us}V_{ub}} R^{l^+l^-}_{\text{quark}}(\hat{s}) \equiv \frac{R^{l^+l^-}_{\text{quark}}(\hat{s}) - R^{l^+l^-}_{\text{quark}}(\hat{s})\Big|_{V^*_{us}V_{ub}=0}}{R^{l^+l^-}_{\text{quark}}(\hat{s})}. \tag{5.44}$$

As will be explained in Section 5.5 the function $h(0,\hat{s})$ receives non-perturbative corrections which can not be addressed in HQE in the region of $\hat{s} < 0.05$. These contributions due to resonant light quark (u,d,s) intermediate states are expected to be of the same size as the perturbative result $h(0,\hat{s})$ itself, after taking an average over a sufficiently wide region of $\hat{s}$. The quantity $\Delta_{h(0,\hat{s})} R^{l^+l^-}_{\text{quark}}(\hat{s})$ measures the relative magnitude of the perturbative $h(0,\hat{s})$ to $R^{l^+l^-}_{\text{quark}}(\hat{s})$ and is shown in Figure 5.10. The solid line corresponds to the NNLL result being only valid up to $\hat{s} = 0.25$ whereas the NLL and the partial NNLL results are shown over the entire range of validity of the HQE. The renormalization scales are fixed to the mean

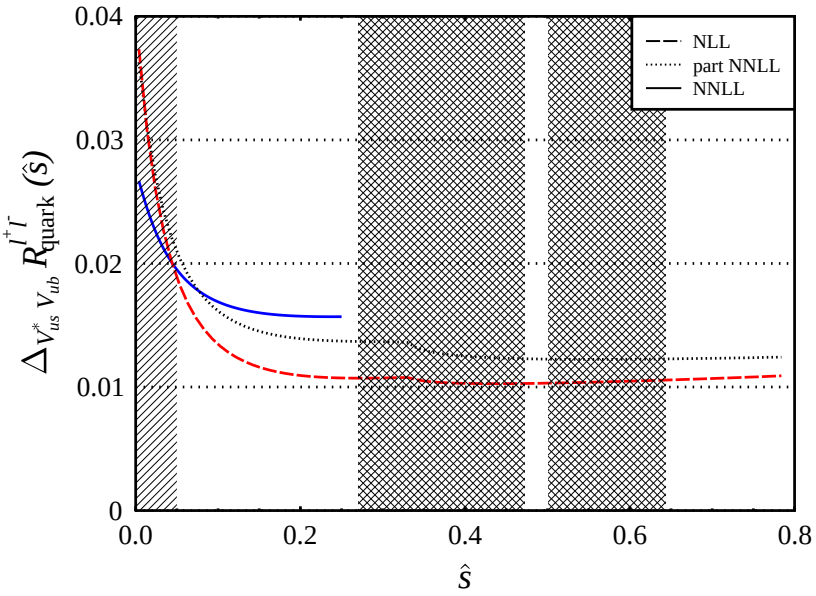

Figure 5.11: The relative contribution of the up-quark sector to $R^{l^+l^-}_{\text{quark}}(\hat{s})$ expressed through $\Delta_{V_{us}^* V_{ub}} R^{l^+l^-}_{\text{quark}}(\hat{s})$.

values of $3/2\mu_0^c = \mu_0^t = 120\,\text{GeV}$ and $\mu = 5\,\text{GeV}$. For all three results the contribution of the perturbative $h(0,\hat{s})$ to the dilepton invariant mass distribution is below 1.5% over the entire region of $\hat{s}$. This allows the conclusions that the tails of the non-perturbative corrections that perhaps continue to the region above $\hat{s} > 0.05$ introduce a negligible uncertainty to $R^{l^+l^-}_{\text{quark}}(\hat{s})$[7]. The shaded region at the left of Figure 5.10 marks the region of $\hat{s} < 0.05$ whereas the two grided regions show the cuts applied by the Belle Collaboration around the J/ψ and ψ' resonances.

The second quantity $\Delta_{V_{us}^* V_{ub}} R^{l^+l^-}_{\text{quark}}(\hat{s})$ yields the size of the contribution of the dilepton invariant mass distribution due to the up-quark sector that is proportional to the CKM element combination $V_{us}^* V_{ub}$ and therefore strongly suppressed. Figure 5.11 displays the NLL, the partial NNLL and the NNLL order result. Here it should be noted again, as already explained in Section 5.3, that the two-loop matrix elements $\mathcal{M}_{7,2}^{u,\{1,2\}}$ and $\mathcal{M}_{9,2}^{u,\{1,2\}}$ are not calculated yet. In view of this the NNLL result should not be considered as complete as for example the corresponding results of the charm sector where the according two-loop matrix elements $\mathcal{M}_{7,2}^{c,\{1,2\}}$ and $\mathcal{M}_{9,2}^{c,\{1,2\}}$ lead to a significant reduction of the μ dependence. Nevertheless, the relative magnitude of the up-quark sector is smaller than 2% for values of $\hat{s} > 0.05$ and does not exceed the 4% level below $0.05 < \hat{s}$. The ignorance of the two-loop matrix elements of the up-quark sector therefore induces only a small theoretical uncertainty in the prediction of $R^{l^+l^-}_{\text{quark}}(\hat{s})$. The significant reduction of the NNLL result in the region $0.05 < \hat{s}$ with respect to the NLL and partial NNLL result and vice versa for $\hat{s} > 0.05$ is a consequence of the contribution of $\mathcal{M}_{7,2}^{u,8}$ and $\mathcal{M}_{9,2}^{u,8}$.

[7]Similar corrections due to $c\bar{c}$ resonances affecting $h(\hat{m}_c,\hat{s})$ will be discussed in Section 5.5 under the key word $\Lambda^2_{\text{QCD}}/m_c^2$ corrections.

Figure	NLL	partial NNLL	NNLL
5.6 (left)	1.78 ± 0.23	1.45 ± 0.06	1.43 ± 0.07
5.6 (right)	1.75 ± 0.03	1.49 ± 0.003	1.47 ± 0.01
5.7	1.76 ± 0.09	1.50 ± 0.19	1.45 ± 0.07
5.8	1.83 ± 0.36	1.44 ± 0.25	1.41 ± 0.14

Table 5.3: The perturbatively calculable branching ratio $\mathcal{B}[b \to X_s l^+ l^-]$ in units of 10^{-6} obtained from the Figures 5.6 – 5.8 by integrating over the low-$\hat{s}$ region $\hat{s} \in [0.05, 0.25]$.

The investigation of the perturbative quantity $R^{l^+l^-}_{\text{quark}}(\hat{s})$ shall be stopped here. As anticipated the existence of non-perturbative effects due to intermediate light hadron states for $\hat{s} < 0.05$ and the intermediate $c\bar{c}$ states at higher values of $\hat{s}$ divides the dilepton invariant mass distribution into several regions. The theoretically favored region is the so-called *low-$\hat{s}$* region

$$\hat{s} \in [0.05,\, 0.25] \tag{5.45}$$

since it is completely free of non-perturbative corrections beyond the HQE and the almost complete NNLL perturbative result is available. A second similar domain is represented by the region

$$\hat{s} \in [0.64,\, 0.78] \tag{5.46}$$

above the ψ' resonance referred to as the *high-$\hat{s}$* region in the following. Within this region the partial NNLL expression will be used for $R^{l^+l^-}_{\text{quark}}(\hat{s})$.

The Branching Ratio

It is illustrative to integrate $R^{l^+l^-}_{\text{quark}}(\hat{s})$ over $\hat{s}$ in the low- and high-$\hat{s}$ regions as introduced above. This quantity corresponds up to the factor of the semileptonic branching ratio $\mathcal{B}[\bar{B} \to X_c e \bar{\nu}_e] \approx 10.58\%$ to the perturbatively calculable branching ratio

$$\mathcal{B}[b \to X_s l^+ l^-] \equiv \mathcal{B}[\bar{B} \to X_c e \bar{\nu}_e] \int d\hat{s}\, R^{l^+l^-}_{\text{quark}}(\hat{s}). \tag{5.47}$$

Table 5.3 collects the results of $\mathcal{B}[b \to X_s l^+ l^-]$ corresponding to the integration over $\hat{s}$ in the low-$\hat{s}$ region. To show the size of the different renormalization scale dependencies the scales μ_0^t, μ_0^c and μ were varied separately and together according to the Figures 5.6–5.8. The variation of μ shows an accidental cancellation of scale dependencies in the NLL order result compared to the partial NNLL order result. The residual scale dependence of the NLL result of 20% can be reduced to a final scale dependence of 10% of the NNLL result. However, the physical measurable hadronic branching ratio $\mathcal{B}[\bar{B} \to X_s l^+ l^-]$ still receives beside the perturbative contribution $\mathcal{B}[b \to X_s l^+ l^-]$ non-perturbative corrections. The discussion of non-perturbative corrections and the associated uncertainties is postponed to Section 5.5.

Figure	NLL	partial NNLL
5.6 (left)	2.91 ± 0.39	2.59 ± 0.09
5.6 (right)	2.87 ± 0.07	2.65 ± 0.02
5.7	2.88 ± 0.21	2.66 ± 0.35
5.8	2.99 ± 0.67	2.57 ± 0.42

Table 5.4: The perturbatively calculable branching ratio $\mathcal{B}[b \to X_s l^+ l^-]$ in units of 10^{-7} obtained by integrating over the high-$\hat{s}$ region $\hat{s} \in [0.64, 0.78]$ and varying the scales as in figures 5.6 – 5.8.

Table 5.4 presents the analogous results $\mathcal{B}[b \to X_s l^+ l^-]$ integrating over the high-$\hat{s}$ region $\hat{s} \in [0.64, 0.78]$. The branching fraction is considerably smaller and the inclusion of the missing two-loop matrix elements is desirable to reduce the low energy scale μ dependence. The accidental cancellation of the scale dependencies again show up in the NLL order result. However, the inclusion of the two-loop matching contributions in the partial NNLL order analysis reduces the residual scale dependence from $\pm 22\%$ to $\pm 16\%$ whereas the absolute value of the branching ratio becomes reduced by 14%. It should be noted that a similar value was reported in the very recent publication [102] in eq. (17). Experimentally the high-$\hat{s}$ region is expected to be as important as the low-$\hat{s}$ region since a comparable number of events is collected here.

We refrain from calculating the so-called "non-resonant" branching ratio at the quark level. The "non-resonant" branching ratio can be found when integrating over the full range of $\hat{s}$. This would imply the inappropriate use of the perturbative quantity $R^{l^+l^-}_{\text{quark}}(\hat{s})$ outside the low- and high-$\hat{s}$ region. Since the theoretical methods are not valid no reliable estimate of uncertainties can be given. Further, for example the $c\bar{c}$ resonances are removed by explicte cuts in the experimental analysis. The inclusion of these regions into the theoretical result by the inappropriate use of $R^{l^+l^-}_{\text{quark}}(\hat{s})$ and analogously on the experimental side to extrapolate to these regions does not add any information. The circumstances do not change when including the non-perturbative corrections that are calculable in the HQE framework being matter of discussion in Section 5.5. This method is not applicable outside the low- and high-$\hat{s}$ region concerning intermediate light quark and $c\bar{c}$ resonances. Values of the "non-resonant" branching ratio can be found for example in [103].

5.4.2 The MSSM

We will adopt the following procedure in the subsequent numerical analysis of the MSSM results within the considered scenario inspired by minimal flavor violation and a heavy decoupled gluino.

We restrict our attention to low values of $\tan\beta$. As already mentioned in section 4.2, this will avoid large neutral Higgs mediated contributions and further non-QCD higher order corrections play a minor role.

The decay $\bar{B} \to X_s l^+ l^-$ essentially involves the CKM element V_{ts}. It is important to emphasize that the presence of new-physics contributions may not only affect the decay modes under study but also B^0_q–$\bar{B}^0_q$ mixing and the CP violation parameter ϵ_K, and consequently the extraction of the CKM elements V_{td} and V_{ts}. In this case, the standard analysis

of the unitarity triangle may lead to false results. In fact, while to a good approximation $|V_{ts}| \approx |V_{cb}|$, is independent of new-physics effects, the value of V_{td} determined using the SM formulae might differ from that obtained in the context of the MSSM [see, e.g., [58,71,104]].

Since we are mainly interested in the renormalization scale dependence and the size of QCD corrections to the dilepton invariant mass spectrum and the branching ratio, rather than on their actual values, we fix $|V_{td}|$ to the SM obtained from the standard parameterization of the CKM matrix as given in Table 5.2. Note that this treatment is different from the analysis of [104], where the new-physics effects on V_{td} have also been taken into account.

Our calculation is based on the assumption of soft supersymmetry breaking terms inspired by minimal flavor violation as outlined in section 4.2. Furthermore, we assume that there are no new CP-violating phases in addition to the single phase residing in the CKM matrix.

Since we ignore flavor-mixing effects among squarks, the matrix in (4.7) decomposes into three 2×2 matrices. A noticeable feature is that the left-right terms are proportional to the masses of the up-type quarks. Hence, large mixing can occur in the scalar top quark sector, leading to a mass eigenstate, say, $\tilde{t}_1$, possibly much lighter than the remaining squarks. We therefore keep left-right mixing only in the stop sector, hence the mass matrix is given by

$$M_{\tilde{t}}^2 = \begin{pmatrix} m_{\tilde{t}_L}^2 + m_t^2 + \frac{1}{6} M_Z^2 \cos 2\beta (3 - 4 s_W^2) & m_t (A_t - \mu \cot \beta) \\ m_t (A_t - \mu \cot \beta) & m_{\tilde{t}_R}^2 + m_t^2 + \frac{2}{3} M_Z^2 \cos 2\beta s_W^2 \end{pmatrix}, \tag{5.48}$$

where $m_{\tilde{t}_{L,R}}$ are the soft SUSY breaking scalar masses and A_t is the trilinear coupling. In this framework, the mixing matrices Γ^{U_L} and Γ^{U_R} (4.12a) take the simple form

$$(\Gamma^{U_L})^{\mathrm{T}} = \begin{pmatrix} 1 & 0 & 0 & 0 & 0 & 0 \\ 0 & 1 & 0 & 0 & 0 & 0 \\ 0 & 0 & \cos\theta_{\tilde{t}} & 0 & 0 & -\sin\theta_{\tilde{t}} \end{pmatrix}, \tag{5.49a}$$

$$(\Gamma^{U_R})^{\mathrm{T}} = \begin{pmatrix} 0 & 0 & 0 & 1 & 0 & 0 \\ 0 & 0 & 0 & 0 & 1 & 0 \\ 0 & 0 & \sin\theta_{\tilde{t}} & 0 & 0 & \cos\theta_{\tilde{t}} \end{pmatrix}. \tag{5.49b}$$

The physical mass eigenstates are then given by

$$\tilde{t}_1 = \cos\theta_{\tilde{t}} \tilde{t}_L + \sin\theta_{\tilde{t}} \tilde{t}_R, \qquad \tilde{t}_2 = -\sin\theta_{\tilde{t}} \tilde{t}_L + \cos\theta_{\tilde{t}} \tilde{t}_R, \tag{5.50}$$

with the mixing angle $(-\pi/2 \leqslant \theta_{\tilde{t}} \leqslant \pi/2)$

$$\sin 2\theta_{\tilde{t}} = \frac{2 m_t (A_t - \mu \cot\beta)}{m_{\tilde{t}_1}^2 - m_{\tilde{t}_2}^2}, \tag{5.51a}$$

$$\cos 2\theta_{\tilde{t}} = \frac{(m_{\tilde{t}_L}^2 - m_{\tilde{t}_R}^2) + \frac{1}{6} M_Z^2 \cos 2\beta (3 - 8 s_W^2)}{m_{\tilde{t}_1}^2 - m_{\tilde{t}_2}^2}, \tag{5.51b}$$

$m_{\tilde{t}_{1,2}}$ being the stop masses with $m_{\tilde{t}_1}^2 < m_{\tilde{t}_2}^2$. (The remaining up-type squark masses are taken to be equal.)

For simplicity, we assume that the scalar partners of the leptons are degenerate in mass. They appear in the functions $[B^{l\bar{l}}]_{\tilde{\chi}}$ originating from box-diagrams which are rather small.

For the results presented below we take into account the following lower bounds on the SUSY particle masses [105–107]

$$m_{\tilde{t}_1,\tilde{b}_1} \gtrsim 100 \text{ GeV}, \quad m_{\tilde{q}\neq\tilde{t}_1,\tilde{b}_1} \gtrsim 260 \text{ GeV}, \quad m_{\tilde{l},\tilde{\nu}} \gtrsim 100 \text{ GeV}, \quad M_{\tilde{\chi}_1} \gtrsim 100 \text{ GeV}. \quad (5.52)$$

As far as the lightest neutral Higgs boson, h^0, is concerned, we must ensure that $M_{h^0} \gtrsim 100$ GeV [107,108], taking into account radiative corrections [109–112] to the tree-level mass defined in (4.2b).

To determine the impact of the QCD corrections on the quantity $R^{l^+l^-}_{\text{quark}}(\hat{s})$, we examine its renormalization scale dependence, namely the matching scale μ_0 dependence, for two points in the SUSY parameter space. For definiteness, we have chosen the following SUSY parameter sets:

$$\text{Point 1:} \quad \begin{cases} m_{\tilde{t}_1} = 150 \text{ GeV}, \ m_{\tilde{t}_2} = 500 \text{ GeV}, \ \theta_{\tilde{t}} = 40^\circ, \\ M_2/\mu = -4, \end{cases} \quad (5.53)$$

$$\text{Point 2:} \quad \begin{cases} m_{\tilde{t}_1} = 200 \text{ GeV}, \ m_{\tilde{t}_2} = 800 \text{ GeV}, \ \theta_{\tilde{t}} = 70^\circ, \\ M_2/\mu = 4. \end{cases} \quad (5.54)$$

Further we set $\tan\beta = 3$, the charged Higgs mass $M_H = 250$ GeV, the gluino mass $M_{\tilde{g}} = 1$ TeV and the slepton masses $m_{\tilde{l},\tilde{\nu}} = 100$ GeV. The lighter chargino mass is fixed to the value $M_{\tilde{\chi}} = 140$ GeV which determines in combination with the ratio M_2/μ and $\tan\beta$ the remaining quantities of the chargino sector completely.

In Figure 5.12 $R^{l^+l^-}_{\text{quark}}(\hat{s})$ is shown when taking into account only the "top-quark – charged Higgs" contribution in addition to the SM. Two different values of the charged Higgs mass are chosen, $M_H = 250$ GeV and $M_H = 450$ GeV, respectively, whereas $\tan\beta = 3$. For comparison also the SM NNLL result is shown. The charged Higgs contributions do not affect the dilepton invariant mass region in the low-$\hat{s}$ region strongly. In this region $R^{l^+l^-}_{\text{quark}}(\hat{s})$ is dominated by $\tilde{C}_9^{\text{eff}}$ and $\tilde{C}_{10}^{\text{eff}}$ as can be seen in Figure 5.5. In both the new physics contribution is proportional to $\cot^2\beta \sim 0.1$ appearing in the functions $[C_9^{l\bar{l}}]_H$ and $[D_9^{l\bar{l}}]_H$ of Appendix C. When going to smaller values of $\hat{s} < 0.05$ the effects become larger due to the increasing influence of $\tilde{C}_7^{\text{eff}}$. For larger values of the charged Higgs mass the effects of new physics become smaller which can be interpreted as a decoupling effect. Both plots show the reduced matching scale dependence due to the inclusion of the two-loop matching conditions of the NNLL result in comparison to the NLL result.

Figure 5.13 represents $R^{l^+l^-}_{\text{quark}}(\hat{s})$ in the considered scenario of the MSSM. The left plot corresponds to the parameter set "Point 1" where the MSSM corrections are rather large for small values of $\hat{s}$. It should be noted, that the NNLL corrections significantly reduce the NLL result. The branching ratio obtained by integration over $\hat{s}$ amounts to $(2.02 \pm 0.26)\,10^{-6}$ and $(1.58 \pm 0.07)\,10^{-6}$ for the NLL and the NNLL result, respectively. These numbers can be compared to the SM result of Table 5.3. The quoted uncertainties are obtained by the variation of the matching scale μ_0 only as in SM shown in Figure 5.6. Choosing the parameter set "Point 1" enhances the branching ratio by 10% compared to the SM prediction.

The right plot of Figure 5.13 shows $R^{l^+l^-}_{\text{quark}}(\hat{s})$ for the choice of the the parameter set "Point 2". The new physics contributions are very small. The comparison with the left plot

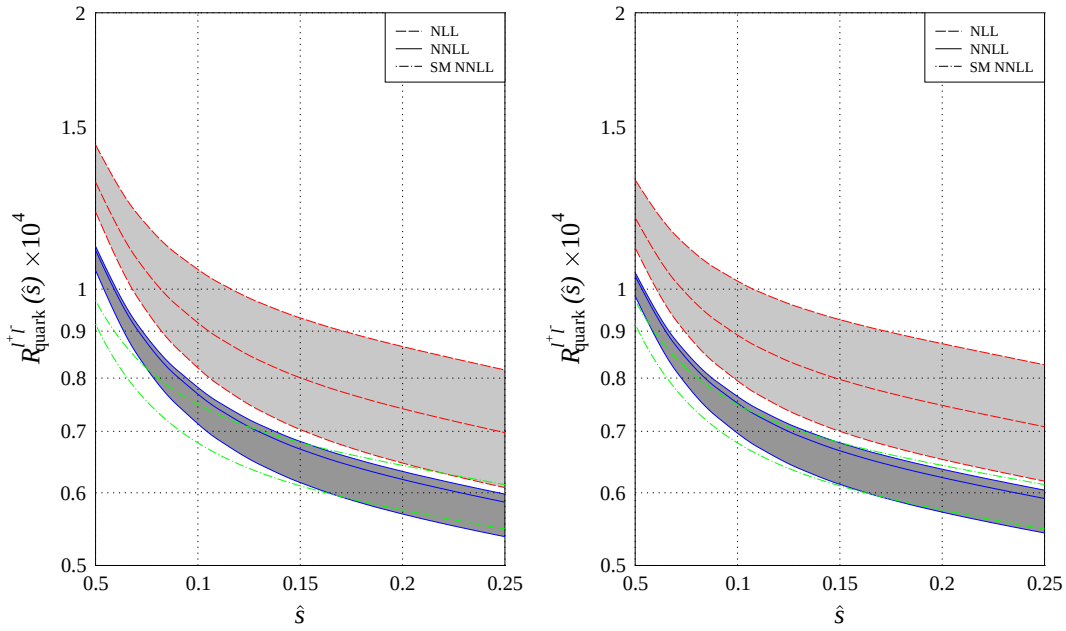

Figure 5.12: Reduction of the μ_0-matching scale dependence of $R^{l^+l^-}_{\text{quark}}(\hat{s})$ when including the "top-quark – charged Higgs" contribution only. In the left plot $M_H = 250$ GeV and in the right plot $M_H = 450$ GeV. Further we set $\tan\beta = 3$.

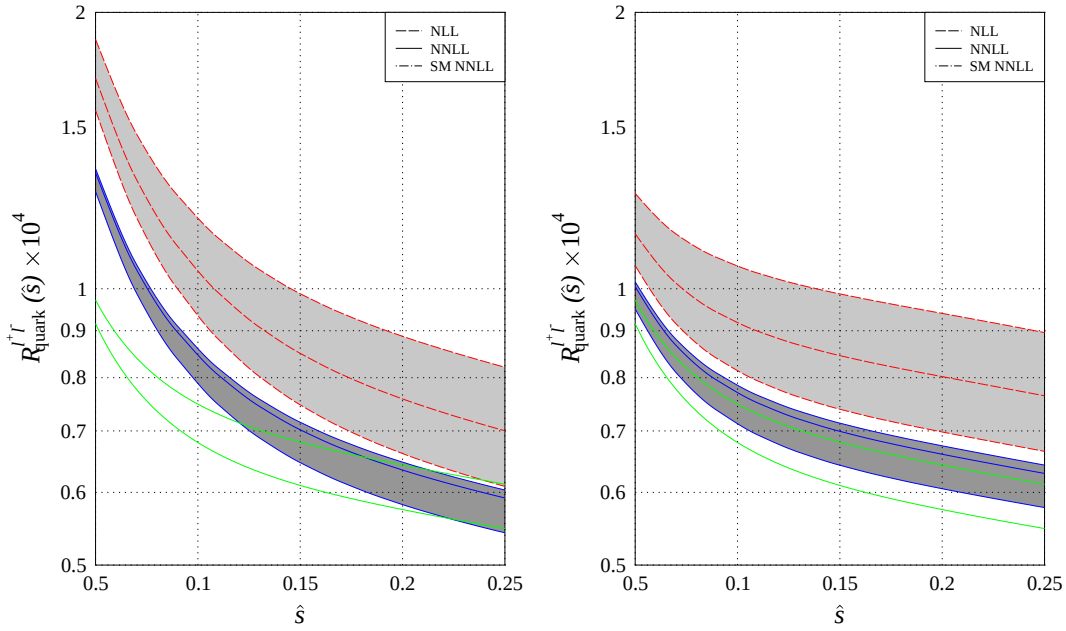

Figure 5.13: Reduction of the μ_0-matching scale dependence of $R^{l^+l^-}_{\text{quark}}(\hat{s})$ in the considered scenario of the MSSM. The left plot corresponds to the choice of the parameter set "Point 1" and the right plot to "Point 2".

of Figure 5.12 shows that a cancellation of the "top-quark – charged Higgs" and the "chargino – up-squark" contribution take place over the entire low-$\hat{s}$ region. The branching ratio of the NLL and the NNLL result is slightly higher than the analogous SM values increasing it by 5%, being $(1.88 \pm 0.25)\,10^{-6}$ and $(1.50 \pm 0.07)\,10^{-6}$, respectively.

The sensitivity of the dilepton invariant mass spectrum to new physics effects seems to be small in the considered scenario of the MSSM. The differential forward-backward asymmetry of the leptons is more sensitive to new physics effects. Here it should be noted, that the leading contribution to this observable arises at NLL order and thus the inclusion of the NNLL corrections presented here will drastically reduce the renormalization scale dependence. In particular, $\hat{s}_0$, the position at which the forward-backward asymmetry vanishes provides an important test of the SM [113] and can constraint the parameter spaces of new physics scenarios.

5.5 Non-perturbative Corrections

As outlined in Section 5.3 the approach of HQE combined with HQET methods allows for a systematic treatment of non-perturbative effects in inclusive decays. The formalism of HQE was first applied to inclusive decays of charmed particles [114] and later extended and combined with HQET techniques to inclusive semileptonic B decays [115–119]. In the following we will compile the results of the dominant HQE/HQET corrections to the differential decay rate $d\Gamma[b \to X_s l^+ l^-]/d\hat{s}$ evaluated in [120–125].

First of all it has to be clarified that the HQE approach has limitations. Especially the validity of the HQE is related to the kinematical configuration under consideration characterized in $\bar{B} \to X_s l^+ l^-$ by the particular value of $\hat{s}$.

The HQE of the dilepton invariant mass distribution of the decay $\bar{B} \to X_s l^+ l^-$ breaks down at the endpoint of the spectrum for $\hat{s} \to 1$ where both leptons fly back to back in the rest frame of the decaying B meson. The final hadronic state X_s remains then almost at rest and the non-pertrubative final state interactions are entirely dictated by scales of the order of $\Lambda_{\rm QCD}$.

In Ref. [124] it was proposed to model the dilepton invariant mass distribution in this region by heavy hadron chiral perturbation theory (HHχPT). Here it is convenient to normalize q^2 to the B meson mass $s_m \equiv q^2/M_B^2$. The inclusive decay degenerates then to the kinematically allowed exclusive decay channels $\bar{B} \to \bar{K}\pi l^+ l^-$ and $\bar{B} \to \bar{K} l^+ l^-$ in the range $0.728 < s_m < 0.821$[8]. The upper bound $s_m = (1 - M_K/M_B)^2 = 0.821$ with $M_K = 0.496\,\text{GeV}$ and $M_B = 5.28\,\text{GeV}$ corresponds to the kinematical threshold of K production in the decay $\bar{B} \to \bar{K} l^+ l^-$ and the lower bound is determined by the kinematical threshold of the decay $\bar{B} \to \bar{K}\pi\pi l^+ l^-$. The authors propose to model the *high* s_m *region* $0.5 < s_m < 0.821$ by using the HQE up to values $s_m \approx 0.65$ and HHχPT in the range $0.73 < s_m < 0.821$. The missing intermediate range $0.65 < s_m < 0.728$ is not reliably accessible by either methods, HQE and HHχPT. The value $s_m \approx 0.65$ corresponds to $\hat{s} \approx 0.78$ using the value $m_{b,pole} = 4.8\,\text{GeV}$ being the upper boundary of the high-$\hat{s}$ region as defined in (5.46).

$b \to X_s c\bar{c} \to X_s l^+ l^-$ Resonances

Apart from the inapplicability of HQE at the endpoint of the dilepton invariant mass

[8] The contribution of the decay $\bar{B} \to \bar{K}\pi l^+ l^-$ turns out to be very small.

l^+l^-	lower cut	$B \to X_s J/\psi$	$B \to X_s \psi'$
Belle Collaboration			
e^+e^-	0.2	$[M_{J/\psi} - 0.6,\ M_{J/\psi} + 0.2]$	$[M_{\psi'} - 0.3,\ M_{\psi'} + 0.15]$
$\mu^+\mu^-$	$2m_\mu$ (none)	$[M_{J/\psi} - 0.35,\ M_{J/\psi} + 0.2]$	$[M_{\psi'} - 0.3,\ M_{\psi'} + 0.15]$
BaBar Collaboration			
e^+e^-	0.2	$[M_{J/\psi} - 0.4,\ M_{J/\psi} + 0.15]$	$[M_{\psi'} - 0.25,\ M_{\psi'} + 0.1]$
$\mu^+\mu^-$	$2m_\mu$ (none)	$[M_{J/\psi} - 0.3,\ M_{J/\psi} + 0.1]$	$[M_{\psi'} - 0.15,\ M_{\psi'} + 0.1]$

Table 5.5: Cuts to the dilepton invariant mass q in units of GeV/c^2 applied by the Belle Collaboration [17] and the BaBar Collaboration [18] to remove backgrounds for the dilepton systems $l^+l^- = e^+e^-$ and $\mu^+\mu^-$. The masses of the $J/\psi(1S)$ and $\psi'(=\psi(2S))$ resonances are $M_{J/\psi} = (3096.87 \pm 0.04)\,\text{MeV}$ and $M_{\psi'} = (3685.96 \pm 0.09)\,\text{MeV}$, respectively.

distribution also intermediate hadron states are not consistently addressable within this framework. The decay $\bar{B} \to X_s l^+ l^-$ can also be mediated besides the simple flavor changing neutral current decay pattern that was investigated so far by intermediate $c\bar{c}$ states proceeding along the decay chain $b \to X_s c\bar{c} \to X_s l^+ l^-$. This decay mechanism forms a very large background to the FCNC signal in the $\hat{s}$ region where the intermediate $c\bar{c}$ resonances are on-shell. The theoretical treatment of these long-distance contributions to $\bar{B} \to X_s l^+ l^-$ goes beyond QCD perturbation theory as used above and also non-perturbative higher order contributions in HQE of Λ_{QCD}/m_b are an inadequate description. So far only model-dependent treatments of the $c\bar{c}$ resonances exist. For example phenomenological resonance saturation models employ a Breit-Wigner form in modeling the resonance peaks [126–129]. Such models rely on the assumption of factorization when estimating the $B \to X_s \psi^{(n)} \to X_s l^+ l^-$[9] matrix elements of the four quark operators resulting in a model-dependent modification of the perturbative result of $h(\hat{m}_c, \hat{s})$. The tails of the resonances extend into regions of $\hat{s}$ far from the resonances. However, it is not clear how a proper connection to the model-independent perturbative short-distant result can be achieved. Often sign ambiguities arise due to unknown phases when combining the amplitudes of the long-distant model-dependent and short-distant model-independent contributions. With regard to the theoretical uncertainties experimental cuts are therefore necessary to remove the part of the dilepton invariant mass distribution dominated by $c\bar{c}$ resonances. These cuts give rise to the identification of the two separate regions already introduced before, the low-$\hat{s}$ region (5.45) below the cut and the high-$\hat{s}$ region (5.46) above.

The cuts applied to the dilepton invariant mass distribution in the experimental analysis of the Belle Collaboration [17] and the BaBar Collaboration [18] are vetoing the two channels $B \to X_s J/\psi$ and $B \to X_s \psi'$. The veto windows for the particular lepton channels $l^+l^- = e^+e^-$ and $\mu^+\mu^-$ can be read off from Table 5.5.

The same mechanism operates also in the case of intermediate resonances of light quarks of the ρ and ω family due to the subsequent decays $b \to X_s q\bar{q} \to X_s l^+ l^-$ with $q = \{u, d, s\}$. For example in [130] it was shown that such contributions are relevant for values of $\hat{s} < 0.05$ using

[9] $\psi^{(n)}$ is the n-th 1^{--} $c\bar{c}$ resonance.

the factorization approximation and dispersion relations. This approach leads to a modification of the perturbative result of the function $h(0,\hat{s})$ introducing model-dependencies.

It should be stressed, that the restriction to the low- and high-$\hat{s}$ regions is essential with respect to the validity of the HQE. The theoretical predictions will be then model-independent just depending on the SM parameters and well defined universal HQE/HQET parameters. The recent status of the $1/m_b$ expansion of the semileptonic decay $\bar{B} \to X_c l \bar{\nu}_l$ and the improved data of moments of the charged lepton energy and the invariant hadronic mass squared will allow for more accurate predictions of $|V_{cb}|$, the b-quark mass and the HQE/HQET parameters [131, 132]. This opens the possibility to test the SM in the decay $\bar{B} \to X_s l^+ l^-$ and to constraint new physics scenarios without further model-dependencies.

$\Lambda^2_{\rm QCD}/m_c^2$ Corrections

Concerning the long-distant effects related to the tails of $c\bar{c}$ resonances it was proposed to estimate their order of magnitude away from the resonance region employing a HQE in inverse powers of the charm quark mass. This approach provides a model-independent systematic treatment determining unambiguously the size and the sign of these contributions. It was first applied in the radiative decay $\bar{B} \to X_s\gamma$ [123, 133–136] and extended to $\bar{B} \to X_s l^+ l^-$ [123]. The result of the non-perturbative $\Lambda^2_{\rm QCD}/m_c^2$ corrections to $R^{l^+l^-}_{\rm quark}(\hat{s})$ have been found with the help of eq. (32) in Ref. [123]

$$\begin{aligned}\delta_{1/m_c^2} R(\hat{s}) = &-\frac{8}{9}\frac{\alpha_{\rm em}^2}{4\pi^2}\frac{|V_{ts}^* V_{tb}|^2}{|V_{cb}|^2}\frac{\lambda_2}{m_c^2}\frac{(1-\hat{s})^2}{f\,\kappa} \\ &\times \mathrm{Re}\left[F\left(\frac{\hat{s}}{4\hat{m}_c^2}\right)\left(C_2 - \frac{1}{6}C_1\right)\left(\frac{1+6\hat{s}-\hat{s}^2}{\hat{s}}\,\tilde{C}_7^{\rm eff*} + (2+\hat{s})\,\tilde{C}_9^{\rm eff*}\right)\right] \end{aligned} \tag{5.55}$$

where

$$F(r) = \frac{3}{2r}\begin{cases} \dfrac{1}{\sqrt{r(1-r)}}\arctan\sqrt{\dfrac{r}{1-r}} - 1 & 0 < r < 1, \\ \dfrac{1}{2\sqrt{r(r-1)}}\left(\ln\dfrac{1-\sqrt{1-1/r}}{1+\sqrt{1-1/r}} + i\pi\right) - 1 & r > 1. \end{cases} \tag{5.56}$$

The $\Lambda^2_{\rm QCD}/m_c^2$ corrections depend on the HQET parameter λ_2 being already introduced in eq. (5.34). The functions f and κ were given in connection with the semileptonic decay rate in eq. (5.42).

$\Lambda^2_{\rm QCD}/m_b^2$ and $\Lambda^3_{\rm QCD}/m_b^3$ Corrections

In consideration of the non-perturbative corrections the hadronic branching ratio of the low-$\hat{s}$ and the high-$\hat{s}$ region is given in terms of the perturbatively calculated quantity $R^{l^+l^-}_{\rm quark}(\hat{s})$ and the $1/m_b^2$ [121, 124], $1/m_b^3$ [125] and $1/m_c^2$ [123] power corrections

$$\mathcal{B}[\bar{B} \to X_s l^+ l^-]_{\hat{s}\in[0.05,\,0.25]} = \mathcal{B}[\bar{B} \to X_c e \bar{\nu}_e] \int_{0.05}^{0.25} d\hat{s} \times \left[R^{l^+l^-}_{\text{quark}}(\hat{s}) + \delta_{1/m_c^2} R(\hat{s}) + \delta_{1/m_b^2} R(\hat{s}) + \delta_{1/m_b^3} R(\hat{s}) \right] . \quad (5.57)$$

The non-perturbative corrections $\delta_{1/m_c^2} R(\hat{s})$ and $\delta_{1/m_b^2} R(\hat{s})$ have been found with the help of eq. (32) in Ref. [123] and eq. (18) in Ref. [124], respectively. The non-perturbative $\delta_{1/m_b^3} R(\hat{s})$ corrections are obtained from [125]. Further the $\Lambda^2_{\text{QCD}}/m_b^2$ corrections to the semileptonic decay rate were calculated in [119] and the according $\Lambda^3_{\text{QCD}}/m_b^3$ corrections in [137].

The quantities $\delta_{1/m_c^2} R(\hat{s})$, $\delta_{1/m_b^2} R(\hat{s})$ and $\delta_{1/m_b^3} R(\hat{s})$ involve HQET parameters characterizing the occurring matrix elements. Both, $\delta_{1/m_c^2} R(\hat{s})$ and $\delta_{1/m_b^2} R(\hat{s})$ depend on the parameter λ_2. This parameter λ_2 is related to the mass splitting

$$\lambda_2 \simeq \frac{M_{B^*}^2 - M_B^2}{4} \approx 0.12\,\text{GeV}^2 \quad (5.58)$$

and is relatively well known. The dependence on the HQET parameter λ_1 cancels due to the normalization to the semileptonic decay rate [124]. This is a welcome feature because no simple relation exists for λ_1 and its value is not well known. It has been for example measured by the CLEO Collaboration [138] by comparing the first moment of the photon spectrum in $\bar{B} \to X_s \gamma$ with the first moment of the invariant mass spectrum. The obtained value is $\lambda_1 = -0.236 \pm 0.071 \pm 0.078\text{GeV}^2$ where the first error is experimental and the second theoretical.

New matrix elements of operators of the HQET appear at the order $\Lambda^3_{\text{QCD}}/m_b^3$ containing the parameters ρ_1, ρ_2 and $\mathcal{T}_{1,\ldots,4}$ [137, 139]. Again $\mathcal{T}_1$ and $\mathcal{T}_2$ cancel in the final expressions of the branching ratio due to the normalization to the semileptonic decay rate. At the present time these parameters are rather poorly known. They where obtained recently from experimental data in two different approaches in [140] and [141], respectively. Both analysis determine beside $|V_{cb}|$ also the heavy quark masses and non-perturbative parameters from measured moments of the charged lepton energy and hadronic mass distributions in semileptonic decays.

The authors of [140] treat both quark masses m_b and m_c as heavy and perform a HQE of all observables in $1/m_b$ and $1/m_c$. In this approach the charm-quark mass is determined by the heavy quark relation following from the HQET. The recent experimental results from CLEO, BaBar and DELPHI are used then for a combined fit of $|V_{cb}|$, m_b and the HQET parameters making use of different mass definitions of m_b.

Instead, in [141], the charm quark mass is not treated as heavy and thus can be determined as a free parameter from the data. This approach avoids the expansion in $1/m_c$ which seems to be questionable and the difficulties can be circumvented associated to non-local correlators affecting meson masses [142–144]. Such non-local correlators are not measured in inclusive B decays and the assumption of a heavy charm quark does not have to be imposed. The analysis uses only the preliminary results of the DELPHI Collaboration that measured moments without cuts on the lepton energy in the B rest frame.

The results of the fit proposes the following ranges for the parameters: $-0.1 \leq \rho_1 \leq 0.3\,\text{GeV}^3$ and $-0.2 \leq \rho 2 \leq 0.1\,\text{GeV}^3$. Concerning $\mathcal{T}_{1,\ldots,4}$ the fit does not provide informations

about uncertainties of the fitted values and thus their values range in $(0.0 \pm 0.5\,\mathrm{GeV})^3$ determined by dimensional analysis.

The hadronic branching ratio integrated over the low-$\hat{s}$ region of the SM is given below to illustrate the order of magnitude of the non-perturbative corrections in comparison to the perturbative contribution $R^{l^+l^-}_{\mathrm{quark}}$. The six equations correspond to the choice of renormalization scales as in the upper and lower boundary curves of the NLL, the partial NNLL and the NNLL result of $R^{l^+l^-}_{\mathrm{quark}}$ shown in Fig. 5.8

$$\mathcal{B}[\bar{B} \to X_s l^+ l^-]^{\mathrm{NLL}}_{\hat{s}\in[0.05,\,0.25]}(\mu_b = 2.5\,\mathrm{GeV},\ 3/2\mu_0^c = \mu_0^t = 240\,\mathrm{GeV}) = \tag{5.59a}$$

$$1.47\left(1 + 0.32\,\lambda_2^b - 0.11\,\lambda_2^c + 0.12\,\rho_1 - 0.06\,\rho_2 + 0.02\,(\mathcal{T}_3 + 3\mathcal{T}_4)\right)10^{-6},$$

$$\mathcal{B}[\bar{B} \to X_s l^+ l^-]^{\mathrm{NLL}}_{\hat{s}\in[0.05,\,0.25]}(\mu_b = 10\,\mathrm{GeV},\ 3/2\mu_0^c = \mu_0^t = 60\,\mathrm{GeV}) = \tag{5.59b}$$

$$2.18\left(1 + 0.32\,\lambda_2^b - 0.16\,\lambda_2^c + 0.13\,\rho_1 - 0.07\,\rho_2 + 0.02\,(\mathcal{T}_3 + 3\mathcal{T}_4)\right)10^{-6},$$

$$\mathcal{B}[\bar{B} \to X_s l^+ l^-]^{\mathrm{part.NNLL}}_{\hat{s}\in[0.05,\,0.25]}(\mu_b = 2.5\,\mathrm{GeV},\ 3/2\mu_0^c = \mu_0^t = 60\,\mathrm{GeV}) = \tag{5.59c}$$

$$1.19\left(1 + 0.34\,\lambda_2^b - 0.15\,\lambda_2^c + 0.12\,\rho_1 - 0.07\,\rho_2 + 0.02\,(\mathcal{T}_3 + 3\mathcal{T}_4)\right)10^{-6},$$

$$\mathcal{B}[\bar{B} \to X_s l^+ l^-]^{\mathrm{part.NNLL}}_{\hat{s}\in[0.05,\,0.25]}(\mu_b = 10\,\mathrm{GeV},\ 3/2\mu_0^c = \mu_0^t = 240\,\mathrm{GeV}) = \tag{5.59d}$$

$$1.69\left(1 + 0.33\,\lambda_2^b - 0.18\,\lambda_2^c + 0.13\,\rho_1 - 0.07\,\rho_2 + 0.02\,(\mathcal{T}_3 + 3\mathcal{T}_4)\right)10^{-6},$$

$$\mathcal{B}[\bar{B} \to X_s l^+ l^-]^{\mathrm{NNLL}}_{\hat{s}\in[0.05,\,0.25]}(\mu_b = 2.5\,\mathrm{GeV},\ 3/2\mu_0^c = \mu_0^t = 60\,\mathrm{GeV}) = \tag{5.59e}$$

$$1.27\left(1 + 0.32\,\lambda_2^b - 0.07\,\lambda_2^c + 0.13\,\rho_1 - 0.07\,\rho_2 + 0.02\,(\mathcal{T}_3 + 3\mathcal{T}_4)\right)10^{-6},$$

$$\mathcal{B}[\bar{B} \to X_s l^+ l^-]^{\mathrm{NNLL}}_{\hat{s}\in[0.05,\,0.25]}(\mu_b = 10\,\mathrm{GeV},\ 3/2\mu_0^c = \mu_0^t = 240\,\mathrm{GeV}) = \tag{5.59f}$$

$$1.55\left(1 + 0.32\,\lambda_2^b - 0.04\,\lambda_2^c + 0.13\,\rho_1 - 0.07\,\rho_2 + 0.02\,(\mathcal{T}_3 + 3\mathcal{T}_4)\right)10^{-6}.$$

The single contributions originating from $\Lambda^2_{\mathrm{QCD}}/m_b^2$ and $\Lambda^2_{\mathrm{QCD}}/m_c^2$ non-perturbative corrections are both proportional to λ_2 which are indicated by λ_2^b and λ_2^c, respectively. The coefficient of the $\Lambda^2_{\mathrm{QCD}}/m_b^2$ correction is rather large being 30% of the perturbative contribution to the branching ratio. The actual value of $\lambda_2 = 0.12\,\mathrm{GeV}^2$ reduces this contribution to a 4% percent correction. The $\Lambda^2_{\mathrm{QCD}}/m_c^2$ power corrections decrease the branching ratio in the low-$\hat{s}$ region. Here the coefficient depends on the Wilson coefficients C_1, C_2, $\tilde{C}_7^{\mathrm{eff}}$ and $\tilde{C}_9^{\mathrm{eff}}$ as given in (5.55). It constitutes a 2% corrections to the perturbative contribution $R^{l^+l^-}_{\mathrm{quark}}$ at NLL and partial NNLL order and reduces to a 1% correction at NNLL order.

The coefficients of $\Lambda^3_{\mathrm{QCD}}/m_b^3$ corrections of ρ_1 and ρ_2 are 13% and 7% of the perturbative result according to the choice of renormalization scales. The possible size of these corrections

can become 4% and 1.5%, respectively for ρ_1 and ρ_2 when they take the maximal values determined from the fit results. The contribution of the combination $\mathcal{T}_3 + 3\mathcal{T}_4$ is below 1%.

The non-perturbative corrections in the low-$\hat{s}$ region add up to approximately 7%. The $\Lambda^2_{\rm QCD}/m_b^2$ and $\Lambda^3_{\rm QCD}/m_b^3$ corrections are equally in size assuming the latter one to be maximal in the range obtained from fits to the data. It should be noted that a further uncertainty is connected to the renormalization scheme adopted for the quark mass m_b (and also m_c) occurring in kinematical factors of the dilepton invariant mass spectrum. The pole mass scheme was used throughout, however other schemes exist which seem preferred since their use can improve the behavior of the QCD perturbation series.

In the following we present similar results for the branching ratio obtained by integrating (5.57) over the high-$\hat{s}$ region (5.46). Varying the scales as above the NLL and partial NNLL expressions according to the upper and lower boundary curves of Figure 5.9 yield the hadronic branching ratios

$$\mathcal{B}[\bar{B} \to X_s l^+ l^-]^{\rm NLL}_{\hat{s}\in[0.64,\,0.78]}(\mu_b = 2.5\,{\rm GeV},\ 3/2\mu_0^c = \mu_0^t = 240\,{\rm GeV}) = \tag{5.60a}$$

$$2.32\left(1 - 0.58\,\lambda_2^b + 0.08\,\lambda_2^c - 0.56\,\rho_1 + 0.12\,\rho_2 - 0.04\,(\mathcal{T}_3 + 3\mathcal{T}_4)\right) 10^{-7},$$

$$\mathcal{B}[\bar{B} \to X_s l^+ l^-]^{\rm NLL}_{\hat{s}\in[0.64,\,0.78]}(\mu_b = 10\,{\rm GeV},\ 3/2\mu_0^c = \mu_0^t = 60\,{\rm GeV}) = \tag{5.60b}$$

$$3.66\left(1 - 0.63\,\lambda_2^b + 0.06\,\lambda_2^c - 0.54\,\rho_1 + 0.13\,\rho_2 - 0.04\,(\mathcal{T}_3 + 3\mathcal{T}_4)\right) 10^{-7},$$

$$\mathcal{B}[\bar{B} \to X_s l^+ l^-]^{\rm part.NNLL}_{\hat{s}\in[0.64,\,0.78]}(\mu_b = 2.5\,{\rm GeV},\ 3/2\mu_0^c = \mu_0^t = 60\,{\rm GeV}) = \tag{5.60c}$$

$$2.15\left(1 - 0.58\,\lambda_2^b + 0.08\,\lambda_2^c - 0.56\,\rho_1 + 0.12\,\rho_2 - 0.04\,(\mathcal{T}_3 + 3\mathcal{T}_4)\right) 10^{-7},$$

$$\mathcal{B}[\bar{B} \to X_s l^+ l^-]^{\rm part.NNLL}_{\hat{s}\in[0.64,\,0.78]}(\mu_b = 10\,{\rm GeV},\ 3/2\mu_0^c = \mu_0^t = 240\,{\rm GeV}) = \tag{5.60d}$$

$$2.99\left(1 - 0.61\,\lambda_2^b + 0.07\,\lambda_2^c - 0.55\,\rho_1 + 0.13\,\rho_2 - 0.04\,(\mathcal{T}_3 + 3\mathcal{T}_4)\right) 10^{-7}.$$

Contrary to the low-$\hat{s}$ region the $\Lambda^2_{\rm QCD}/m_b^2$ and $\Lambda^3_{\rm QCD}/m_b^3$ corrections lead to a reduction of the perturbative result in the high-$\hat{s}$ region. The contributions due to λ_2, ρ_1 and ρ_2 are of the order of 7%, 16% and 3%, respectively, assuming the maximal possible values of ρ_1 and ρ_2. Especially here the unknown value of ρ_1 induces a large uncertainty comparable to the scale uncertainty of the perturbative result as can be seen in Table 5.4. The combination of $\mathcal{T}_3 + 3\mathcal{T}_4$ can contribute up to 2% varying $\mathcal{T}_3$ and $\mathcal{T}_4$ as given above. The power corrections $\Lambda^2_{\rm QCD}/m_c^2$ receive a reversed sign compared to the low-$\hat{s}$ region increasing the branching ratio by around 1%.

The branching ratio of the high-$\hat{s}$ region composes out of the perturbative result and about $-(10-25)\%$ correction when adding up the single non-perturbative contributions. The uncertainties induced by the unknown $\Lambda^3_{\rm QCD}/m_b^3$ HQET parameters are of the order of 15% which has to be combined with the uncertainties of the perturbative result of similar size [see Table 5.4].

Concluding, the analysis of the branching ratios of the low-$\hat{s}$ and high-$\hat{s}$ regions in the SM has shown that the current theoretical uncertainties can be reduced when including NNLL order corrections. In the low-$\hat{s}$ region the uncertainties of the NNLL result due to renormalization scale dependencies are estimated to be of the order of 10% [see Table 5.3] compared to the uncertainties due to $\Lambda^3_{\rm QCD}/m_b^3$ corrections of the order of 5%. The final branching ratio can be found in (5.59) at NLL, partial NNLL and NNLL order respectively.

The branching ratio of the high-$\hat{s}$ region can not be predicted with the same accuracy. The complete perturbative NNLL result requires the knowledge of two-loop matrix elements of four-quark operators for values $\hat{s} > 0.25$. Their inclusion should significantly reduce the remaining low energy scale μ dependence of the partial NNLL result given in Table 5.4. The uncertainties of the perturbative result due to renormalization scale dependencies are of the order of 16%. The uncertainties connected to the $\Lambda^3_{\rm QCD}/m_b^3$ corrections are of the same size preventing at present as precise tests as using the low-$\hat{s}$ region. The final branching ratio is given in (5.60) at the NLL and partial NNLL order.

6 Conclusions and Outlook

In this thesis we have presented the results of the calculation of NNLL order matching contributions to the operators mediating $b \to s l^+ l^-$ within the SM. In addition the results of the matching contributions within a special scenario of the MSSM were presented. This scenario is characterized by a heavy decoupled gluino and a texture of the soft supersymmetry breaking parameters inspired by minimal flavor violation. The explicit calculation requires the evaluation of two-loop diagrams in the SM and the MSSM.

The inclusion of the NNLL corrections to the Wilson coefficients leads to a significant reduction of the renormalization scale dependence (matching scale) associated to heavy particles. In the SM this concerns the renormalization scale dependence which arises mainly due to the $\overline{\text{MS}}$ top-quark mass. As a result we are able to remove a $\pm 16\%$ uncertainty of the dilepton invariant mass spectrum. The remaining $\pm 6\%$ uncertainty is found to be due to $\tilde{C}_{10}^{\text{eff}}$ and to smaller extend $\tilde{C}_{9}^{\text{eff}}$. Within the considered scenario of the MSSM the analogous renormalization scale dependencies become reduced in the same way. Here the uncertainties arise due to the renormalization scale dependence of the $\overline{\text{MS}}$ top-quark mass in the charged Higgs contribution and due to the renormalization scale dependence of the up-squark masses in the "chargino – up-squark" contribution.

The status of the perturbative calculation of the dilepton invariant mass distribution at the parton level is summarized and the impact of the NNLL corrections on the magnitude and the uncertainties of the theoretical prediction are given. This corresponds to the evaluation of the NNLL renormalization group running of the Wilson coefficients and the inclusion of two-loop matrix elements and bremsstrahlung corrections of the operators of the effective theory. In particular, the point of special emphasis is the investigation of the remaining uncertainties due to renormalization scale dependencies. The overall uncertainty due to the matching scale μ_0 and the low energy scale μ dependence can be reduced from $\pm 20\%$ to $\pm 10\%$ in the low-$\hat{s}$ region and from $\pm 22\%$ to $\pm 16\%$ in the high-$\hat{s}$ region, respectively.

Within the framework of HQE the perturbative result of the dilepton invariant mass distribution is the leading contribution whereas a systematical expansion in inverse powers of the b-quark mass (and c-quark mass) yields non-perturbative corrections. The HQE is reliably applicable in the low- and high-$\hat{s}$ region due to the absence of intermediate light quark and $c\bar{c}$-resonances. We have included the results of $\Lambda^2_{\text{QCD}}/m_b^2$, $\Lambda^3_{\text{QCD}}/m_b^3$ and $\Lambda^2_{\text{QCD}}/m_c^2$ non-perturbative corrections to the dilepton invariant mass spectrum and calculated the according branching ratios.

The branching ratio of the low-$\hat{s}$ region can be predicted with a 10% uncertainty due to renormalization scale dependencies. The non-perturbative corrections vary between $+(2-7)\%$ depending on the actual values of the $\Lambda^3_{\text{QCD}}/m_b^3$ HQET parameters thus introducing a further uncertainty of 5%.

This optimistic picture is not valid for the branching ratio obtained from the high-$\hat{s}$ region. Here the current result of the partial NNLL analysis suffers from 16% uncertainty due to

renormalization scale dependencies. In addition the non-perturbative corrections involving the $\Lambda^3_{\rm QCD}/m_b^3$ HQET parameters decrease the branching ratio by $(10-25)\%$ introducing further uncertainties of 15% originating from the $\Lambda^3_{\rm QCD}/m_b^3$ HQET parameters.

Apart from the reported achievements and the associated uncertainties discussed here, still some improvements towards a complete NNLL QCD calculation are missing. The first point to mention concerns the renormalization group evolution of the Wilson coefficients. Here the inclusion of the contribution $U_{92}^{c(2)}$ seems to be available in the close future. The authors of [83] have recently presented the results of the three-loop mixing of the four-quark operators $\mathcal{O}^Q_{1,\ldots,6}$ into the operator $\mathcal{O}_9$ and announced the publication of the three-loop self-mixing of the four-quark operators [90]. The size of the induced uncertainty in the branching ratio due to the variation of $U_{92}^{c(2)}$ from -10 to 10 was shown to be small [85]. However, the exact result of $U_{92}^{c(2)}$ will remove this uncertainty and might even decrease the overall uncertainty due to the exact knowledge of the correlated renormalization scale dependence.

Within the high-$\hat{s}$ region the prediction of the partial NNLL result of the branching ratio still suffers from large renormalization scale uncertainties due to the missing two-loop matrix elements of the four-quark operators $\mathcal{O}^Q_{1,2}$. The inclusion of these matrix elements should remove this uncertainty to a large extent as it happens in the low-$\hat{s}$ region. The authors of [93, 100, 101] report about a calculation, using a procedure for calculating the two-loop matrix elements that is valid in the entire range of $\hat{s}$, however the results are not yet publicly available. Furthermore, the two-loop matrix elements of the four-quark operators $\mathcal{O}_{3,\ldots,6}$ are not calculated yet. They are suppressed by the small Wilson coefficients C_3-C_6 in the SM and expected to give a negligible contribution. This conclusion is supported by the result of the calculation of the two-loop matrix elements of these operators contributing to $\bar{B} \to X_s\gamma$ [96]. In this decay the branching ratio becomes reduced by 1%.

The two-loop matrix element of the operator $\mathcal{O}_9$ and the according bremsstrahlung corrections denoted by $\omega_{99}^{(2)}(\hat{s})$ in (5.40) are another missing part of the complete NNLL prediction of the dilepton invariant mass distribution. This quantity requires a complicated calculation of two-loop integrals with general kinematical configurations. Such calculations had been performed in connection with the semileptonic charmless decay $\bar{B} \to X_u l\bar{\nu}_l$ being almost similar to $\bar{B} \to X_s l^+l^-$. In [145] the total decay rate was considered providing an estimate when integrating over the entire $\hat{s}$ range. In [146] the expression of the dilepton invariant mass spectrum was obtained by the expansion in the parameter $\delta = (1-\hat{s})$ that can be used for the high-$\hat{s}$ region. At least the use of these approximations will provide a reliable estimate of the size of $\omega_{99}^{(2)}(\hat{s})$ to the dilepton invariant mass distribution.

Beside the corrections and the correlated uncertainties investigated so far other issues concerning the decay $\bar{B} \to X_s l^+l^-$ deserve a more accurate treatment. It was realized in the radiative decay $\bar{B} \to X_s\gamma$ that large uncertainties occur due to the choice of the renormalization scheme [15] of the charm quark mass. Two different origins of the charm quark mass have to be considered. The leading contribution depending on the charm quark mass in $\bar{B} \to X_s\gamma$ appears only when evaluating the two-loop matrix elements of the four-quark operators. The *MSbar* scheme seems more appropriate here, due to their off-shellness. In contrast the semileptonic decay width, that is used as normalization, involves the charm quark mass in the pole mass scheme. Here it enters due to the kinematics and phase space integration. In the decay $\bar{B} \to X_s l^+l^-$ the situation seems not so dramatic, since the leading contribution is already given by the one-loop matrix elements and the two-loop matrix elements are taken into account. Nevertheless, the explicite investigation [103] and [92] have shown that the variation of the ratio $m_c/m_b \in [0.25,\ 0.33]$ also leads to sizeable uncertainties

in $\bar{B} \to X_s l^+ l^-$ of the order of 15% in the dilepton invariant mass spectrum and in the branching ratio. In the case of $\bar{B} \to X_s \gamma$ the authors of [15] proposed to use the charmless semileptonic decay width in combination with the "non-perturbative semileptonic phase-space factor". This allows to separate the charm quark mass determination from the problem of convergence of the perturbation series. This idea was applied very recently [102] to $\bar{B} \to X_s l^+ l^-$ and the authors found the reduced uncertainty due to the charm-quark mass of 6%.

Furthermore in the analysis of $\bar{B} \to X_s \gamma$ [15] all kinematical factors of $m_{b,pole}$ where expressed in terms of the the bottom mass "1S mass" m_b^{1S}. The only exception was the factor m_b of the electro-magnetic operator $\mathcal{O}_7$ appearing in the top-quark sector. The use of the m_b^{1S} mass avoids renormalon ambiguities that are present in $m_{b,pole}$ and the behavior of the QCD perturbation series improves with respect to the pole mass scheme.

Another source of uncertainty is related to the electromagnetic corrections to the running and mixing of especially $\mathcal{O}_9$ and $\mathcal{O}_{10}$. This would imply corrections of the order $[\alpha_{\rm em} \ln(\mu_0^2/\mu^2)\ \alpha_s^n \ln^n(\mu_0^2/\mu^2)]$. The simple estimate of this effect is reported in [102] which leads to an uncertainty of the order of 8% due to the variation of $\alpha_{\rm em}$ between 1/128 and 1/133. The explicite calculation of these corrections would reduce this additional source of uncertainty.

Appendix A MSSM Lagrangian

In this appendix we present general expressions of the parts of the MSSM Lagrangian needed for the calculation of matching conditions to operators mediating FCNC B decays such as $\bar{B} \to X_s\gamma$, $\bar{B} \to X_s l^+ l^-$ or $\bar{B} \to X_s \nu\bar{\nu}$. A general introduction to the MSSM and the complete list of all Feynman rules for perturbative calculations can be found in Ref. [49].

The "up-quark – down-quark – charged Higgs" coupling has the form

$$\mathcal{L}_{udH} = \frac{g_2}{\sqrt{2}M_W}\Big[\cot\beta\,(\bar{u}\,M_U V_{\rm CKM} P_L\,d) \;+\; \tan\beta\,(\bar{u}\,V_{\rm CKM} M_D P_R\,d)\Big] H^+ + \text{h.c.}\,. \quad \text{(A.1)}$$

$M_U \equiv \text{diag}(m_u, m_c, m_t)$ and $M_D \equiv \text{diag}(m_d, m_s, m_b)$ are the up and down quark mass matrices, respectively.

The physical dirac charginos are denoted by $\tilde{\chi}_i^-$ $(i = 1, 2)$, whereas the charge conjugated spinor is defined as $\tilde{\chi}_i^+ \equiv (\tilde{\chi}_i^-)^c$. The neutral higgsinos, the wino and the bino mix to form four Majorana fermions called neutralinos $\tilde{\chi}_i^0$ $(i = 1, \ldots, 4)$ and the superpartners of the gluons called gluinos form Majorana spinors $\tilde{g}_a$ $(a = 1, \ldots, 8)$ too. The interaction of the charginos $\tilde{\chi}_i^-$, neutralinos $\tilde{\chi}_i^0$ and gluinos $\tilde{g}_a$ with fermions and sfermions is given by

$$\begin{aligned}
\mathcal{L}_{\tilde{\chi}\tilde{f}f} \;=\; & \sum_{i=1}^{2}\Bigg\{\overline{\tilde{\chi}_i^-}\,\Big[\,\tilde{\nu}^\dagger(X_i^{N_L}P_L + X_i^{N_R}P_R)\,l \;+\; \tilde{u}^\dagger(X_i^{U_L}P_L + X_i^{U_R}P_R)\,d\,\Big] \\
& \qquad + \overline{\tilde{\chi}_i^+}\,\Big[\,\tilde{l}^\dagger(X_i^{E_L}P_L + X_i^{E_R}P_R)\,\nu\,\Big]\Bigg\} + \text{h.c.} \\
+ \; & \sum_{i=1}^{4}\Bigg\{\overline{\tilde{\chi}_i^0}\,\Big[\,\tilde{d}^\dagger(Z_i^{D_L}P_L + Z_i^{D_R}P_R)\,d \;+\; \tilde{l}^\dagger(Z_i^{E_L}P_L + Z_i^{E_R}P_R)\,l \\
& \qquad + \tilde{\nu}^\dagger(Z_i^{N_L}P_L + Z_i^{N_R}P_R)\,\nu\,\Big]\Bigg\} + \text{h.c.} \\
- \; & \sqrt{2}g\sum_{a=1}^{8}\Bigg\{\overline{\tilde{g}_a}\,\Big[\,\tilde{u}^\dagger(\Gamma^{U_L}P_L - \Gamma^{U_R}P_R)\mathbf{T}^a u \;+\; \tilde{d}^\dagger(\Gamma^{D_L}P_L - \Gamma^{D_R}P_R)\mathbf{T}^a d\,\Big]\Bigg\} + \text{h.c.},
\end{aligned} \quad \text{(A.2)}$$

where

$$X_i^{U_L} = -g_2 \left[V_{i1}^* \, \Gamma^{U_L} - V_{i2}^* \, \Gamma^{U_R} \frac{M_U}{\sqrt{2} M_W \sin\beta} \right] V_{\rm CKM}, \tag{A.3}$$

$$X_i^{U_R} = g_2 \, U_{i2} \, \Gamma^{U_L} \, V_{\rm CKM} \frac{M_D}{\sqrt{2} M_W \cos\beta}, \tag{A.4}$$

$$X_i^{N_L} = -g_2 \, V_{i1}^* \, \Gamma^N, \qquad X_i^{N_R} = g_2 \, U_{i2} \, \Gamma^N \, \frac{M_E}{\sqrt{2} M_W \cos\beta}, \tag{A.5}$$

$$X_i^{E_L} = -g_2 \left[U_{i1}^* \, \Gamma^{E_L} - U_{i2}^* \, \Gamma^{E_R} \, \frac{M_E}{\sqrt{2} M_W \cos\beta} \right], \qquad X_i^{E_R} = 0, \tag{A.6}$$

$$Z_i^{D_L} = -\frac{g_2}{\sqrt{2}} \left[\left(\frac{1}{3} t_W N_{i1}^* - N_{i2}^* \right) \Gamma^{D_L} + N_{i3}^* \Gamma^{D_R} \frac{M_D}{M_W \cos\beta} \right], \tag{A.7}$$

$$Z_i^{D_R} = -\frac{g_2}{\sqrt{2}} \left[\frac{2}{3} t_W N_{i1} \Gamma^{D_R} + N_{i3} \Gamma^{D_L} \frac{M_D}{M_W \cos\beta} \right], \tag{A.8}$$

$$Z_i^{E_L} = -\frac{g_2}{\sqrt{2}} \left[-(t_W N_{i1}^* + N_{i2}^*) \Gamma^{E_L} + N_{i3}^* \Gamma^{E_R} \frac{M_E}{M_W \cos\beta} \right], \tag{A.9}$$

$$Z_i^{E_R} = -\frac{g_2}{\sqrt{2}} \left[2 \, t_W N_{i1} \Gamma^{E_R} + N_{i3} \Gamma^{E_L} \frac{M_E}{M_W \cos\beta} \right], \tag{A.10}$$

$$Z_i^{N_L} = \frac{g_2}{\sqrt{2}} \Gamma^N \left(t_W N_{i1}^* - N_{i2}^* \right), \qquad Z_i^{N_R} = 0. \tag{A.11}$$

The diagonalization matrices U, V and N of the chargino and neutralino mass matrices were introduced in eqs. (4.4) and (4.6) whereas the diagonalization matrices of the squarks and sleptons can be found in eqs. (4.11) and (4.15). Further $t_W \equiv \tan\theta_W = s_W / c_W$.

The gauge interactions of charginos with neutral gauge bosons A_μ and Z_μ are as follows

$$\mathcal{L}_{\tilde{\chi}\tilde{\chi}A} = -e \sum_{i=1}^{2} \overline{\tilde{\chi}_i^+} \, \gamma^\mu \, \tilde{\chi}_i^+ \, A_\mu, \tag{A.12}$$

$$\mathcal{L}_{\tilde{\chi}\tilde{\chi}Z} = -\frac{g_2}{2 c_W} \sum_{i,j=1}^{2} \overline{\tilde{\chi}_i^+} \, \gamma^\mu (V_{i1} V_{j1}^* P_L + U_{i1}^* U_{j1} P_R + \cos 2\theta_W \, \delta_{ij}) \, \tilde{\chi}_j^+ \, Z_\mu. \tag{A.13}$$

The squark – gauge boson (Photon, Gluon, Z boson) interactions are

$$\mathcal{L}_{\tilde{q}\tilde{q}V} = -\frac{ie}{3}A_\mu\left[2(\tilde{u}_a^*\overset{\leftrightarrow}{\partial^\mu}\tilde{u}_a) - (\tilde{d}_a^*\overset{\leftrightarrow}{\partial^\mu}\tilde{d}_a)\right] - igG_\mu^a\left[(\tilde{u}_b^*\mathbf{T}^a\overset{\leftrightarrow}{\partial^\mu}\tilde{u}_b) + (\tilde{d}_b^*\mathbf{T}^a\overset{\leftrightarrow}{\partial^\mu}\tilde{d}_b)\right]$$
$$-\frac{ig_2}{2c_W}Z_\mu\left\{\left[(\Gamma^{U_L}\Gamma^{U_L\dagger})_{ab} - \frac{4}{3}s_W^2\delta_{ab}\right](\tilde{u}_a^*\overset{\leftrightarrow}{\partial^\mu}\tilde{u}_b)\right.$$
$$\left.-\left[(\Gamma^{D_L}\Gamma^{D_L\dagger})_{ab} - \frac{2}{3}s_W^2\delta_{ab}\right](\tilde{d}_a^*\overset{\leftrightarrow}{\partial^\mu}\tilde{d}_b)\right\}, \tag{A.14}$$

The quartic self-interaction of the squarks reads

$$\mathcal{L}_4 \equiv \mathcal{L}^g_{\tilde{u},\tilde{d}} = -\frac{1}{4}g^2\left[\tilde{u}^*P_U\mathbf{T}^a\tilde{u} + \tilde{d}^*P_D\mathbf{T}^a\tilde{d}\right]^2, \tag{A.15}$$

where

$$P_U \equiv \Gamma^{U_L}\Gamma^{U_L\dagger} - \Gamma^{U_R}\Gamma^{U_R\dagger}, \qquad P_D \equiv \Gamma^{D_L}\Gamma^{D_L\dagger} - \Gamma^{D_R}\Gamma^{D_R\dagger}. \tag{A.16}$$

It should be emphasized that $\mathcal{L}_4$ represents only the part of the quartic squark interaction vertex which is proportional to the strong coupling constant α_s.

Appendix B Non-Physical Operators

In this appendix we shall present the non-physical operators namely the EOM-vanishing and evanescent operators relevant to the off-shell matching of $b \to s+$(light particles).

The EOM-vanishing operators appear in the off-shell calculation of the $b \to s\gamma$ and $b \to sg$ Greens functions. Once the off-shell photon (gluon) decays into a lepton (quark) pair their Wilson coefficients contribute to the process $b \to sl^+l^-$ ($b \to sq\bar{q}$). Here it is convenient to use a background field version to maintain explicit gauge invariance which allows to perform the matching without making use of the CKM-matrix unitarity. As a consequence the relevant EOM-vanishing operators contain background fields and are invariant with respect to gauge transformations of the background field. The gauge-invariant EOM-vanishing operators can be chosen as

$$\begin{aligned}
\mathcal{O}_{31} &= \frac{1}{g_s}(\bar{s}\,\gamma^\mu P_L \mathbf{T}^a\, b) D^\nu_{ab} G^b_{\mu\nu} + \mathcal{O}_4, \\
\mathcal{O}_{32} &= \frac{1}{g_s^2} m_b \bar{s}\, \not{D}\not{D} P_R\, b, \\
\mathcal{O}_{33} &= \frac{i}{g_s^2} \bar{s}\, \not{D}\not{D}\not{D} P_L\, b, \\
\mathcal{O}_{34} &= \frac{i}{g_s} \left[\bar{s}\, \overleftarrow{\not{D}}\, \sigma^{\mu\nu} P_L \mathbf{T}^a\, b G^a_{\mu\nu} - G^a_{\mu\nu} \bar{s}\, \mathbf{T}^a \sigma^{\mu\nu} \not{D} P_L\, b\right] + \mathcal{O}_8, \\
\mathcal{O}_{35} &= \frac{ie}{g_s^2} \left[\bar{s}\, \overleftarrow{\not{D}}\, \sigma^{\mu\nu} P_L\, b F_{\mu\nu} - F_{\mu\nu} \bar{s}\, \sigma^{\mu\nu} \not{D} P_L\, b\right] + \mathcal{O}_7, \\
\mathcal{O}_{36} &= \frac{e}{g_s^2} (\bar{s}\,\gamma^\mu P_L\, b) \partial^\nu F_{\mu\nu} - \mathcal{O}_9.
\end{aligned} \tag{B.1}$$

Here D_μ denotes the covariant derivative of the gauge group $SU(3)_C \otimes U(1)_Q$. The sign convention in the covariant derivative acting on a quark field ψ is

$$D_\mu \psi = \left(\partial_\mu + ieQ_\psi A_\mu + ig_s G^a_\mu \mathbf{T}^a\right) \psi. \tag{B.2}$$

The according sign convention in the covariant derivative acting on the gluon field-strength tensor $G^a_{\mu\nu}$ is

$$D^\nu_{ab} G^b_{\mu\nu} = \left(\partial^\nu \delta_{ab} + g_s f_{abc} G^{c,\nu}\right) G^b_{\mu\nu}. \tag{B.3}$$

The EOM-vanishing operators can be assumed to contain the background field only, because in the off-shell matching procedure nothing but their tree-level matrix elements are needed. However, a systematic off-shell renormalization of the effective theory requires introducing EOM-vanishing operators that contain the quantum fields as well. Further other non-physical operators such as gauge-variant EOM-vanishing operators containing quantum fields have to be considered. The explicit form of those operators as well as details concerning the complete off-shell renormalization of the effective theory can be found in [83, 147, 148] and references therein. Here it is emphasized that the gauge invariant EOM-vanishing operators of eq. (B.1) are needed for the matching calculation of the Wilson coefficients of the physical operators. Besides also other non-physical operators enter the effective Lagrangian $\mathcal{L}_{\text{eff}}$ that are needed in the course of a complete renormalization of the effective theory.

In intermediate steps of the calculation structures like

$$(\gamma_{\mu_1}\gamma_{\mu_2}\gamma_{\mu_3}P_A)\otimes(\gamma^{\mu_1}\gamma^{\mu_2}\gamma^{\mu_3}P_B) \tag{B.4}$$

occur with $P_{A,B}$ being either P_L or P_R. They cannot be reduced using D dimensional Dirac algebra, due to the appearance of the matrix γ_5. Only after the matching all divergencies cancel and the limit $D \to 4$ can be taken. Consequently, evanescent operators must be introduced in the effective theory.

The evanescent operators appearing in the calculation of the anomalous dimensions [82,83] of the processes $b \to s\gamma$, $b \to sg$, $b \to sc\bar{c}$ and $b \to sq\bar{q}$ are defined as follows

$$\begin{aligned}
\mathcal{O}_{11}^{Q} &= (\bar{s}\,\gamma_{\mu_1}\gamma_{\mu_2}\gamma_{\mu_3}P_L\mathbf{T}^a\,Q)(\bar{Q}\,\gamma^{\mu_1}\gamma^{\mu_2}\gamma^{\mu_3}P_L\mathbf{T}^a\,b) - 16\,\mathcal{O}_1^{Q},\\
\mathcal{O}_{12}^{Q} &= (\bar{s}\,\gamma_{\mu_1}\gamma_{\mu_2}\gamma_{\mu_3}P_L\,Q)(\bar{Q}\,\gamma^{\mu_1}\gamma^{\mu_2}\gamma^{\mu_3}P_L\,b) - 16\,\mathcal{O}_2^{Q},\\
\mathcal{O}_{15} &= (\bar{s}\,\gamma_{\mu_1}\gamma_{\mu_2}\gamma_{\mu_3}\gamma_{\mu_4}\gamma_{\mu_5}P_L\,b)\sum_q(\bar{q}\,\gamma^{\mu_1}\gamma^{\mu_2}\gamma^{\mu_3}\gamma^{\mu_4}\gamma^{\mu_5}\,q) - 20\,\mathcal{O}_5 + 64\,\mathcal{O}_3,\\
\mathcal{O}_{16} &= (\bar{s}\,\gamma_{\mu_1}\gamma_{\mu_2}\gamma_{\mu_3}\gamma_{\mu_4}\gamma_{\mu_5}P_L\mathbf{T}^a\,b)\sum_q(\bar{q}\,\gamma^{\mu_1}\gamma^{\mu_2}\gamma^{\mu_3}\gamma^{\mu_4}\gamma^{\mu_5}\mathbf{T}^a\,q) - 20\,\mathcal{O}_6 + 64\,\mathcal{O}_4,\\
\mathcal{O}_{21}^{Q} &= (\bar{s}\,\gamma_{\mu_1}\gamma_{\mu_2}\gamma_{\mu_3}\gamma_{\mu_4}\gamma_{\mu_5}P_L\mathbf{T}^a\,Q)(\bar{Q}\,\gamma^{\mu_1}\gamma^{\mu_2}\gamma^{\mu_3}\gamma^{\mu_4}\gamma^{\mu_5}P_L\mathbf{T}^a\,b) - 20\,\mathcal{O}_{11}^{Q} - 256\,\mathcal{O}_1^{Q},\\
\mathcal{O}_{22}^{Q} &= (\bar{s}\,\gamma_{\mu_1}\gamma_{\mu_2}\gamma_{\mu_3}\gamma_{\mu_4}\gamma_{\mu_5}P_L\,Q)(\bar{Q}\,\gamma^{\mu_1}\gamma^{\mu_2}\gamma^{\mu_3}\gamma^{\mu_4}\gamma^{\mu_5}P_L\,b) - 20\,\mathcal{O}_{12}^{Q} - 256\,\mathcal{O}_2^{Q}.
\end{aligned} \tag{B.5}$$

Their explicit form defines what the "MS" scheme means in the effective theory. Modifying the scheme by changing the evanescent operators by terms proportional to $\epsilon = 2 - D/2$ will not affect their property to vanish in the limit of $D \to 4$, however Wilson coefficients, anomalous dimensions and matrix elements of physical operators will undergo changes.

Further evanescent operators appear in box diagrams in the SM and in the MSSM when calculating the process $b \to sl^+l^-$. For example, in the SM we define the evanescent operator for $b \to sl^+l^-$ as follows [149, 150]

$$\mathcal{O}_1^{E} = (\bar{s}\,\gamma_{\mu_1}\gamma_{\mu_2}\gamma_{\mu_3}P_L\,b)(\bar{l}\,\gamma^{\mu_3}\gamma^{\mu_2}\gamma^{\mu_1}P_L\,l) - 4\,(\bar{s}\,\gamma_{\mu}P_L\,b)(\bar{l}\,\gamma^{\mu}P_L\,l). \tag{B.6}$$

In the chargino sector of the MSSM, operators with a different spinor ordering show up in box diagrams [86]

$$\tilde{\mathcal{O}}_{SAB} = (\bar{s}\, P_A\, l)(\bar{l}\, P_B\, b),$$
$$\tilde{\mathcal{O}}_{VAB} = (\bar{s}\, \gamma_\mu P_A\, l)(\bar{l}\, \gamma^\mu P_B\, b),$$
$$\tilde{\mathcal{O}}_{TAA} = (\bar{s}\, \sigma_{\mu\nu} P_A\, l)(\bar{l}\, \sigma^{\mu\nu} P_B\, b), \tag{B.7}$$

with $\sigma_{\mu\nu} \equiv [\gamma_\mu, \gamma_\nu]/2$. We are not allowed to project these operators onto the physical operators $\mathcal{O}_9$ and $\mathcal{O}_{10}$ given in eq. (5.5). For such a projection we would have to apply Fierz identities which cannot be continued to D dimensions. For this reason, we have to define the following so-called *"Fierz-vanishing" evanescent* operators [151, 152]:

$$\tilde{\mathcal{O}}^E_{SLL} = \tilde{\mathcal{O}}_{SLL} + \frac{1}{2}\mathcal{O}_{SLL} - \frac{1}{8}\mathcal{O}_{TLL},$$
$$\tilde{\mathcal{O}}^E_{SLR} = \tilde{\mathcal{O}}_{SLR} + \frac{1}{2}\mathcal{O}_{VRL},$$
$$\tilde{\mathcal{O}}^E_{VLL} = \tilde{\mathcal{O}}_{VLL} - \mathcal{O}_{VLL},$$
$$\tilde{\mathcal{O}}^E_{VLR} = \tilde{\mathcal{O}}_{VLR} + 2\mathcal{O}_{SRL},$$
$$\tilde{\mathcal{O}}^E_{TLL} = \tilde{\mathcal{O}}_{TLL} - 6\mathcal{O}_{SLL} - \frac{1}{2}\mathcal{O}_{TLL}, \tag{B.8}$$

as well as operators which can be obtained by an interchange of $P_L \leftrightarrow P_R$. The operators without tilde are identical to the ones given in eqs. (B.7), but with exchanged l and b spinors. Due to a finite mixing into the physical operators the "Fierz-vanishing" evanescent operators contribute at next-to-leading order. A similar situation was described in [149] concerning the SM calculation. From (B.8) it is evident that we cannot neglect the contributions to the scalar and tensor operators $\tilde{\mathcal{O}}_{SAB}$ and $\tilde{\mathcal{O}}_{TAA}$ as it affects the Wilson coefficients of the vector operators $\tilde{\mathcal{O}}_{VAB}$.

Furthermore the following two evanescent operators are necessary at intermediate steps

$$\tilde{\mathcal{O}}^E_1 = (\bar{s}\, \gamma_{\mu_1}\gamma_{\mu_2}\gamma_{\mu_3} P_L\, l)(\bar{l}\, \gamma^{\mu_1}\gamma^{\mu_2}\gamma^{\mu_3} P_L\, b) - 16\, \tilde{\mathcal{O}}_{VLL},$$
$$\tilde{\mathcal{O}}^E_2 = (\bar{s}\, \gamma_{\mu_1}\gamma_{\mu_2}\gamma_{\mu_3} P_L\, l)(\bar{l}\, \gamma^{\mu_1}\gamma^{\mu_2}\gamma^{\mu_3} P_R\, b) - 4\, \tilde{\mathcal{O}}_{VLR}. \tag{B.9}$$

Appendix C Wilson Coefficients

This appendix summarizes the matching results relevant to $\bar{B} \to X_s l^+ l^-$ in the SM and the considered scenario of the MSSM as introduced in Chapter 4.2. It provides the formulae of the functions $[X]_i^n$ introduced in eq. (5.11) and appearing in the eqs. (5.8) and (5.9).

The values of the Wilson coefficients are found in the matching procedure by requiring equality of $b \to s+$(light particles) Greens functions calculated in the effective theory and in the full theory, up to order $\mathcal{O}[(\text{external momenta and light masses})^2/M^2_{\text{heavy}}]$. The perturbative expansion in coupling constants in the matching procedure includes the orders $\sim G_F$, $G_F\alpha_s$ and $G_F\alpha_s^2$ of the process $b \to sc\bar{c}$ and $b \to sq\bar{q}$. Further the processes $b \to s\gamma$ and $b \to sg$ have to be considered to the orders $G_F\, e$, $G_F\, e\, \alpha_s$ and $G_F\, g_s$, $G_F\, g_s\, \alpha_s$, respectively, whereas the process $b \to sl^+l^-$ analogously to the order $G_F\, e^2$ and $G_F\, e^2\, \alpha_s$.

Dimensional regularization with fully anti-commuting γ_5 and the $\overline{\text{MS}}$ scheme is used for all QCD counterterms, both in the full and in the effective theory for the light degrees of freedom. The only exceptions are the top quark and squark loop contributions to the renormalization of the light-quark and gluon wave functions on the full theory side. The corresponding terms in the propagators are subtracted in the MOM scheme at $q^2 = 0$. In consequence, no top quark and squark loop contribution remains in the (W boson)–(light quark) effective vertex after renormalization. This non-minimal renormalization of heavy particle effects guarantees the equality of the fields of the light degrees of freedom and the couplings (α_s and α_{em}) of the effective theory and their corresponding counterparts of the full theory.

The only relevant off-shell electroweak counterterm in the full theory proportional to $\bar{s}\not{D}b$ has been taken in the MOM scheme as well, at $q^2 = 0$ for the $\bar{s}\not{\partial}b$, and at vanishing external momenta for terms containing gauge bosons.

As a consequence of this special choice of the renormalization all masses of quarks and squarks appearing in this appendix are the running $\overline{\text{MS}}$ masses. The masses of particles which do not interact strongly (QCD) do not become renormalized and thus might interpreted as their tree-level masses.

We define the mass ratios

$$
\begin{aligned}
x &= \frac{m_t^2}{M_W^2}, & y &= \frac{m_t^2}{M_H^2}, & x_{\tilde{u}_a} &= \frac{m_{\tilde{u}_a}^2}{M_W^2}, & x_{\tilde{d}_a} &= \frac{m_{\tilde{d}_a}^2}{M_W^2}, \\
x_{ij} &= \frac{M_{\tilde{\chi}_i}^2}{M_{\tilde{\chi}_j}^2}, & y_{ai} &= \frac{m_{\tilde{u}_a}^2}{M_{\tilde{\chi}_i}^2}, & v_{fi} &= \frac{m_{\tilde{\nu}_f}^2}{M_{\tilde{\chi}_i}^2},
\end{aligned}
\tag{C.1}
$$

and introduce the abbreviations

$$L_t = \ln \frac{\mu_0^2}{m_t^2}, \qquad L_{\tilde{u}_a} = \ln \frac{\mu_0^2}{m_{\tilde{u}_a}^2}, \qquad \kappa = \frac{1}{g_2 V_{tb} V_{ts}^*}. \tag{C.2}$$

In these equations m_t denotes the top quark mass, $m_{\tilde{u}_a}$ and $m_{\tilde{d}_a}$ up and down squark masses, M_W the W boson mass, M_H the charged Higgs mass, $M_{\tilde{\chi}_i}$ the chargino masses and finally $m_{\tilde{\nu}_f}$ sneutrino masses.

The decoupling of the heavy gluino modifies the "down-quark – up-squark – chargino" couplings $X^{U_{L,R}}$ [see (A.3) and (A.4)]. Therefore, throughout the formulae presented in Appendix C.3 and C.4 the corresponding expressions of the "effective MSSM" given (4.27) and (4.28) have to be used.

The integral representations for the functions $\mathrm{Li}_2(s)$ and $\mathrm{Cl}_2(x)$ are as follows

$$\mathrm{Li}_2(z) = -\int_0^z dt \frac{\ln(1-t)}{t}, \tag{C.3}$$

$$\mathrm{Cl}_2(x) = \mathrm{Im}\left[\mathrm{Li}_2\left(e^{ix}\right)\right] = -\int_0^x d\theta \ln|2\sin(\theta/2)|. \tag{C.4}$$

C.1 $i = W$ – "top quark – W boson"

The evaluation of Feynman diagrams contributing to $b \to s+$(light particles) Greens functions within the SM mediated by "top quark – W boson" loops and denoted by the index $i = W$ in eq. (5.11) yields

$$[A_7]_W^0 = \tfrac{-3x^3+2x^2}{2(x-1)^4} \ln x + \tfrac{-22x^3+153x^2-159x+46}{36(x-1)^3}, \tag{C.5}$$

$$[B_9^{l\bar{l}}]_W^0 = [B_{10}^{l\bar{l}}]_W^0 = \tfrac{x}{4(x-1)^2} \ln x - \tfrac{1}{4(x-1)}, \tag{C.6}$$

$$[C_9^{l\bar{l}}]_W^0 = \tfrac{3x^2+2x}{8(x-1)^2} \ln x + \tfrac{x^2-6x}{8(x-1)}, \tag{C.7}$$

$$[D_9]_W^0 = \tfrac{-3x^4+30x^3-54x^2+32x-8}{18(x-1)^4} \ln x + \tfrac{47x^3-237x^2+312x-104}{108(x-1)^3}, \tag{C.8}$$

$$[E_4]_W^0 = \tfrac{-9x^2+16x-4}{6(x-1)^4} \ln x + \tfrac{7x^3+21x^2-42x-4}{36(x-1)^3}, \tag{C.9}$$

$$[F_8]_W^0 = \tfrac{3x^2}{2(x-1)^4} \ln x + \tfrac{-5x^3+9x^2-30x+8}{12(x-1)^3}, \tag{C.10}$$

$$[A_7]_W^1 = \tfrac{32x^4+244x^3-160x^2+16x}{9(x-1)^4} \mathrm{Li}_2\left(1-\tfrac{1}{x}\right) + \tfrac{774x^4+2826x^3-1994x^2+130x-8}{81(x-1)^5} \ln x + \tfrac{-94x^4-18665x^3+20682x^2-9113x+2006}{243(x-1)^4}$$

$$+ \left[\tfrac{12x^4+92x^3-56x^2}{3(x-1)^5}\ln x + \tfrac{-68x^4-202x^3-804x^2+794x-152}{27(x-1)^4}\right] L_t, \tag{C.11}$$

$$[B_9^{l\bar{l}}]_W^1 = [B_{10}^{l\bar{l}}]_W^1 =$$
$$\tfrac{-2x}{(x-1)^2}\mathrm{Li}_2\big(1-\tfrac{1}{x}\big) + \tfrac{x^2-17x}{3(x-1)^3}\ln x + \tfrac{13x+3}{3(x-1)^2} + \left[\tfrac{-2x^2-2x}{(x-1)^3}\ln x + \tfrac{4x}{(x-1)^2}\right] L_t, \tag{C.12}$$

$$[C_9^{l\bar{l}}]_W^1 = \tfrac{-x^3-4x}{(x-1)^2}\mathrm{Li}_2\big(1-\tfrac{1}{x}\big) + \tfrac{-3x^3-14x^2-23x}{3(x-1)^3}\ln x + \tfrac{4x^3+7x^2+29x}{3(x-1)^2}$$
$$+ \left[\tfrac{-8x^2-2x}{(x-1)^3}\ln x + \tfrac{x^3+x^2+8x}{(x-1)^2}\right] L_t, \tag{C.13}$$

$$[D_9]_W^1 = \tfrac{380x^4-1352x^3+1656x^2-784x+256}{81(x-1)^4}\mathrm{Li}_2\big(1-\tfrac{1}{x}\big) + \tfrac{-304x^4-1716x^3+4644x^2-2768x+720}{81(x-1)^5}\ln x$$
$$+ \tfrac{-6175x^4+41608x^3-66723x^2+33106x-7000}{729(x-1)^4}$$
$$+ \left[\tfrac{-648x^4+720x^3+232x^2+160x-32}{81(x-1)^5}\ln x + \tfrac{-352x^4+4912x^3-8280x^2+3304x-880}{243(x-1)^4}\right] L_t, \tag{C.14}$$

$$[E_4]_W^1 = \tfrac{515x^4-614x^3-81x^2-190x+40}{54(x-1)^4}\mathrm{Li}_2\big(1-\tfrac{1}{x}\big) + \tfrac{1030x^4-435x^3-1373x^2-1950x+424}{108(x-1)^5}\ln x$$
$$+ \tfrac{-29467x^4+45604x^3-30237x^2+66532x-10960}{1944(x-1)^4}$$
$$+ \left[\tfrac{1125x^3-1685x^2-380x+76}{54(x-1)^5}\ln x + \tfrac{133x^4-2758x^3-2061x^2+11522x-1652}{324(x-1)^4}\right] L_t, \tag{C.15}$$

$$[F_8]_W^1 = \tfrac{4x^4-40x^3-41x^2-x}{3(x-1)^4}\mathrm{Li}_2\big(1-\tfrac{1}{x}\big) + \tfrac{144x^4-3177x^3-3661x^2-250x+32}{108(x-1)^5}\ln x$$
$$+ \tfrac{-247x^4+11890x^3+31779x^2-2966x+1016}{648(x-1)^4}$$
$$+ \left[\tfrac{-17x^3-31x^2}{(x-1)^5}\ln x + \tfrac{-35x^4+170x^3+447x^2+338x-56}{18(x-1)^4}\right] L_t, \tag{C.16}$$

$$[G_3]_W^1 = \tfrac{10x^4-100x^3+30x^2+160x-40}{27(x-1)^4}\mathrm{Li}_2\big(1-\tfrac{1}{x}\big) + \tfrac{30x^3-42x^2-332x+68}{81(x-1)^4}\ln x$$
$$+ \tfrac{6x^3+293x^2-161x-42}{81(x-1)^3} + \left[\tfrac{90x^2-160x+40}{27(x-1)^4}\ln x + \tfrac{-35x^3-105x^2+210x+20}{81(x-1)^3}\right] L_t, \tag{C.17}$$

$$[T_1]_W^1 = -(16x+8)\sqrt{4x-1}\,\mathrm{Cl}_2\Big(2\arcsin\tfrac{1}{2\sqrt{x}}\Big) + \big(16x+\tfrac{20}{3}\big)\ln x + 32x + \tfrac{112}{9}. \tag{C.18}$$

The result of the functions

- $[A_7]_W^1$ and $[F_8]_W^1$ are given in [57, 153–156],
- $[B_9]_W^1$ and $[C_9]_W^1$ are given in [149, 150, 157, 158],
- $[D_9]_W^1$, $[E_4]_W^1$, $[G_3]_W^1$ and $[T_1]_W^1$ are given in [85].

C.2 $i = H$ – "top quark – charged Higgs"

The evaluation of Feynman diagrams contributing to $b \to s+$(light particles) Greens functions within the MSSM (but also Two Higgs doublet models (2HDM) of type II) mediated by "top quark – charged Higgs boson" loops and denoted by the index $i = H$ in eq. (5.11) yields

$$[A_7]_H^0 = \tfrac{-3y^2+2y}{3(y-1)^3}\ln y + \tfrac{5y^2-3y}{6(y-1)^2} + \cot^2\beta\left\{\tfrac{-3y^3+2y^2}{6(y-1)^4}\ln y + \tfrac{8y^3+5y^2-7y}{36(y-1)^3}\right\}, \tag{C.19}$$

$$[B_9^{l\bar{l}}]_H^0 = [B_{10}^{l\bar{l}}]_H^0 = 0, \tag{C.20}$$

$$[C_9^{l\bar{l}}]_H^0 = \tfrac{M_H^2}{8M_W^2}\cot^2\beta\left\{\tfrac{-y^2}{(y-1)^2}\ln y + \tfrac{y^2}{y-1}\right\}, \tag{C.21}$$

$$[D_9]_H^0 = \cot^2\beta\left\{\tfrac{-3y^4+6y^2-4y}{18(y-1)^4}\ln y + \tfrac{47y^3-79y^2+38y}{108(y-1)^3}\right\}, \tag{C.22}$$

$$[E_4]_H^0 = \cot^2\beta\left\{\tfrac{3y^2-2y}{6(y-1)^4}\ln y + \tfrac{7y^3-29y^2+16y}{36(y-1)^3}\right\}, \tag{C.23}$$

$$[F_8]_H^0 = \tfrac{y}{(y-1)^3}\ln y + \tfrac{y^2-3y}{2(y-1)^2} + \cot^2\beta\left\{\tfrac{y^2}{2(y-1)^4}\ln y + \tfrac{y^3-5y^2-2y}{12(y-1)^3}\right\}, \tag{C.24}$$

$$\begin{aligned}[A_7]_H^1 = {} & \tfrac{-64y^3+224y^2-96y}{9(y-1)^3}\mathrm{Li}_2\Big(1-\tfrac{1}{y}\Big) + \tfrac{-28y^3+256y^2-132y}{9(y-1)^4}\ln y + \tfrac{16y^3-104y^2+56y}{3(y-1)^3} \\ & + \left[\tfrac{24y^3+112y^2-64y}{9(y-1)^4}\ln y + \tfrac{32y^3-188y^2+84y}{9(y-1)^3}\right]L_t \\ & + \cot^2\beta\left\{\tfrac{-32y^4+148y^3-72y^2}{9(y-1)^4}\mathrm{Li}_2\Big(1-\tfrac{1}{y}\Big) + \tfrac{-126y^4+1614y^3-926y^2+14y}{81(y-1)^5}\ln y\right. \\ & \left. + \tfrac{1202y^4-7569y^3+5436y^2-797y}{243(y-1)^4} + \left[\tfrac{12y^4+92y^3-56y^2}{9(y-1)^5}\ln y + \tfrac{28y^4-270y^3+36y^2+62y}{27(y-1)^4}\right]L_t\right\},\end{aligned} \tag{C.25}$$

$$[B_9^{l\bar{l}}]_H^1 = [B_{10}^{l\bar{l}}]_H^1 = 0, \tag{C.26}$$

$$\begin{aligned}[C_9^{l\bar{l}}]_H^1 = {} & \tfrac{M_H^2}{8M_W^2}\cot^2\beta\left\{\tfrac{-8y^3+16y^2}{(y-1)^2}\mathrm{Li}_2\Big(1-\tfrac{1}{y}\Big) + \tfrac{-24y^3+88y^2}{3(y-1)^3}\ln y + \tfrac{32y^3-96y^2}{3(y-1)^2}\right. \\ & \left. + \left[\tfrac{16y^2}{(y-1)^3}\ln y + \tfrac{8y^3-24y^2}{(y-1)^2}\right]L_t\right\},\end{aligned} \tag{C.27}$$

$$\begin{aligned}[D_9]_H^1 = {} & \cot^2\beta\left\{\tfrac{380y^4-528y^3+72y^2+128y}{81(y-1)^4}\mathrm{Li}_2\Big(1-\tfrac{1}{y}\Big) + \tfrac{596y^4-672y^3+64y^2+204y}{81(y-1)^5}\ln y\right. \\ & + \tfrac{-6175y^4+9138y^3-3927y^2-764y}{729(y-1)^4} \\ & \left. + \left[\tfrac{432y^4-456y^3+40y^2+128y}{81(y-1)^5}\ln y + \tfrac{-352y^4-972y^3+1944y^2-1052y}{243(y-1)^4}\right]L_t\right\},\end{aligned} \tag{C.28}$$

$$[E_4]_H^1 = \cot^2\beta \left\{ \tfrac{515y^4-906y^3+99y^2+182y}{54(y-1)^4}\mathrm{Li}_2\Big(1-\tfrac{1}{y}\Big) + \tfrac{1030y^4-2763y^3-15y^2+980y}{108(y-1)^5}\ln y \right.$$
$$+ \tfrac{-29467y^4+68142y^3-6717y^2-18134y}{1944(y-1)^4}$$
$$\left. + \left[\tfrac{-375y^3-95y^2+182y}{54(y-1)^5}\ln y + \tfrac{133y^4-108y^3+4023y^2-2320y}{324(y-1)^4}\right] L_t \right\}, \tag{C.29}$$

$$[F_8]_H^1 = \tfrac{-17y^3+25y^2-36y}{3(y-1)^3}\mathrm{Li}_2\Big(1-\tfrac{1}{y}\Big) + \tfrac{-34y^3+7y^2-165y}{6(y-1)^4}\ln y + \tfrac{29y^3-44y^2+143y}{4(y-1)^3}$$
$$+ \left[\tfrac{-34y^2-38y}{3(y-1)^4}\ln y + \tfrac{7y^3-16y^2+81y}{3(y-1)^3}\right] L_t$$
$$+ \cot^2\beta \left\{ \tfrac{-13y^4+17y^3-30y^2}{3(y-1)^4}\mathrm{Li}_2\Big(1-\tfrac{1}{y}\Big) + \tfrac{-468y^4+321y^3-2155y^2-2y}{108(y-1)^5}\ln y \right.$$
$$\left. + \tfrac{4451y^4-7650y^3+18153y^2-1130y}{648(y-1)^4} + \left[\tfrac{-17y^3-31y^2}{3(y-1)^5}\ln y + \tfrac{7y^4-18y^3+261y^2+38y}{18(y-1)^4}\right] L_t \right\}, \tag{C.30}$$

$$[G_3]_H^1 = \cot^2\beta \left\{ \tfrac{10y^4+30y^2-20y}{27(y-1)^4}\mathrm{Li}_2\Big(1-\tfrac{1}{y}\Big) + \tfrac{30y^3-66y^2-56y}{81(y-1)^4}\ln y + \tfrac{6y^3-187y^2+213y}{81(y-1)^3} \right.$$
$$\left. + \left[\tfrac{-30y^2+20y}{27(y-1)^4}\ln y + \tfrac{-35y^3+145y^2-80y}{81(y-1)^3}\right] L_t \right\}, \tag{C.31}$$

$$[T_1]_H^1 = 0. \tag{C.32}$$

The result of the functions

- $[A_7]_H^1$ and $[F_8]_H^1$ are given in [57, 155, 159],
- $[B_{10}]_H^1$ and $[C_9]_H^1$ are given in [86].

The results of the functions $[D_9]_H^1$, $[E_4]_H^1$, $[G_3]_H^1$ and $[T_1]_H^1$ are new. Note that $[B_9]_H^1$ and $[B_{10}]_H^1$ vanish due to the approximation of vanishing lepton masses.

C.3 $i = \tilde{\chi}$ – "chargino – up-squark"

The evaluation of Feynman diagrams contributing to $b \to s+$(light particles) Greens functions within the MSSM mediated by "chargino – up squark" loops and denoted by the index $i = \tilde{\chi}$ in eq. (5.11) yields

$$[A_7]_{\tilde{\chi}}^0 = \kappa \sum_{i=1}^{2}\sum_{a=1}^{6} \frac{M_W^2}{M_{\tilde{\chi}_i}^2} \left\{ [X_i^{U_L\dagger}]_{2a}[X_i^{U_L}]_{a3}\, h_1^{(0)}(y_{ai}) + \frac{M_{\tilde{\chi}_i}}{m_b}[X_i^{U_L\dagger}]_{2a}[X_i^{U_R}]_{a3}\, h_2^{(0)}(y_{ai}) \right\}, \tag{C.33}$$

$$[B_{9,10}^{l\bar{l}}]_{\tilde{\chi}}^0 = \mp\kappa \frac{M_W^2}{2e^2} \sum_{i,j=1}^{2}\sum_{a=1}^{6}\sum_{b=1}^{3} \frac{[X_j^{U_L\dagger}]_{2a}[X_i^{U_L}]_{a3}}{M_{\tilde{\chi}_i}^2}$$
$$\times \left\{ \frac{1}{2}[X_i^{N_L\dagger}]_{lb}[X_j^{N_L}]_{bl} f_5^{(0)}(x_{ji}, y_{ai}, v_{bi}) \mp [X_i^{N_R\dagger}]_{lb}[X_j^{N_R}]_{bl}\sqrt{x_{ji}} f_6^{(0)}(x_{ji}, y_{ai}, v_{bi}) \right\}, \tag{C.34}$$

$$[C_9^{l\bar{l}}]^0_{\tilde{\chi}} = [C_L^{\nu\bar{\nu}}]^0_{\tilde{\chi}}, \tag{C.35}$$

$$[D_9]^0_{\tilde{\chi}} = \kappa \sum_{i=1}^{2}\sum_{a=1}^{6} \frac{M_W^2}{M_{\tilde{\chi}_i}^2} [X_i^{U_L\dagger}]_{2a}[X_i^{U_L}]_{a3}\; h_3^{(0)}(y_{ai}), \tag{C.36}$$

$$[E_4]^0_{\tilde{\chi}} = \kappa \sum_{i=1}^{2}\sum_{a=1}^{6} \frac{M_W^2}{M_{\tilde{\chi}_i}^2} [X_i^{U_L\dagger}]_{2a}[X_i^{U_L}]_{a3}\; h_4^{(0)}(y_{ai}), \tag{C.37}$$

$$[F_8]^0_{\tilde{\chi}} = \kappa \sum_{i=1}^{2}\sum_{a=1}^{6} \frac{M_W^2}{M_{\tilde{\chi}_i}^2} \left\{ [X_i^{U_L\dagger}]_{2a}[X_i^{U_L}]_{a3}\; h_5^{(0)}(y_{ai}) + \frac{M_{\tilde{\chi}_i}}{m_b} [X_i^{U_L\dagger}]_{2a}[X_i^{U_R}]_{a3}\; h_6^{(0)}(y_{ai}) \right\}, \tag{C.38}$$

$$[A_7]^1_{\tilde{\chi}} = \kappa \sum_{i=1}^{2}\sum_{a=1}^{6} \frac{M_W^2}{M_{\tilde{\chi}_i}^2} \left\{ [X_i^{U_L\dagger}]_{2a}[X_i^{U_L}]_{a3}\; h_1^{(1)}(y_{ai}) + \frac{M_{\tilde{\chi}_i}}{m_b} [X_i^{U_L\dagger}]_{2a}[X_i^{U_R}]_{a3}\; h_2^{(1)}(y_{ai}) \right\}, \tag{C.39}$$

$$\begin{aligned}[B_{9,10}^{l\bar{l}}]^1_{\tilde{\chi}} = {} & \mp\kappa \frac{M_W^2}{2e^2} \sum_{i,j=1}^{2}\sum_{a=1}^{6}\sum_{b=1}^{3} \frac{[X_j^{U_L\dagger}]_{2a}[X_i^{U_L}]_{a3}}{M_{\tilde{\chi}_i}^2} \\ & \times \left\{ \frac{1}{2}[X_i^{N_L\dagger}]_{lb}[X_j^{N_L}]_{bl} \left[f_8^{(1)}(x_{ji}, y_{ai}, v_{bi}) + 4\left(1 + y_{ai}\frac{\partial}{\partial y_{ai}}\right) f_5^{(0)}(x_{ji}, y_{ai}, v_{bi})\; L_{\tilde{u}_a} \right] \right. \\ & \left. \mp [X_i^{N_R\dagger}]_{lb}[X_j^{N_R}]_{bl}\sqrt{x_{ji}} \left[f_9^{(1)}(x_{ji}, y_{ai}, v_{bi}) + 4\left(1 + y_{ai}\frac{\partial}{\partial y_{ai}}\right) f_6^{(0)}(x_{ji}, y_{ai}, v_{bi})\; L_{\tilde{u}_a} \right] \right\}, \end{aligned} \tag{C.40}$$

$$[C_9^{l\bar{l}}]^1_{\tilde{\chi}} = [C_L^{\nu\bar{\nu}}]^1_{\tilde{\chi}}, \tag{C.41}$$

$$[D_9]^1_{\tilde{\chi}} = \kappa \sum_{i=1}^{2}\sum_{a=1}^{6} \frac{M_W^2}{M_{\tilde{\chi}_i}^2} [X_i^{U_L\dagger}]_{2a}[X_i^{U_L}]_{a3}\; h_3^{(1)}(y_{ai}), \tag{C.42}$$

$$[E_4]^1_{\tilde{\chi}} = \kappa \sum_{i=1}^{2}\sum_{a=1}^{6} \frac{M_W^2}{M_{\tilde{\chi}_i}^2} [X_i^{U_L\dagger}]_{2a}[X_i^{U_L}]_{a3}\; h_4^{(1)}(y_{ai}), \tag{C.43}$$

$$[F_8]^1_{\tilde{\chi}} = \kappa \sum_{i=1}^{2}\sum_{a=1}^{6} \frac{M_W^2}{M_{\tilde{\chi}_i}^2} \left\{ [X_i^{U_L\dagger}]_{2a}[X_i^{U_L}]_{a3}\; h_5^{(1)}(y_{ai}) + \frac{M_{\tilde{\chi}_i}}{m_b} [X_i^{U_L\dagger}]_{2a}[X_i^{U_R}]_{a3}\; h_6^{(1)}(y_{ai}) \right\}, \tag{C.44}$$

$$[G_3]^1_{\tilde{\chi}} = \kappa \sum_{i=1}^{2} \sum_{a=1}^{6} \frac{M_W^2}{M^2_{\tilde{\chi}_i}} [X_i^{U_L\dagger}]_{2a} [X_i^{U_L}]_{a3}\, h_7^{(1)}(y_{ai}), \tag{C.45}$$

$$\begin{aligned}[T_1]^1_{\tilde{\chi}} = \sum_{a=1}^{6} \Bigg\{ & (8x_{\tilde{u}_a} - 2)\sqrt{4x_{\tilde{u}_a} - 1}\, \mathrm{Cl}_2\Big(2 \arcsin \tfrac{1}{2\sqrt{x_{\tilde{u}_a}}}\Big) - \Big(8x_{\tilde{u}_a} - \frac{8}{3}\Big) \ln x_{\tilde{u}_a} - 16 x_{\tilde{u}_a} + \frac{52}{9} \\ & + (8x_{\tilde{d}_a} - 2)\sqrt{4x_{\tilde{d}_a} - 1}\, \mathrm{Cl}_2\Big(2 \arcsin \tfrac{1}{2\sqrt{x_{\tilde{d}_a}}}\Big) - \Big(8x_{\tilde{d}_a} - \frac{8}{3}\Big) \ln x_{\tilde{d}_a} - 16 x_{\tilde{d}_a} + \frac{52}{9} \Bigg\}. \end{aligned} \tag{C.46}$$

The result of the functions

- $[A_7]^1_{\tilde{\chi}}$ and $[F_8]^1_{\tilde{\chi}}$ are given in [57, 58],
- $[B_{10}]^1_{\tilde{\chi}}$ and $[C_9]^1_{\tilde{\chi}}$ are given in [86].

The results of the functions $[D_9]^1_{\tilde{\chi}}$, $[E_4]^1_{\tilde{\chi}}$, $[G_3]^1_{\tilde{\chi}}$ and $[T_1]^1_{\tilde{\chi}}$ are new. The expression of the functions $[C_L^{\nu\bar{\nu}}]^0_{\tilde{\chi}}$ and $[C_L^{\nu\bar{\nu}}]^1_{\tilde{\chi}}$ correspond to the leading and the next-to leading contribution of the function $[C_L^{\nu\bar{\nu}}]_{\tilde{\chi}} = [C_L^{\nu\bar{\nu}}]^0_{\tilde{\chi}} + \alpha_s/(4\pi)[C_L^{\nu\bar{\nu}}]^1_{\tilde{\chi}}$ given in (3.14) of [86].

C.4 $i = 4$ – "chargino – up-squark (quartic)"

The evaluation of Feynman diagrams contributing to $b \to s+$(light particles) Greens functions within the MSSM mediated by "chargino – up squark" loops containing the quartic squark vertex[1] instead of gluon corrections and denoted by the index $i = 4$ in eq. (5.11) yields

$$\begin{aligned}[A_7]^1_4 = {} & \kappa \sum_{i=1}^{2} \sum_{a,b,c=1}^{6} \frac{M_W^2}{M^2_{\tilde{\chi}_i}}\, P^U_{ab}\, y_{bi}\, P^U_{bc}\, (1 + L_{\tilde{u}_b}) \\ & \times \Bigg\{ [X_i^{U_L\dagger}]_{2a} [X_i^{U_L}]_{c3}\, [-q_1^{(1)}(y_{ai}, y_{ci}) + \frac{2}{3} q_2^{(1)}(y_{ai}, y_{ci})] \\ & + \frac{M_{\tilde{\chi}_i}}{m_b} [X_i^{U_L\dagger}]_{2a} [X_i^{U_R}]_{c3}\, [-q_3^{(1)}(y_{ai}, y_{ci}) + \frac{2}{3} q_4^{(1)}(y_{ai}, y_{ci})] \Bigg\}, \end{aligned} \tag{C.47}$$

$$\begin{aligned}[B^{l\bar{l}}_{9,10}]^1_4 = {} & \pm \frac{\kappa}{2e^2} \frac{4}{3} \sum_{i,j=1}^{2} \sum_{f=1}^{3} \sum_{a,b,c=1}^{6} \frac{M_W^2}{M^2_{\tilde{\chi}_i}}\, P^U_{ab}\, y_{bi}\, P^U_{bc}\, (1 + L_{\tilde{u}_b})\, [X_j^{U_L\dagger}]_{2a} [X_i^{U_L}]_{c3} \\ & \times \Bigg\{ \frac{1}{2} f_9^{(0)}(x_{ji}, y_{ai}, y_{ci}, v_{fi}) [X_i^{N_L\dagger}]_{lf} [X_j^{N_L}]_{fl} \\ & \mp \sqrt{x_{ji}} f_{10}^{(0)}(x_{ji}, y_{ai}, y_{ci}, v_{fi}) [X_i^{N_R\dagger}]_{lf} [X_j^{N_R}]_{fl} \Bigg\}, \end{aligned} \tag{C.48}$$

[1] Strictly speaking these matching contributions originate from the part of the quartic squark vertex proportional to the strong coupling constant α_s.

$$[C_9^{l\bar{l}}]_4^1 = \frac{\kappa}{6}\sum_{i,j=1}^{2}\sum_{a,\ldots,e,g,k=1}^{6} P_{gk}^U\, y_{ki}\, P_{ke}^U\, (1+L_{\tilde{u}_k})\, [X_j^{U_L\,\dagger}]_{2d}[X_i^{U_L}]_{a3}$$
$$\times\Big\{2\sqrt{x_{ji}}f_6^{(0)}(x_{ji},y_{ai},y_{di})U_{j1}U_{i1}^*\delta_{ae}\delta_{gd} - f_5^{(0)}(x_{ji},y_{ai},y_{di})V_{j1}^*V_{i1}\delta_{ae}\delta_{gd}$$
$$+ f_5^{(0)}(y_{ai},y_{bi},y_{ci})(\Gamma^{U_L}\Gamma^{U_L\dagger})_{bc}\delta_{ij}\delta_{ae}\delta_{bg}\delta_{cd} + f_5^{(0)}(y_{ai},y_{ci},y_{di})(\Gamma^{U_L}\Gamma^{U_L\dagger})_{bc}\delta_{ij}\delta_{ab}\delta_{ce}\delta_{dg}\Big\}, \tag{C.49}$$

$$[D_9]_4^1 = \kappa\sum_{i=1}^{2}\sum_{a,b,c=1}^{6}\frac{M_W^2}{M_{\tilde{\chi}_i}^2}\, P_{ab}^U\, y_{bi}\, P_{bc}^U\, (1+L_{\tilde{u}_b})\, [X_i^{U_L\,\dagger}]_{2a}[X_i^{U_L}]_{c3}\, q_5^{(1)}(y_{ai},y_{ci}), \tag{C.50}$$

$$[E_4]_4^1 = \kappa\sum_{i=1}^{2}\sum_{a,b,c=1}^{6}\frac{M_W^2}{M_{\tilde{\chi}_i}^2}\, P_{ab}^U\, y_{bi}\, P_{bc}^U\, (1+L_{\tilde{u}_b})\, [X_i^{U_L\,\dagger}]_{2a}[X_i^{U_L}]_{c3}\, q_6^{(1)}(y_{ai},y_{ci}), \tag{C.51}$$

$$[F_8]_4^1 = \kappa\sum_{i=1}^{2}\sum_{a,b,c=1}^{6}\frac{M_W^2}{M_{\tilde{\chi}_i}^2}\, P_{ab}^U y_{bi}\, P_{bc}^U\, (1+L_{\tilde{u}_b})$$
$$\times\left\{[X_i^{U_L\,\dagger}]_{2a}[X_i^{U_L}]_{c3}\, q_2^{(1)}(y_{ai},y_{ci}) + \frac{M_{\tilde{\chi}_i}}{m_b}[X_i^{U_L\,\dagger}]_{2a}[X_i^{U_R}]_{c3}\, q_4^{(1)}(y_{ai},y_{ci})\right\}, \tag{C.52}$$

$$[G_3]_4^1 = 0, \tag{C.53}$$

$$[T_1]_4^1 = 0. \tag{C.54}$$

The result of the functions

- $[A_7]_4^1$ and $[F_8]_4^1$ are given in [57],
- $[B_{10}]_4^1$ and $[C_9]_4^1$ are given in [86].

The result of the functions $[D_9]_4^1$, $[E_4]_4^1$, $[G_3]_4^1$ and $[T_1]_4^1$ are new.

Appendix D Auxiliary Functions

Here we present explicit formulae for the loop functions $h_i^{(0)}(x)$, $h_i^{(1)}(x)$ and $q_i^{(1)}(x,y)$ introduced in Appendix C. They read

$$h_1^{(0)}(x) = \tfrac{3x^2-2x}{3(x-1)^4}\ln x + \tfrac{-8x^2-5x+7}{18(x-1)^3}, \tag{D.1}$$

$$h_2^{(0)}(x) = \tfrac{-6x^2+4x}{3(x-1)^3}\ln x + \tfrac{7x-5}{3(x-1)^2}, \tag{D.2}$$

$$h_3^{(0)}(x) = \tfrac{-6x^3+9x^2-2}{9(x-1)^4}\ln x + \tfrac{52x^2-101x+43}{54(x-1)^3}, \tag{D.3}$$

$$h_4^{(0)}(x) = \tfrac{-1}{3(x-1)^4}\ln x + \tfrac{2x^2-7x+11}{18(x-1)^3}, \tag{D.4}$$

$$h_5^{(0)}(x) = \tfrac{-x}{(x-1)^4}\ln x + \tfrac{-x^2+5x+2}{6(x-1)^3}, \tag{D.5}$$

$$h_6^{(0)}(x) = \tfrac{2x}{(x-1)^3}\ln x + \tfrac{-x-1}{(x-1)^2}, \tag{D.6}$$

$$\begin{aligned} h_1^{(1)}(x) = {} & \tfrac{-48x^3-104x^2+64x}{9(x-1)^4}\mathrm{Li}_2\big(1-\tfrac{1}{x}\big) + \tfrac{-378x^3-1566x^2+850x+86}{81(x-1)^5}\ln x \\ & + \tfrac{2060x^3+3798x^2-2664x-170}{243(x-1)^4} + \left[\tfrac{12x^3-124x^2+64x}{9(x-1)^5}\ln x + \tfrac{-56x^3+258x^2+24x-82}{27(x-1)^4}\right] L_{\tilde{u}_a}, \end{aligned} \tag{D.7}$$

$$\begin{aligned} h_2^{(1)}(x) = {} & \tfrac{224x^2-96x}{9(x-1)^3}\mathrm{Li}_2\big(1-\tfrac{1}{x}\big) + \tfrac{-24x^3+352x^2-128x-32}{9(x-1)^4}\ln x + \tfrac{-340x^2+132x+40}{9(x-1)^3} \\ & + \left[\tfrac{-24x^3+176x^2-80x}{9(x-1)^4}\ln x + \tfrac{-28x^2-108x+64}{9(x-1)^3}\right] L_{\tilde{u}_a}, \end{aligned} \tag{D.8}$$

$$\begin{aligned} h_3^{(1)}(x) = {} & \tfrac{32x^3+120x^2-384x+128}{81(x-1)^4}\mathrm{Li}_2\big(1-\tfrac{1}{x}\big) + \tfrac{-108x^4+1058x^3-898x^2-1098x+710}{81(x-1)^5}\ln x \\ & + \tfrac{-304x^3-13686x^2+29076x-12062}{729(x-1)^4} \\ & + \left[\tfrac{540x^3-972x^2+232x+56}{81(x-1)^5}\ln x + \tfrac{-664x^3+54x^2+1944x-902}{243(x-1)^4}\right] L_{\tilde{u}_a}, \end{aligned} \tag{D.9}$$

$$h_4^{(1)}(x) = \tfrac{-562x^3+1101x^2-420x+101}{54(x-1)^4}\mathrm{Li}_2\big(1-\tfrac{1}{x}\big) + \tfrac{-562x^3+1604x^2-799x+429}{54(x-1)^5}\ln x$$

$$+\frac{17470x^3-47217x^2+31098x-13447}{972(x-1)^4}+\left[\frac{89x+55}{27(x-1)^5}\ln x+\frac{38x^3-135x^2+54x-821}{162(x-1)^4}\right]L_{\tilde{u}_a}, \tag{D.10}$$

$$h_5^{(1)}(x)=\frac{9x^3+46x^2+49x}{6(x-1)^4}\mathrm{Li}_2\left(1-\tfrac{1}{x}\right)+\frac{81x^3+594x^2+1270x+71}{54(x-1)^5}\ln x$$
$$+\frac{-923x^3-3042x^2-6921x-1210}{324(x-1)^4}+\left[\frac{10x^2+38x}{3(x-1)^5}\ln x+\frac{-7x^3+30x^2-141x-26}{9(x-1)^4}\right]L_{\tilde{u}_a}, \tag{D.11}$$

$$h_6^{(1)}(x)=\frac{-32x^2-24x}{3(x-1)^3}\mathrm{Li}_2\left(1-\tfrac{1}{x}\right)+\frac{-52x^2-109x-7}{3(x-1)^4}\ln x+\frac{95x^2+180x+61}{6(x-1)^3}$$
$$+\left[\frac{-20x^2-52x}{3(x-1)^4}\ln x+\frac{-2x^2+60x+14}{3(x-1)^3}\right]L_{\tilde{u}_a}, \tag{D.12}$$

$$h_7^{(1)}(x)=\frac{-20x^3+60x^2-60x-20}{27(x-1)^4}\mathrm{Li}_2\left(1-\tfrac{1}{x}\right)+\frac{-60x^2+240x+4}{81(x-1)^4}\ln x+\frac{132x^2-382x+186}{81(x-1)^3}$$
$$+\left[\frac{20}{27(x-1)^4}\ln x+\frac{-20x^2+70x-110}{81(x-1)^3}\right]L_{\tilde{u}_a}, \tag{D.13}$$

$$q_1^{(1)}(x,y)=\frac{4}{3(x-y)}\left[\frac{x^2\ln x}{(x-1)^4}-\frac{y^2\ln y}{(y-1)^4}\right]+\frac{4x^2y^2+10xy^2-2y^2+10x^2y-44xy+10y-2x^2+10x+4}{9(x-1)^3(y-1)^3}, \tag{D.14}$$

$$q_2^{(1)}(x,y)=\frac{4}{3(x-y)}\left[\frac{x\ln x}{(x-1)^4}-\frac{y\ln y}{(y-1)^4}\right]+\frac{-2x^2y^2+10xy^2+4y^2+10x^2y-20xy-14y+4x^2-14x+22}{9(x-1)^3(y-1)^3}, \tag{D.15}$$

$$q_3^{(1)}(x,y)=\frac{8}{3(x-y)}\left[\frac{-x^2\ln x}{(x-1)^3}+\frac{y^2\ln y}{(y-1)^3}\right]+\frac{-12xy+4y+4x+4}{3(x-1)^2(y-1)^2}, \tag{D.16}$$

$$q_4^{(1)}(x,y)=\frac{8}{3(x-y)}\left[\frac{-x\ln x}{(x-1)^3}+\frac{y\ln y}{(y-1)^3}\right]+\frac{-4xy-4y-4x+12}{3(x-1)^2(y-1)^2}, \tag{D.17}$$

$$q_5^{(1)}(x,y)=\frac{4}{27(x-y)}\left[\frac{(6x^3-9x^2+2)\ln x}{(x-1)^4}-\frac{(6y^3-9y^2+2)\ln y}{(y-1)^4}\right]$$
$$+\frac{104x^2y^2-202xy^2+86y^2-202x^2y+380xy-154y+86x^2-154x+56}{81(x-1)^3(y-1)^3}, \tag{D.18}$$

$$q_6^{(1)}(x,y)=\frac{4}{9(x-y)}\left[\frac{\ln x}{(x-1)^4}-\frac{\ln y}{(y-1)^4}\right]+\frac{4x^2y^2-14xy^2+22y^2-14x^2y+52xy-62y+22x^2-62x+52}{27(x-1)^3(y-1)^3}, \tag{D.19}$$

$$f_5^{(0)}(x,y,z)=\frac{x^2\ln x}{(x-1)(x-y)(x-z)}+(x\leftrightarrow y)+(x\leftrightarrow z), \tag{D.20}$$

$$f_6^{(0)}(x,y,z)=\frac{x\ln x}{(x-1)(x-y)(x-z)}+(x\leftrightarrow y)+(x\leftrightarrow z). \tag{D.21}$$

Bibliography

[1] P. W. Higgs, Phys. Lett. **12** (1964) 132, Phys. Rev. Lett. **13** (1964) 508, Phys. Rev. **145** (1966) 1156.

[2] F. Englert and R. Brout, Phys. Rev. Lett. **13** (1964) 321.

[3] G. S. Guralnik, C. R. Hagen and T. W. B. Kibble, Phys. Rev. Lett. **13** (1964) 585.

[4] T. W. B. Kibble, Phys. Rev. **155** (1967) 1554.

[5] G. 't Hooft and M. Veltman, Nucl. Phys. **B44** (1972) 189; Nucl. Phys. **B50** (1972) 318.

[6] B. W. Lee and J. Zinn-Justin, Phys. Rev. **D5** (1972) 3121, 3137, 3155; Phys. Rev. **D7** (1973) 1049.

[7] N. Cabibbo, Phys. Rev. Lett. **10** (1963) 531.

[8] M. Kobayashi and K. Maskawa, Prog. Theor. Phys. **49** (1973) 652.

[9] Y. Fukuda, *et al.*, [Super-Kamiokande Collaboration], Phys. Rev. Lett. **81** (1998) 1562, hep-ex/9807003.

[10] Q. R. Ahmad, *et al.*, [SNO Collaboration], Phys. Rev. Lett. **98** (2002) 011301, nucl-ex/0204008.

[11] J. H. Christenson J. W. Cronin, V. L. Fitch and R. Turlay, Phys. Rev. Lett. **13** (1964) 138.

[12] T. Affolder *et al.* [CDF Collaboration], Phys. Rev. **D61** (2000) 072005, hep-ex/9909003.

[13] M. Battaglia *et al.*, hep-ph/0304132.

[14] S. Chen *et al.* [CLEO Collaboration], Phys. Rev. Lett. **87** (2001) 251807, hep-ex/0108032.

[15] P. Gambino and M. Misiak, Nucl. Phys. **B611** (2001) 338, hep-ph/0104034.

[16] A. J. Buras and M. Misiak, Acta Phys. Polon. B **33** (2002) 2597, hep-ph/0207131.

[17] J. Kaneko *et al.* [Belle Collaboration], Phys. Rev. Lett. **90** (2003) 021801, hep-ex/0208029.

[18] B. Aubert *et al.* [BaBar Collaboration], hep-ex/0308016.

[19] Z. Ligeti and M. B. Wise, Phys. Rev. **D53** (1996) 4937, hep-ph/9512225.

[20] B. Grinstein, M. J. Savage and M. B. Wise, Nucl. Phys. **B319** (1989) 271.

[21] R. Grigjanis, P. J. O'Donnell, M. Sutherland and H. Navelet, Phys. Lett. **B223** (1989) 239.

[22] G. Cella, G. Ricciardi and A. Vicere, Phys. Lett. **B258** (1991) 212.

[23] M. Misiak, Nucl. Phys. **B393** (1993) 23, Erratum: Nucl. Phys. **B439** (1995) 461.

[24] A. J. Buras and M. Münz, Phys. Rev. **D52** (1995) 186, hep-ph/9501281.

[25] S. L. Glashow, Nucl. Phys. **B22** (1961) 579.

[26] S. Weinberg, Phys. Rev. Lett. **19** (1967) 1264.

[27] A. Salam, in "Elementary Particle Theory", ed. N. Svartholm, Amquist ans Wiksells, Stockholm (1969) p. 376.

[28] J. C. Taylor, Nucl. Phys. **B33** (1971) 436.

[29] A. A. Slavnov, Theor. Math. Phys. **10**(1972)99.

[30] M. Gell-Mann, P. Ramond and R. Slansky, in: P. van Nieuwenhuizen, D. Freedman (Eds.), Proceedings of the Supergravity Stony Brook Workshop, New York 1979, North-Holland, Amsterdam.

[31] T. Yanagida, in: A. Sawada, A. Sugamoto (Eds.), Proceedings of the Workshop on Unified Theories and Baryon Number in the Universe, Tsukuba, Japan 1979, KEK Report No. 79-18, Tsukuba.

[32] R. Mohapatra and G. Senjanovic, Phys. Lett. **44** (1980) 912.

[33] D. J. Gross and F. Wilczek, Phys. Rev. Lett. **30** (1973) 1343.

[34] H. D. Politzer, Phys. Rev. Lett. **30** (1973) 1346.

[35] S. R. Coleman and D. J. Gross, Phys. Rev. Lett. **31** (1973) 851.

[36] C. Itzykson and J. B. Zuber, "Quantum Field Theory,", McGraw-Hill Book Co., Singapore, 1980.

[37] K. G. Wilson, Phys. Rev. **179** (1969) 1499.

[38] G. 't Hooft and M. Veltman, Nucl. Phys. **B44** (1972) 189.

[39] C. G. Bollini and J. J. Giamiagi, Phys. Lett. **B40** (1972) 566.

[40] J. F. Ashmore, Nuovo Cimento Lett. **4** (1972) 289.

[41] G. M. Cicuta and E. Montaldi, Nuovo Cimento Lett. **4** (1972) 329.

[42] G. Leibbrandt, Rev. Mod. Phys. **47** (1975) 849.

[43] G. 't Hooft, Nucl. Phys. **B61** (1973) 455.

[44] W. A. Bardeen, A. J. Buras, D. W. Duke and T. Muta, Phys. Rev. **D18** (1978) 3998.

[45] P. Breitenlohner and D. Maison, Commun. Math. Phys. **52** (1977) 11.

[46] D. A. Akyeampong and R. Delbourgo, Nuovo Cimento A **17** (1973) 578.

[47] K. Chetyrkin, M. Misiak and M. Münz, Nucl. Phys. **B520** (1998) 279, hep-ph/9711280.

[48] H. E. Haber and G. L. Kane, Phys. Rept. **117** (1985) 75.

[49] J. Rosiek, Phys. Rev. **D41** (1990) 3464, Erratum: hep-ph/9511250.

[50] S. P. Martin, hep-ph/9709356.

[51] M. Misiak, S. Pokorski and J. Rosiek, Adv. Ser. Direct. High Energy Phys. **15**(1998)795, also in: A. J. Buras, M. Lindner (Eds.), "Heavy Flavors II", World Scientific, Singapore, 1998, p.795, hep-ph/9703442.

[52] S. Ferrara and E. Remiddi, Phys. Lett. **B53** (1974) 347.

[53] R. Barbieri and G. F. Giudice, Phys. Lett. **B309** (1993) 86, hep-ph/9303270.

[54] S. Bertolini, F. Borzumati, A. Masiero and G. Ridolfi, Nucl. Phys. **B353** (1991) 591.

[55] P. L. Cho, M. Misiak and D. Wyler, Phys. Rev. **D54** (1996) 3329, hep-ph/9601360.

[56] F. Borzumati, C. Greub, T. Hurth and D. Wyler, Phys. Rev. **D62** (2000) 075005, hep-ph/9911245.

[57] C. Bobeth, M. Misiak and J. Urban, Nucl. Phys. **B567** (2000) 153, hep-ph/9904413.

[58] M. Ciuchini, G. Degrassi, P. Gambino and G. F. Giudice, Nucl. Phys. **B534** (1998) 3, hep-ph/9806308.

[59] A. Ali and D. London, Eur. Phys. J. C **9** (1999) 687, hep-ph/9903535.

[60] S. Bergmann and G. Perez, Phys. Rev. **D64** (2001) 115009, hep-ph/0103299.

[61] A. J. Buras and R. Fleischer, Phys. Rev. **D64** (2001) 115010, hep-ph/0104238.

[62] A. J. Buras, P. H. Chankowski, J. Rosiek and L. Slawianowska, Nucl. Phys. **B619** (2001) 434, hep-ph/0107048.

[63] S. Laplace, Z. Ligeti, Y. Nir and G. Perez, Phys. Rev. **D65** (2002) 094040, hep-ph/0202010.

[64] G. D'Ambrosio, G. F. Giudice, G. Isidori and A. Strumia, Nucl. Phys. **B645** (2002) 155, hep-ph/0207036.

[65] A. J. Buras, P. Gambino, M. Gorbahn, S. Jäger and L. Silvestrini, Phys. Lett. **B500** (2001) 161, hep-ph/0007085

[66] C. S. Huang, W. Liao and Q. S. Yan Phys. Rev. **D59** (1999) 011701, hep-ph/9803460.

[67] C. S. Huang, W. Liao, Q. S. Yan and S. H. Zhu, Phys. Rev. **D63** (2001) 114021, Erratum: Phys. Rev. **D64** (2001) 059902, hep-ph/0006250.

[68] K. S. Babu and C. Kolda, Phys. Rev. Lett. **84** (2000) 228, hep-ph/9909476.

[69] P. H. Chankowski and Ł. Sławianowska, Phys. Rev. **D63** (2001) 054012, hep-ph/0008046.

[70] C. Bobeth, T.Ewerth, F.Krüger and J. Urban, Phys. Rev. **D64** (2001) 074014, hep-ph/0104284; Phys. Rev. **D66** (2002) 074021, hep-ph/0204225.

[71] A. J. Buras, P. H. Chankowski, J. Rosiek and Ł. Sławianowska, Nucl. Phys. **B619** (2001) 434, hep-ph/0107048; Phys. Lett. **B546** (2002) 96, hep-ph/0207241; hep-ph/0210145.

[72] G. Isidori and A. Retico, J. High Energy Phys. **0111** (2001) 001, hep-ph/0110121; J. High Energy Phys. **0209** (2002) 063, hep-ph/0208159.

[73] M. Carena, D. Garcia, U. Nierste and C. E. Wagner, Nucl. Phys. **B577** (2000) 88, hep-ph/9912516; Phys. Lett. **B499** (2001) 141, hep-ph/0010003.

[74] G. Degrassi, P. Gambino and G. F. Giudice, J. High Energy Phys. **0012** (2000) 009, hep-ph/0009337.

[75] S. Mori *et al.* [Belle Collaboration], Nucl. Instrum. Meth. A **479** (2002) 117.

[76] B. Aubert *et al.* [BaBar Collaboration], Nucl. Instrum. Meth. A **479** (2002) 1, hep-ex/0105044.

[77] K. Abe *et al.* [Belle Collaboration], Phys. Rev. Lett. **88** (2002) 021801, hep-ex/0109026; BELLE-CONF-0241; hep-ex/0308044.

[78] B. Aubert *et al.* [BaBar Collaboration], Phys. Rev. Lett. **88** (2002) 241801, hep-ex/0201008; hep-ex/0207082; hep-ex/0308042.

[79] A. J. Buras and P. H. Weisz, Nucl. Phys. **B333** (1990) 66.

[80] M. J. Dugan and B. Grinstein, Phys. Lett. **256** (1991) 239.

[81] S. Herrlich and U. Nierste, Nucl. Phys. **B455** (1995) 39, hep-ph/9412375.

[82] K. Chetyrkin, M. Misiak and M. Münz, Phys. Lett. **B400** (1997) 206, hep-ph/9612313, Erratum: Phys. Lett. **B425** (1998) 414.

[83] P. Gambino, M. Gorbahn and U. Haisch, hep-ph/0306079.

[84] H. D. Politzer, Nucl. Phys. **B172** (1980) 349.

[85] C. Bobeth, M. Misiak and J. Urban, Nucl. Phys. **B574** (2000) 291, hep-ph/9910220.

[86] C. Bobeth, A. J. Buras, F. Krüger and J. Urban, Nucl. Phys. **B630** (2002) 87, hep-ph/0112305.

[87] A. Djouadi, P. Gambino, S. Heinemeyer, W. Hollik, C. Jünger and G. Weiglein, Phys. Rev. **D57** (1998) 4179, hep-ph/9710438.

[88] A. J. Buras, Rev. Mod. Phys. **52** (1980) 199.

[89] M. Beneke, T. Feldmann and D. Seidel, Nucl. Phys. **B612** (2001) 25, hep-ph/0106067.

[90] P. Gambino, M. Gorbahn and U. Haisch, private communication, to be published.

[91] H. H. Asatrian, H. M. Asatrian, C. Greub and M. Walker, Phys. Lett. **B507** (2001) 162, hep-ph/0103087; Phys. Rev. **D65** (2002) 074004, hep-ph/0109140.

[92] H. H. Asatrian, H. M. Asatrian, C. Greub and M. Walker, Phys. Rev. **D66** (2002) 034009, hep-ph/0204341.

[93] A. Ghinculov, T. Hurth, G. Isidori and Y.-P. Yao, Nucl. Phys. **B648** (2003) 254, hep-ph/0208088.

[94] H. M. Asatrian, K. Bieri, C. Greub and A. Hovhannisyan, Phys. Rev. **D66** (2002) 094013, hep-ph/0209006.

[95] M. P. Walker, PhD Thesis, University Bern, 2002.

[96] A. J. Buras, A. Czarnecki, M. Misiak and J. Urban, Nucl. Phys. **B631** (2002) 219, hep-ph/0203135.

[97] N. Cabibbo and L. Maiani, Phys. Lett. **B79** (1978) 109.

[98] Y. Nir, Phys. Lett. **B221** (1989) 184.

[99] L. L. Chau and W. Y. Keung, Phys. Rev. Lett. **53** (1984) 1802.

[100] A. Ghinculov, T. Hurth, G. Isidori and Y. P. Yao, Nucl. Phys. Proc. Suppl. **116**, 284 (2003), hep-ph/0211197.

[101] A. Ghinculov, hep-ph/0305313.

[102] P. H. Chankowski and Ł. Sławianowska, hep-ph/308032.

[103] A. Ali, E. Lunghi, C. Greub and G. Hiller, Phys. Rev. **D66** (2002) 034002, hep-ph/0112300.

[104] A. J. Buras, P. Gambino, M. Gorbahn, S. Jäger and L. Silvestrini, Nucl. Phys. **B592** (2001) 55, hep-ph/.

[105] K. Hagiwara *et al.* [Particle Data Group Collaboration], Phys. Rev. **D66** (2002) 010001.

[106] A. Djouadi, M. Drees and J. L. Kneur, J. High Energy Phys. **0108** (2001) 055, hep-ph/0107316.

[107] G. G. Hanson, Talk given at XX International Symposium on Lepton and Photon Interactions at High Energies, July 23–28, 2001, Rome, Italy, hep-ex/0111058.

[108] [LEP Higgs Working Group Collaboration], hep-ex/0107030.

[109] A. Dabelstein, Z. Phys. C **67** (1995) 495, hep-ph/9409375.

[110] R. Hempfling and A. H. Hoang, Phys. Lett. **B331** (1994) 99, hep-ph/9401219.

[111] M. Carena, P. H. Chankowski, S. Pokorski and C. E. Wagner, Phys. Lett. **B441** (1998) 205, hep-ph/9805349.

[112] S. Heinemeyer, W. Hollik and G. Weiglein, Phys. Lett. **B455** (1999) 179, hep-ph/9903404.

[113] G. Burdman, Phys. Rev. **D52** (1995) 6400, hep-ph/9505352; Phys. Rev. **D57** (1998) 4254, hep-ph/9710550.

[114] M. B. Voloshin and M. A. Shifman, in: "Heavy Quarks" ed. V. A. Khoze and M. A. Shifman, Sov. Phys. Usp. **26** (1983) 387; Sov. J. Nucl. Phys. **41** (1985) 120; Sov. Phys.-JETP **64** (1986) 698.

[115] J. Chay, H. Georgi and B. Grinstein, Phys. Lett. **B247** (1990) 399.

[116] I. I. Bigi, N. G. Uraltsev and A. I. Vainshtein, Phys. Lett. **B293** (1992) 430, Erratum: Phys. Lett. **B297** (1993) 477, hep-ph/9207214.

[117] I. I. Bigi, M. A. Shifman, N. G. Uraltsev and A. I. Vainshtein, Phys. Rev. Lett. **71** (1993) 496, hep-ph/9304225;.

[118] B. Blok, L. Koyrakh, M. A. Shifman and A. I. Vainshtein, Phys. Rev. **D49** (1994) 3356, Erratum: Phys. Rev. **D50** (1994) 3572, hep-ph/9307247.

[119] A. V. Manohar and M. B. Wise, Phys. Rev. **D49** (1994) 1310, hep-ph/9308246.

[120] A. F. Falk, M. E. Luke and M. J. Savage, Phys. Rev. **D49** (1994) 3367, hep-ph/9308288.

[121] A. Ali, G. Hiller, L. T. Handoko and T. Morozumi, Phys. Rev. **D55** (1997) 4105, hep-ph/9609449.

[122] J. W. Chen, G. Rupak and M. J. Savage, Phys. Lett. **B410** (1997) 285, hep-ph/9705219.

[123] G. Buchalla, G. Isidori and S. J. Rey, Nucl. Phys. **B511** (1998) 594, hep-ph/9705253.

[124] G. Buchalla and G. Isidori, Nucl. Phys. **B525** (1998) 333, hep-ph/9801456.

[125] C. W. Bauer and C. N. Burrell, Phys. Lett. **B469** (1999) 248, hep-ph/9907517; Phys. Rev. **D62** (2000) 114028, hep-ph/9911404.

[126] C. S. Lim, T. Morozumi and A. I. Sanda, Phys. Lett. **B218** (1989) 343.

[127] N. G. Deshpande, J. Trampetic and K. Panose, Phys. Rev. **D39** (1989) 1461.

[128] P. J. O'Donnell, M. Sutherland and H. K. Tung, Phys. Rev. **D46** (1992) 4091.

[129] P. J. O'Donnell and H. K. Tung, Phys. Rev. **D43** (1991) 2067.

[130] F. Krüger and L. M. Sehgal, Phys. Lett. **B380** (1996) 199, hep-ph/9603237; Phys. Rev. **D55** (1997) 2799, hep-ph/9608361.

[131] N. Uraltsev, hep-ph/0306290.

[132] M. Luke, hep-ph/0307378.

[133] M. B. Voloshin, Phys. Lett. **B397** (1997) 275, hep-ph/9612483.

[134] A. Khodjamirian, R. Rückl, G. Stoll and D. Wyler, Phys. Lett. **B402** (1997) 167, hep-ph/9702318.

[135] Z. Ligeti, L. Randall and M. B. Wise Phys. Lett. **B402** (1997) 178, hep-ph/9702322.

[136] A. K. Grant, A. G. Morgan, S. Nussinov and R. D. Peccei, Phys. Rev. **D56** (1997) 3151, hep-ph/9702380.

[137] M. Gremm and A. Kapustin, Phys. Rev. **D55** (1997) 6924, hep-ph/9603448.

[138] D. Cronin-Hennessy *et al.* [CLEO Collaboration], Phys. Rev. Lett. **87** (2001) 251808, hep-ex/0108033.

[139] T. Mannel, Phys. Rev. **D50** (1994) 428, hep-ph/9403249.

[140] C. W. Bauer, Z. Ligeti, M. Luke and A. V. Manohar, Phys. Rev. **D67** (2003) 054012, hep-ph/0210027.

[141] M. Battaglia *et al.*, Phys. Lett. **B556** (2003) 41, hep-ph/0210319.

[142] R. F. Lebed and N. G. Uraltsev, Phys. Rev. **D62** (2000) 094011, hep-ph/0006346.

[143] A. S. Kronfeld and J. N. Simone, Phys. Lett. **B490** (2000) 228, Erratum: Phys. Lett. **B495** (2000) 441, hep-ph/0006345.

[144] N. Uraltsev, Phys. Lett. **B545** (2002) 337, hep-ph/0111166.

[145] T. van Ritbergen, Phys. Lett. **B454** (1999) 353, hep-ph/9903226.

[146] A. Czarnecki and K. Melnikov, Phys. Lett. **B88** (2002) 131801, hep-ph/0112264.

[147] M. Misiak and M. Münz, Phys. Lett. **B344** (1995) 308, hep-ph/9409454.

[148] K. Chetyrkin, M. Misiak and M. Münz, Nucl. Phys. **B518** (1998) 473, hep-ph/9711266; Nucl. Phys. **B520** (1998) 279, hep-ph/9711280.

[149] M. Misiak and J. Urban, Phys. Lett. **B451** (1999) 161, hep-ph/9901278.

[150] G. Buchalla and A. J. Buras, Nucl. Phys. **B548** (1999) 309, hep-ph/9901288.

[151] A. J. Buras, M. Misiak and J. Urban, Nucl. Phys. **B586** (2000) 397, hep-ph/0005183.

[152] M. Jamin and A. Pich, Nucl. Phys. **B425** (1994) 15, hep-ph/9402363.

[153] K. Adel and Y. P. Yao, Phys. Rev. **D49** (1994) 4945, hep-ph/9308349.

[154] C. Greub and T. Hurth, Phys. Rev. **D56** (1997) 2934, hep-ph/9703349.

[155] M. Ciuchini, G. Degrassi, P. Gambino and G. F. Giudice, Nucl. Phys. **B527** (1998) 21, hep-ph/9710335.

[156] A. J. Buras, A. Kwiatkowski and N. Pott, Nucl. Phys. **B517** (1998) 353, hep-ph/9710336.

[157] G. Buchalla and A. J. Buras, Nucl. Phys. **B398** (1993) 285.

[158] G. Buchalla and A. J. Buras, Nucl. Phys. **B400** (1993) 225.

[159] F. Borzumati and C. Greub, Phys. Rev. **D58** (1998) 074004, hep-ph/9802391; Addendum: Phys. Rev. **D59** (1999) 057501, hep-ph/9809438.

Acknowledgments

I am indebted to many persons who participated and have been instrumental during my studies in many respects aside from this work.

First and foremost I would like to thank my advisor Prof. Andrzej Buras for the possibility to work on the subject of B physics, for his continuous support throughout the years and for his encouraging advises and discussions. As a collaborator I have learned to appreciate his profound knowledge of the subject and intuition for the essential. I am also grateful for proofreading the manuscript.

Next I would like to thank Dr. Mikolaj Misiak who guided my way into the field of B physics, effective theories, the technical details of two loop calculations, for navigating me safely through tedious calculations, for always patiently giving me well considered answers to all my questions. I have enjoyed the collaboration with him which is one of the best experiences I ever had but I thank him also for his enthusiasm and kind hospitality.

Moreover, a special thank goes to Dr. Jörg Urban as a long-term workmate. I want to thank him for his dedicated efforts in all our joined work since the very beginning, for the time we spent to solve problems and to understand physics. Furthermore, I also want to thank him for the time we spent discussing about the rest of the world, his friendship and continuous care. Thank you!

I particularly want to thank my collaborators Thorsten Ewerth and Dr. Frank Krüger. I appreciate the collaboration with Thorsten, his straight way to approach things and his careful and steady manner. I want to thank Frank for the numerous discussions, explanations and insights concerning the phenomenology of B physics.

Furthermore, I would like to thank my roommate Michael Spranger for the relaxed and friendly atmosphere in our common office. I also thank Ulrich Haisch for discussions and for providing some checks of the numeric contained in this thesis. Moreover, it is a great pleasure to thank all current and former members of the physics department at the Technische Universität München for numerous discussions, chats and the pleasant social environment, not only during lunchtime. My thanks go to Dr. Rouzbeh Allahverdi, Cyrille Barbot, Dr. Athanasios Dedes, Prof. Manuel Drees, Benedikt Gaißmaier, Martin Gorbahn, Sebastian Jäger, Dr. Kin-ya Oda, Dr. Janusz Rosiek, Anton Poschenrieder, Michael Rauch, Dr. Stefan Recksiegel, Felix Schwab, Chung Lin Shan, Andreas Weiler and Elmar Wyszomirski.

An dieser Stelle möchte ich auch meinen Eltern und meiner Familie für ihre uneingeschränkte Unterstützung, ihre Sorge und die Freiräume danken.

Un grande bacio serio per Rita, for her great heart and all the patience.